GA-A14098
UC-77

A STRUCTURAL ANALYSIS OF THE GAS-COOLED FAST BREEDER REACTOR CORE SUPPORT

by

K. H. Chang, A. S. Chuang,
and C. E. Washington

Prepared under
Contract EY-76-C-03-0167
Project Agreement No. 23
for the
San Francisco Operations Office
U.S. Energy Research and Development Administration

General Atomic Project 3228

Date Published: June 1977

ABSTRACT

This report presents the results of a comprehensive study of the effect of pressure loading on the gas-cooled fast breeder reactor (GCFR) core support structure. Two theories are investigated for the core support grid plate: thin plate theory and anisotropic elasticity theory. The case of an isotropic thick plate is also presented. The effect of transverse shear and normal stress in a thick plate and the effect of the outer solid rim of the perforated interior portion of the grid plate are studied. The grid plate support structure upper flange, support cylinder, and lower flange are analyzed, and the structural interaction between the grid plate and the support structure is discussed. Numerical results are presented for each analysis. The stresses obtained in the grid plate and the support structure are evaluated according to the requirements of the ASME Boiler and Pressure Vessel Code, Section III, Division 1, and the deflections of the grid plate are examined to determine whether the reactivity insertion limitation on the plant safety requirements is met.

Since the final dimensions of the core support structure are not certain at this time, this report is not considered to be a final design stress report; however, it does examine the feasibility of the design and also demonstrates the analytical methods used to solve the grid plate problem from the standpoint of pressure loading.

NOMENCLATURE

a_{11}	independent coefficient of deformation
a_{12}	independent coefficient of deformation
a_{13}	independent coefficient of deformation
a_{33}	independent coefficient of deformation
a_{44}	independent coefficient of deformation
E	Young's modulus for isotropic material or Young's modulus in the plane of isotropy for transversely isotropic material
E'	Young's modulus in the plane perpendicular to the plane of isotropy for transversely isotropic material
E^*	effective Young's modulus for equivalent solid plate
G	shear modulus for isotropic material or shear modulus in the plane of isotropy for transversely isotropic material
G'	shear modulus in the plane perpendicular to the plane of isotropy for transversely isotropic material
G^*	effective shear modulus for equivalent solid plate
H	radial width of solid ring or flange
h	thickness of grid plate
M	radial moment of plate
p	pressure load
Q	radial force of plate
R_0	radius of grid plate
R_1	radius of perforated plate or equivalent solid plate
R^*	radius of perforated plate or equivalent solid plate
r	cylindrical coordinate

t	thickness of solid ring or flange
u	displacement in x direction
u_r	displacement in r direction
u_θ	displacement in θ direction
V'	transverse shear of plate
v	displacement in y direction
w	displacement in z direction
x	Cartesian coordinate
y	Cartesian coordinate
z	Cartesian or cylindrical coordinate
γ_{rz}	shear strain in cylindrical coordinate
$\gamma_{r\theta}$	shear strain in cylindrical coordinate
γ_{xy}	shear strain in Cartesian coordinate
γ_{xz}	shear strain in Cartesian coordinate
γ_{yz}	shear strain in Cartesian coordinate
$\gamma_{\theta z}$	shear strain in cylindrical coordinate
ε_r	normal strain in cylindrical coordinate
ε_x	normal strain in Cartesian coordinate
ε_y	normal strain in Cartesian coordinate
ε_z	normal strain in Cartesian or cylindrical coordinate
ε_θ	normal strain in cylindrical coordinate
θ	cylindrical coordinate
σ_r	normal stress in cylindrical coordinate
σ_x	normal stress in Cartesian coordinate
σ_y	normal stress in Cartesian coordinate

σ_z	normal stress in Cartesian or cylindrical coordinate
σ_θ	normal stress in cylindrical coordinate
τ_{rz}	shear stress in cylindrical coordinate
$\tau_{r\theta}$	shear stress in cylindrical coordinate
τ_{xy}	shear stress in Cartesian coordinate
τ_{xz}	shear stress in Cartesian coordinate
τ_{yz}	shear stress in Cartesian coordinate
$\tau_{\theta z}$	shear stress in cylindrical coordinate
ν	Poisson's ratio for isotropic material or Poisson's ratio in the plane of isotropy for transversely isotropic material
ν'	Poisson's ratio in the plane perpendicular to the plane of isotropy for transversely isotropic material
ν^*	effective Poisson's ratio for equivalent solid plate
χ	stress function, $\chi = \psi/(1 - \nu)$
ψ	stress function

CONTENTS

FIGURES

FIGURES (Continued)

1. INTRODUCTION

The gas-cooled fast breeder reactor (GCFR) core support structure consists basically of two structural members: the grid plate and the grid plate support cylinder. The grid plate is a thick circular disk which is perforated throughout the central region and surrounded by a narrow solid outer rim, and there are 265 circular holes which accommodate the bayonet sections of the core assemblies. The primary function of the grid plate is to accurately hold the fuel and blanket assemblies in position so that the reactivity change associated with core distortion due to deformation of the structure is minimized to an acceptable value set by plant safety requirements. As a result, the grid plate is a deflection-limited rather than stress-limited structural component.

The structural analysis problem of perforated plates has been extensively investigated ever since Gardner (Refs. 1 through 3) introduced the equivalent solid plate concept. Not long after Gardner's first paper, Horvay (Refs. 4 through 6) and Malkin (Ref. 7) separately proposed basing the equivalent solid plate concept on the use of fictitious elastic constants called effective elastic constants. The present investigation employs the concept of an equivalent solid plate for the grid plate. The effective elastic constants are derived from the existing literature, such as the ASME Code and work by Slot (Ref. 8). Thin plate theory and anisotropic elasticity theory are applied and the results compared.

The grid plate support structure consists of a cylinder and upper and lower flanges. The cylinder and the lower flange are analyzed by elastic thin shell theory, and the upper flange is treated as a ring. Compatibility conditions are used to determine the redundant forces and moments at the geometrical discontinuity.

The reactivity change associated with deflection of the grid plate is considered, and a computer program has been developed for the purpose of finding an optimum design. The interrelationship of plate thickness, ligament efficiency, and reactivity is also studied, as shown in Fig. 1. The interaction between the grid plate and the support structure is also considered (Section 5). The interactive force and moment between the grid plate and the support cylinder are analytically formulated, and a computer program has been written to obtain numerical results.

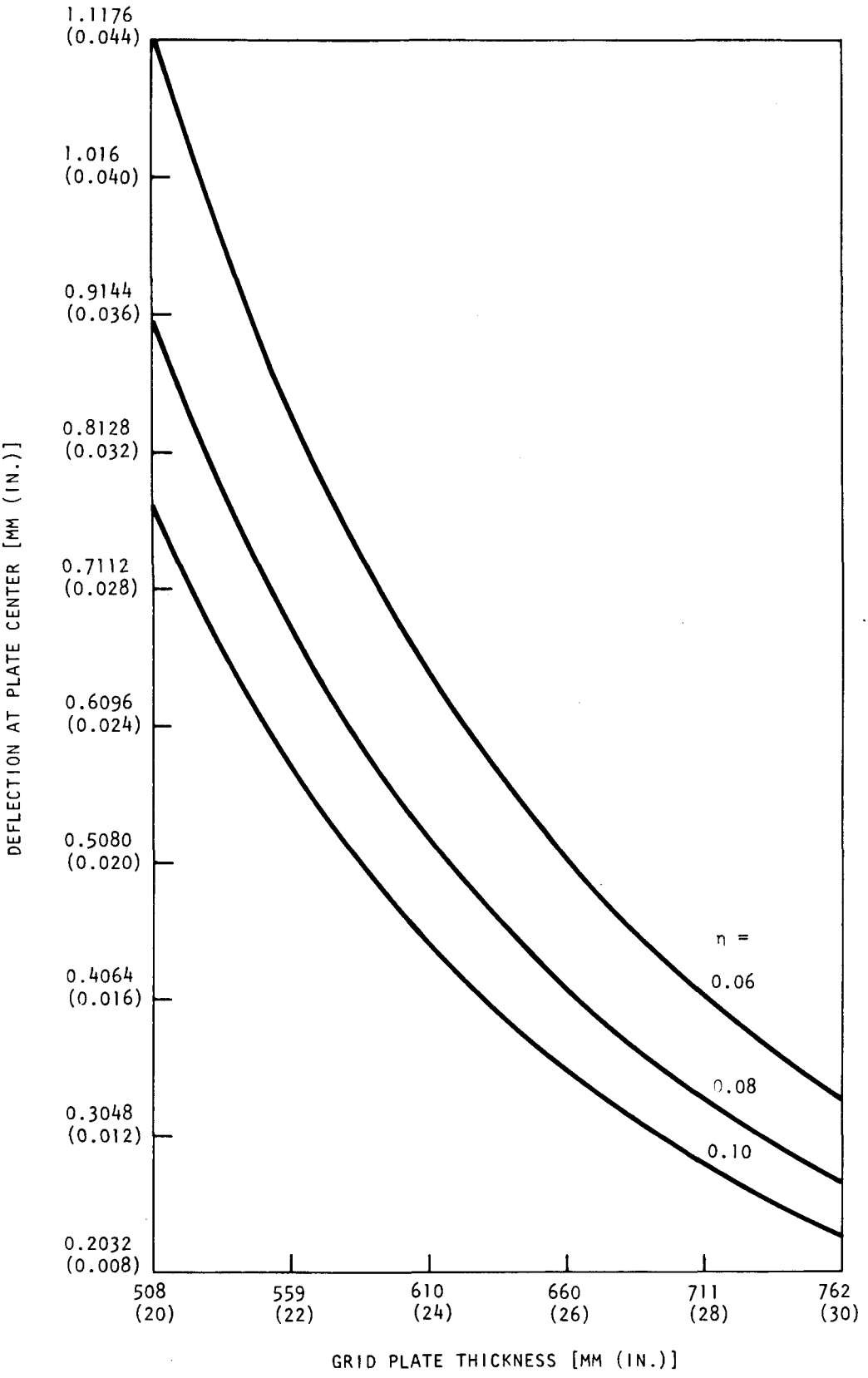

Fig. 1. Parametric study of grid plate thickness and center deflection for different ligament efficiencies

2. DESIGN PHILOSOPHY

2.1. DESIGN CONSIDERATION

Conformance of the core support structure to the reactivity requirement and available codes and standards is investigated. Experience with the 300-MW(e) demonstration plant design indicates that the reactivity change associated with deflection of the grid plate is more critical than the stresses in the grid plate due to expected loads during normal and transient operation. When the plant is operating at a steady power output, the reactor is in the critical condition. However, if there is a partial or total loss of coolant, a reduction of pressure drop across the grid plate is accompanied by a decrease in deflection, resulting in a positive reactivity insertion in the core owing to inward movement of the fuel assembly. Because of the more stringent requirement of positive reactivity insertion associated with the plant safety operation, the grid plate design is deflection-limited rather than stress-limited.

2.2. GRID PLATE DEFLECTION REACTIVITY EFFECT

The reactivity effect resulting from core expansion causes (1) changes in neutron leakage owing to the increase in core size and (2) a decrease in the densities of fuel, cladding, and structural materials because the total material inventory remains unchanged (this is reflected by a decrease of all nuclide densities). This is a strongly negative effect owing primarily to the decrease in fissile density dominating the leakage distribution. Thus, the overall reactivity effect of core expansion is negative. Conversely, a reduction in core size results in a positive reactivity insertion.

During normal operation, grid plate deflection is composed of two components. The first component, which is always present, is the dead

weight of the grid plate; the second is the coolant pressure drop across the core during normal operation. The reactivity change of the latter component is of interest because it can vary under transient conditions such as depressurization and is therefore a safety-related problem.

The relationship between reactivity change and radial core expansion is derived (Ref. 9) in the following form:

$$\Delta\psi = C_r \frac{\Delta R}{R} \quad , \tag{1}$$

where $\Delta\psi$ = reactivity change,

R = core radius,

C_r = core radial expansion coefficient,

ΔR = increment of core radius at core midplane.

The core radial expansion coefficient is obtained from a two-dimensional diffusion theory calculation which results in

$$C_r = -0.64 \quad .$$

It is desirable to derive a formula relating the deflection of the grid plate to the increment of the core and incorporate the expression into an equation (Eq. 1). Then, the reactivity change due to grid plate deflection can be easily evaluated.

The geometric relation of grid plate deflection and the increment of the core radius at the midplane of the core is shown in Fig. 2. In this figure, L is the distance from the bottom of the grid plate to the midplane of the core, R_c is the equivalent cylindrical radius of the outermost fuel rod assemblies, and ΔR is the core radial increment at the core midplane.

The total axial displacement of the grid plate based on the transversely isotropic elasticity theory is derived in Eq. 87 to be

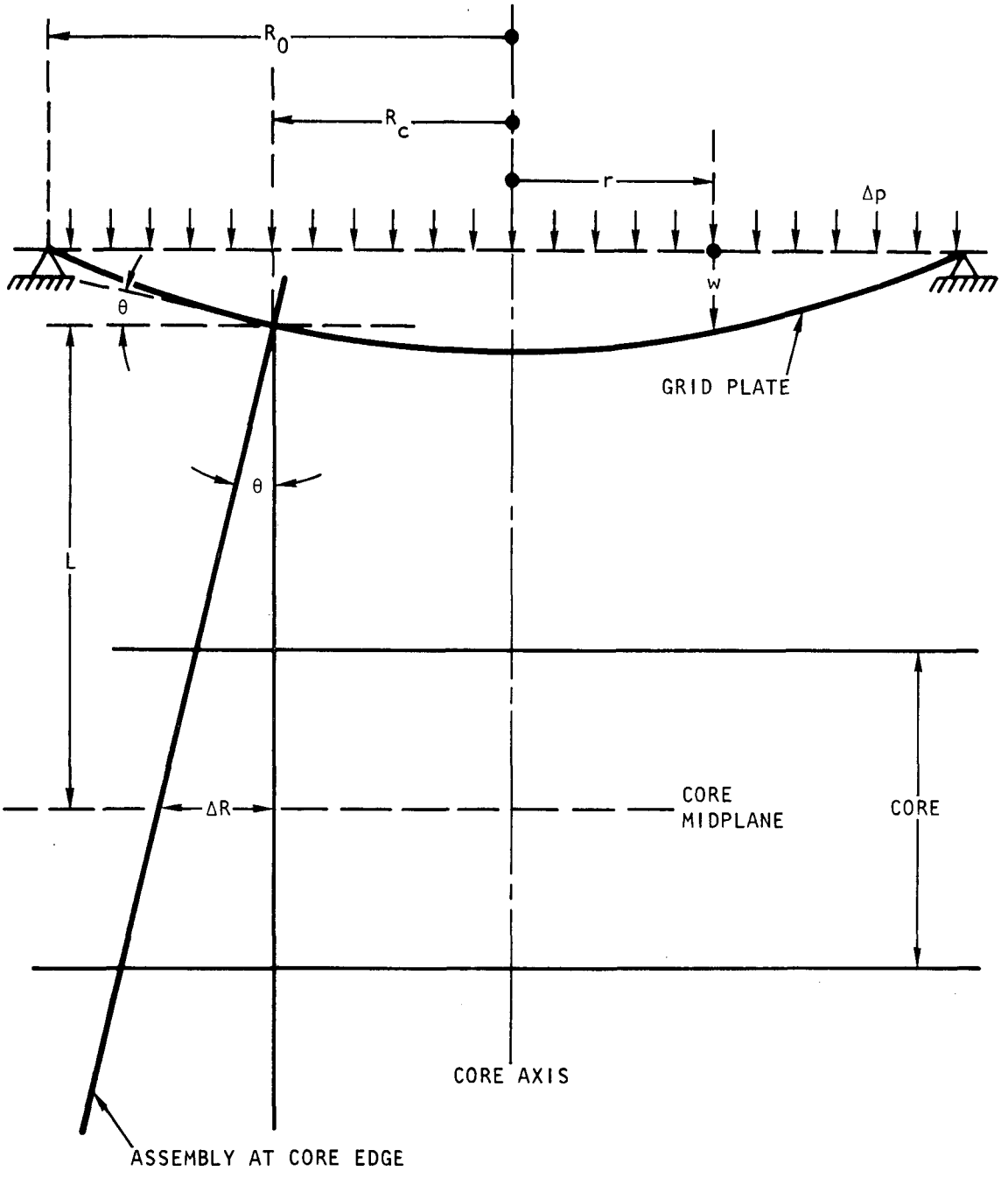

Fig. 2. Computational model

$$w = \frac{p}{64D}(R_1^2 - r^2)\left[\frac{5 + \nu^*}{1 + \nu^*}R_1^2 - r^2\right]$$

$$+ \frac{3p}{10h}\left[\frac{1}{G'} - \frac{\nu'(7 - \nu^*)}{4E'}\right](R_1^2 - r^2)$$

$$+ \frac{pZ}{E'}\left\{-\frac{1}{2} - \frac{3\nu'Z}{4E'h^3}\left[(3 + \nu^*)R_1^2 - 2(1 + \nu^*)r^2\right]\right.$$

$$\left. + \frac{3Z}{20h}(m\nu' + 5) - \frac{Z^3}{2h^3}(m\nu' + 1)\right\}$$

$$- \frac{6}{h^3}\left[\frac{(1 - \nu^*)}{E^*}(R_1^2 - r^2) - \frac{2\nu'}{E^*}Z^2\right]M + \frac{2\nu'}{E'}\frac{Z}{h}H$$

$$+ \frac{pR_2(R_1^2 + R_0^2)\Delta R^2}{4EI} \quad ,$$

where

$$D = \frac{E^*h^3}{12(1 - \nu^2)} \quad ,$$

$$M = \frac{\dfrac{pR_1^3}{8D(1 + \nu^*)} - \dfrac{pR_2(R_1^2 + R_0^2)\Delta R}{4EI} + \dfrac{3pR_1}{5h}\left[\dfrac{1}{G'} - \dfrac{\nu'(7 - \nu^*)}{4E'}\right]}{\dfrac{R_1R_2}{EI} + \dfrac{12R_1(1 - \nu^*)}{E^*h^3}} \quad ,$$

$$H = \frac{pEE^*\nu'h\Delta R}{2E'[E^*R_2 + (1 - \nu^*)E\Delta R]} \quad .$$

Deflections of the grid plate midplane can be obtained by letting $z = 0$ in Eq. 81, and the expression can be simplified:

$$w = \frac{p}{64D}(R_1^2 - r^2)\left[\frac{5 + \nu^*}{1 + \nu^*}R_1^2 - r^2\right]$$

$$+ \frac{3p}{10h}\left[\frac{1}{G'} - \frac{\nu'(7 - \nu^*)}{4E'}\right](R_1^2 - r^2)$$

$$- \frac{6}{h^3}\left[\frac{(1 - \nu^*)}{E^*}(R_1^2 - r^2)\right]M$$

$$+ \frac{pR_2(R_1^2 + R_0^2)\Delta R^2}{4EI} \quad . \tag{2}$$

Differentiating the expression of Eq. 2 with respect to r, the slope of the grid plate meridian yields

$$\frac{dw}{dr} = \frac{pr^3}{16D} + r\left\{\frac{12(1 - \nu^*)}{E^*h^3}M - \frac{p}{32D}\left[R_1^2\left(\frac{5 + \nu^*}{1 + \nu^*} + 1\right)\right]\right.$$

$$\left. - \frac{3p}{5h}\left[\frac{1}{G'} - \frac{\nu'(7 - \nu^*)}{4E'}\right]\right\} \quad . \tag{3}$$

For a fuel assembly at the edge of the core ($r = R_c$), which results in the greatest radial displacement due to grid plate deflection, the following geometric relation can be obtained from Fig. 2:

$$\tan\theta = \frac{\Delta R}{L} = \left.\frac{dw}{dr}\right|_{r = R_c} \quad .$$

This implies that

$$\Delta R = L \left.\frac{dw}{dr}\right|_{r = R_c} . \tag{4}$$

Therefore, the reactivity change can be written as

$$\Delta\psi = C_r \left(\frac{L}{R}\right) \left.\frac{dw}{dr}\right|_{r = R_c} . \tag{5}$$

For the current 300-MW(e) demonstration plant design, the reactivity change due to core grid plate deflection under a pressure load of 289.58 kPa (42.0 psi) can be estimated as follows:

R_0 = 1.6986 m (66.875 in.),
R_1 = 1.5535 m (61.16 in.),
R_c = 1.1367 m (44.75 in.),
L = 1.6050 m (63.19 in.),
h = 609.6 mm (24.0 in.),
E^* = 6.102 x 10^3 MPa (0.885 x 10^6 psi),
E = 172.37 x 10^3 MPa (25.0 x 10^6 psi),
E' = 39.851 x 10^3 MPa (5.78 x 10^6 psi),
G' = 7.943 x 10^3 MPa (1.152 x 10^6 psi),
ν^* = 0.734,
ν' = 0.3,
p = 289.58 kPa (42.0 psi).

Substituting these geometric dimensions, material constants, and pressure loading into Eq. 3, the value of dw/dr at r = 1.1367 m (44.75 in.) yields

$$\left.\frac{dw}{dr}\right|_{r = 1.1367\ m} = 0.26959 \times 10^{-3} .$$

Therefore,

$$\Delta\psi = C_r\left(\frac{L}{R}\right)\frac{dw}{dr}\Bigg|_{r = 1.1367\ \text{m (44.75 in.)}}$$

$$= -0.64\left(\frac{1.6050}{1.1367}\right)\left(\frac{0.26959 \times 10^{-3}}{3.5 \times 10^{-3}}\right)$$

$$= -\$0.0696 \quad .$$

Thus, the reactivity change corresponding to the 289.58-kPa (42-psi) pressure loading across the grid plate has a value of -$0.07, which is within the tentative plant safety requirement of a reactivity change of -$0.10.

3. THEORY AND ANALYSIS OF THE GRID PLATE

3.1. CONCEPT OF THE EQUIVALENT SOLID PLATE

One established procedure for determination of stresses in thick perforated plates is based on the concept of treating the perforated material as an equivalent solid material with modified elastic constants (Ref. 10, 11). This approach is based on the concept that these modified constants, called effective elastic constants, are determined in such a way that gross deformations in the perforated plate and the equivalent solid plate are identical under the same loading and boundary conditions. Once these effective elastic constants have been established, the stress analysis problem of perforated plates involves essentially two steps:

1. Nominal stresses in the equivalent solid plate are computed by means of established continuum mechanics analytical methods.

2. Physically meaningful stresses in the perforated plate are determined from nominal stresses using appropriate stress multipliers.

The effective elastic constants and the stress multipliers can be determined by experimental measurement. They are calculated from doubly periodic stress and strain fields produced in perforated plates of infinite extent under uniform loading conditions.

The equivalent solid plate approach as it is currently used (Ref. 10) was originally developed (Ref. 11) for solving problems involving equivalent solid plate stresses which were either uniform or linear through the thickness of the plate. This approach is too restrictive for solving problems in which the state of stress in the equivalent solid plate is more complex than can be described by a combination of membrane and bending stress. A more general equivalent solid plate concept is necessary for such problems.

In Section 3.3, a generalized equivalent solid plate approach has been formulated which permits analysis of thick perforated plate problems.

3.2. THIN PLATE THEORY

3.2.1. Mathematical Formulation

3.2.1.1. Analytical Procedure. The central portion of the grid plate is perforated and surrounded by a solid ring. A uniformly distributed load resulting from the pressure difference across the plate is applied on the top surface of the plate, and it is assumed that the plate is simply supported around the edge. This method of analysis is based on Article 8000, Section III, of the ASME Boiler and Pressure Vessel Code (Ref. 10).

In the following analysis, the perforated plate is replaced by a solid plate which is geometrically similar to the perforated plate but has the modified value of the elastic constants. The outer solid rim is considered to be a ring, and the elastic modulus E and Poisson's ratio ν are replaced by the effective elastic modulus E^* and effective Poisson's ratio ν^* of the perforated plate. Conventional formulas for the plate are used to determine the deformations and nominal stresses for the equivalent solid plate. The deformations are computed so that they may be directly used in evaluating interaction effects.

The effective elastic constants are functions of the ligament efficiency η. These values are given in Fig. A-8131-1 of Section III, ASME Boiler and Pressure Vessel Code (Ref. 10) for the range $0.05 \leq \eta \leq 1.0$ in the form ν^* versus η (for a material with $\nu = 0.3$) and E^*/E versus η.

3.2.1.2. Structural Analysis. In the structural analysis, the grid plate is first separated at the junction of the perforated portion and the solid ring, and the following variables are assigned:

M = radial redundant moment [N·m/m (in.·lb/in.)] of circumference,
Q = radial redundant force [N/m (lb/in.)] of circumference,

V' = transverse shear [N/m (lb/in.)] of circumference,

p = uniformly distributed pressure [Pa (lb/in.^{2})].

This analysis, in which Q is assumed to be zero, is illustrated below.

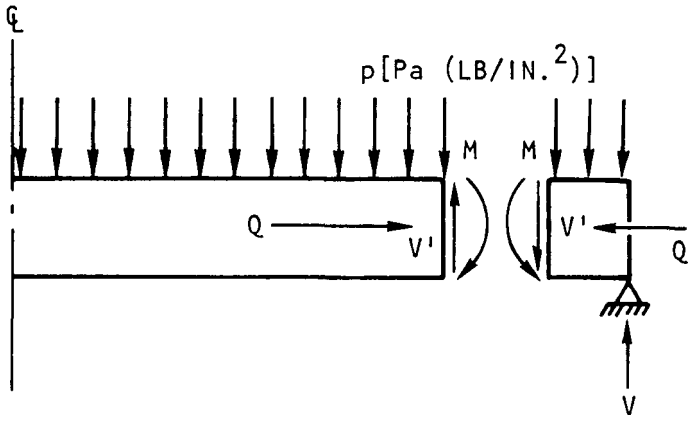

Next, the edge deformation due to the redundant moment is calculated. For the perforated plate, the rotation of the plate edge at the midplane caused by moment M is

$$\theta_{pl} = \frac{12R^*}{E^* t_2^3}(1 - \nu^*)M \quad \text{(radian)} \quad . \tag{5}$$

This can be depicted as follows:

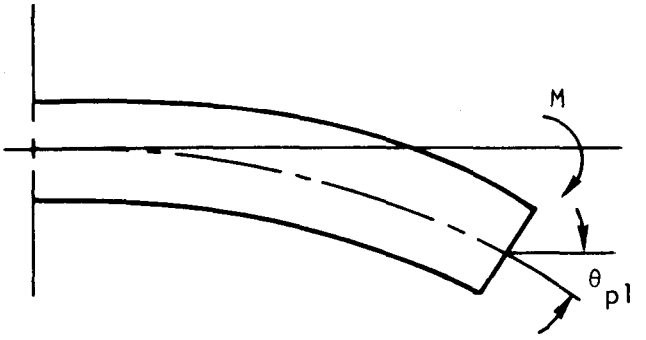

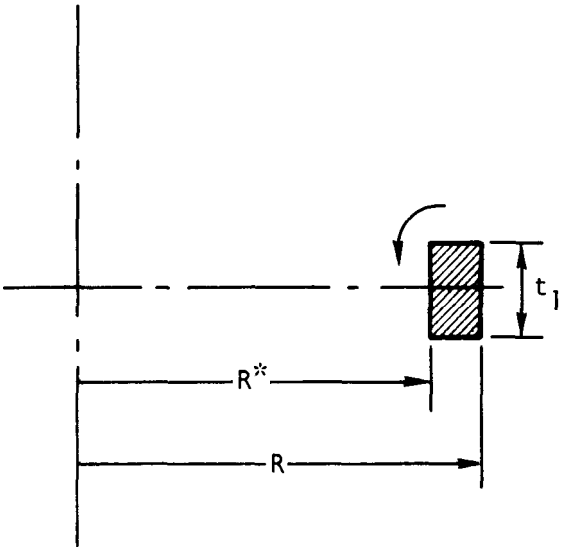

The rotation of the ring cross section in its own plane about its centroid caused by M is (Ref. 12)

$$\theta_{rl} = \frac{\frac{M(2\pi R^*)}{2\pi \bar{R}} \bar{R}^2}{EI} = \frac{M R^* R}{EI} \quad , \tag{6}$$

where $\bar{R} = (R + R^*)/2$,

I = moment of inertia about the central axis of the cross section in the plane of the ring

$$= \frac{t_1^3 \Delta R}{12} \quad ,$$

$$\Delta R = R - R^* \quad .$$

The edge deformations caused by loads other than redundant loads are shown below and calculated as follows. For the perforated plate,

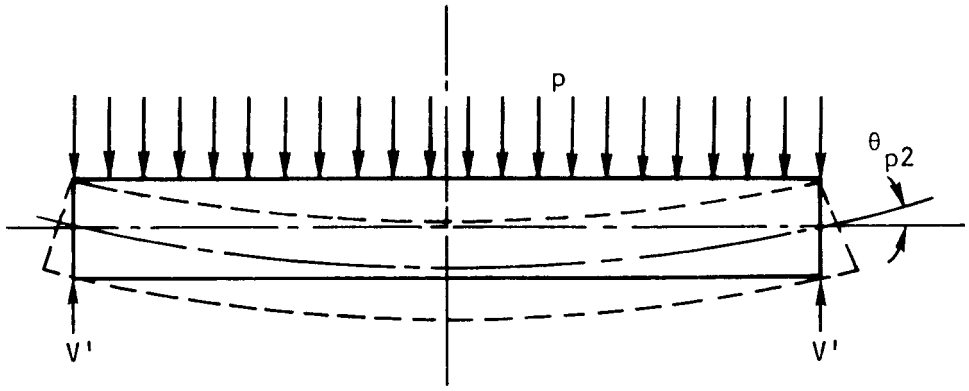

$$V_1' = \frac{\pi R^{*2} \omega}{2\pi R^*} = \frac{R^* p}{2} \quad , \tag{7}$$

$$\theta_{p2} = \frac{3 (R^*)^3}{2 E^* t_2^3} (1 - \nu^*) p \quad , \tag{8}$$

where $p = \Delta p$ and is the normal distributed load due to the net pressure acting on the plate.

For the solid ring,

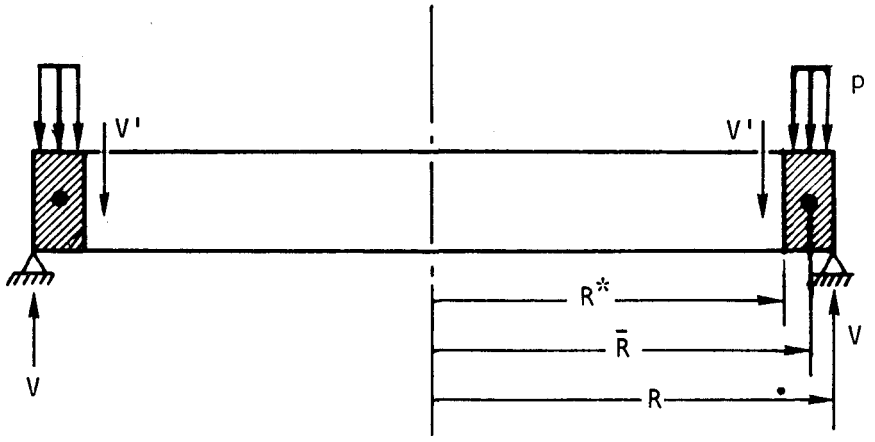

$$V = \frac{\pi R^2 p}{2\pi R} = \frac{Rp}{2} \quad . \tag{9}$$

The twist moment per unit length of the mean circumference of the ring due to the load is

$$M_\ell = \frac{V(2\pi R)\frac{\Delta R}{2}}{2\pi \bar{R}} + \frac{V_1(2\pi R^*)\frac{R}{2}}{2\pi \bar{R}}$$

$$= \frac{\frac{pR}{2} R \frac{\Delta R}{2}}{\bar{R}} + \frac{\frac{pR^*}{2} R^* \frac{\Delta R}{2}}{\bar{R}}$$

$$= \frac{p\Delta R(R^2 + R^{*2})}{4\bar{R}} \quad . \tag{10}$$

The rotation of the ring cross section in its own plane about its centroid due to M_ℓ is

$$\theta_{rz} = \frac{M_\ell \bar{R}^2}{EI} = \frac{p\Delta R(R^2 + R^{*2})}{4\bar{R}} \frac{\bar{R}}{EI}$$

$$= \frac{p\Delta R\bar{R}}{4EI} (R^{*2} + R^2) \quad . \tag{11}$$

For the compatibility condition, the total rotations of the perforated plate and solid ring at the junction must be equated as follows:

$$\theta_p = \theta_r \quad ,$$

where $\theta_p = \theta_{p2} - \theta_{p1}$,

$\theta_r = \theta_{r1} + \theta_{r2}$.

Thus,

$$\theta_p = \frac{3}{2}\frac{(R^*)^3}{E^* t_2^3}(1 - \nu^*)\, p - \frac{12R^*}{E^* t_2^3}(1 - \nu^*)M \quad , \tag{12}$$

$$\theta_r = \frac{MR^*\bar{R}}{EI} + \frac{p\Delta R\bar{R}}{4EI}(R^{*2} + R^2)$$

$$= \frac{6R^*(R + R^*)}{(R - R^*)Et_1^3} M + \frac{1.5(R + R^*)(R^2 + R^{*2})}{Et_1^3} p \quad , \tag{13}$$

$$\frac{R^*(1 - \nu^*)}{E^* t_2^3}\left[12 + 6\frac{E^*}{E}\left(\frac{t_2}{t_1}\right)^3 \frac{(R + R^*)}{(1 - \nu^*)(R - R^*)}\right]M$$

$$= \frac{R^*(1 - \nu^*)}{E^* t_2^3}\left[1.5R^{*2} p - 1.5\left(\frac{E^*}{E}\right)\left(\frac{t_2}{t_1}\right)^3 \frac{(R + R^*)(R^2 + R^{*2})}{R^*(1 - \nu)}\right]p \quad . \tag{14}$$

The redundant moment then becomes

$$M = \frac{R^{*2} p - \frac{E^*}{E}\left(\frac{t_2}{t_1}\right)^3 \frac{(R + R^*)(R^2 + R^{*2})}{R^*(1 - \nu^*)} p}{8 + 4\frac{E^*}{E}\left(\frac{t_2}{t_1}\right)^3 \frac{R + R^*}{(1 - \nu^*)(R - R^*)}} \quad . \tag{15}$$

The deflection at the center of the grid plate is shown below and calculated as follows:

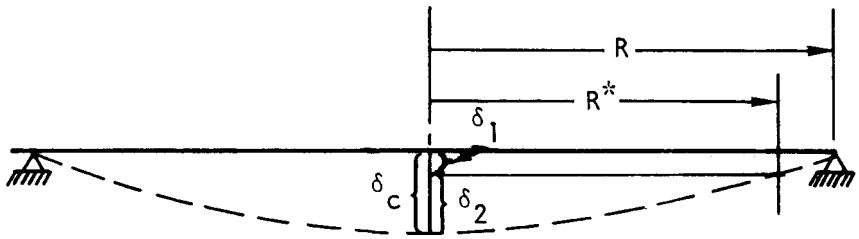

$$\delta_c = \delta_1 + \delta_2 \quad ,$$

where

$$\left.\begin{aligned}
\delta_1 &= \theta_R \cdot \Delta R = \left[\frac{6R^*(R + R^*)M}{(R - R^*)Et_1^3} + \frac{1.5(R + R^*)(R^2 + R^{*2})p}{E^*t_1^3}\right](R - R^*) \quad , \\
\delta_2 &= \left(\delta_2\right)^M_{\text{due to M}} + \left(\delta_2\right)^p_{\text{due to p}} \quad , \\
(\delta_2)^M &= \frac{6(1 - \nu^*)R^{*2}M}{E^*t_2^3} \qquad \text{(see Ref. 12)} \quad , \\
(\delta_2)^p &= \frac{3R^{*4}(1 - \nu^*)(5 + \nu^*)}{16E^*t_2^3} \qquad \text{(see Ref. 12)} \quad ,
\end{aligned}\right\} \qquad (16)$$

$$\delta_c = \frac{6R^*(R + R^*)M}{Et_1^3} + \frac{1.5(R^4 - R^{*4})}{Et_1^3} p$$

$$- \frac{6(1 - \nu^*)R^{*2} M}{E^* t_2^3} + \frac{3R^{*4}(1 - \nu^*)(5 + \nu^*)}{16E^* t_2^3} \quad ,$$

$$\delta_c = \left[\frac{6R^*(R + R^*)}{Et_1^3} - \frac{6(1 - \nu^*)R^{*2}}{E^* t_2^3}\right] M$$

$$+ \left[\frac{1.5(R^4 - R^{*4})}{Et_1^3} + \frac{3R^{*4}(1 - \nu^*)(5 + \nu^*)}{16E^* t_2^3}\right] p \quad . \qquad (16)$$

Finally, the slope at the edge of the core is calculated as shown below.

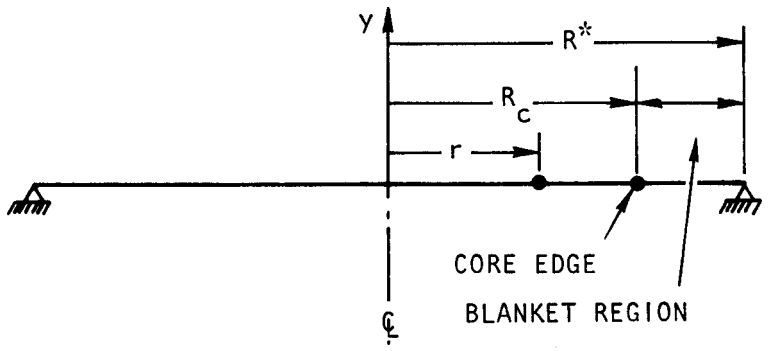

The deflection at any given point a distance r from the center of the plate due to M and p is given as follows (Ref. 12):

$$w = \frac{3\pi(R^*)^2 p(1 - \nu^{*2})}{8\pi E^* t_2^3}\left[\frac{(5 + \nu^*)(R^*)^2}{2(1 + \nu^*)} + \frac{r^4}{2R^{*2}} - \frac{(3 + \nu^*)r^2}{1 + \nu^*}\right]$$

$$+ \frac{6(1 - \nu^*)(R^{*2} - r^2)M}{Et_2^3} \quad . \tag{17}$$

The slope at the core edge R_c is therefore

$$\left.\frac{dw}{dr}\right|_{r = R_c} = -\frac{3R^{*2} p(1 - \nu^{*2})}{8E^* t_2^3}\left[\frac{2R_c^3}{R^{*2}} - \frac{2(3 + \nu^*)R_c}{1 + \nu^*}\right]$$

$$- \frac{12(1 - \nu^*)MR_c}{E^* t_2^3} \quad . \tag{18}$$

3.2.2. Numerical Results

The numerical calculations were done using a computer program. Deflections at the center of the grid plate were evaluated for different sets of values of plate thickness, ligament efficiency, and solid rim width in the ranges of interest. The optimal dimensions of the grid plate were then determined by the reactivity insertion limit; material and fabrication cost were also considered. The computational model is shown in Fig. 3, and the numerical data for calculations are listed as follows:

T = 349°C (660°F),

E = 172.645 x 10^3 MPa [25.04 x 10^6 psi (for 316 stainless steel at T = 349°C, Section III, ASME Code)],

P = pitch = 196.85 mm (7.75 in.),

R_o = 1.6986 m (66.875 in.),

R^* = 1.5335 m (61.16 in.).

A parametric study on the optimal design of the grid plate was performed using grid plate radius, thickness, and ligament efficiency as

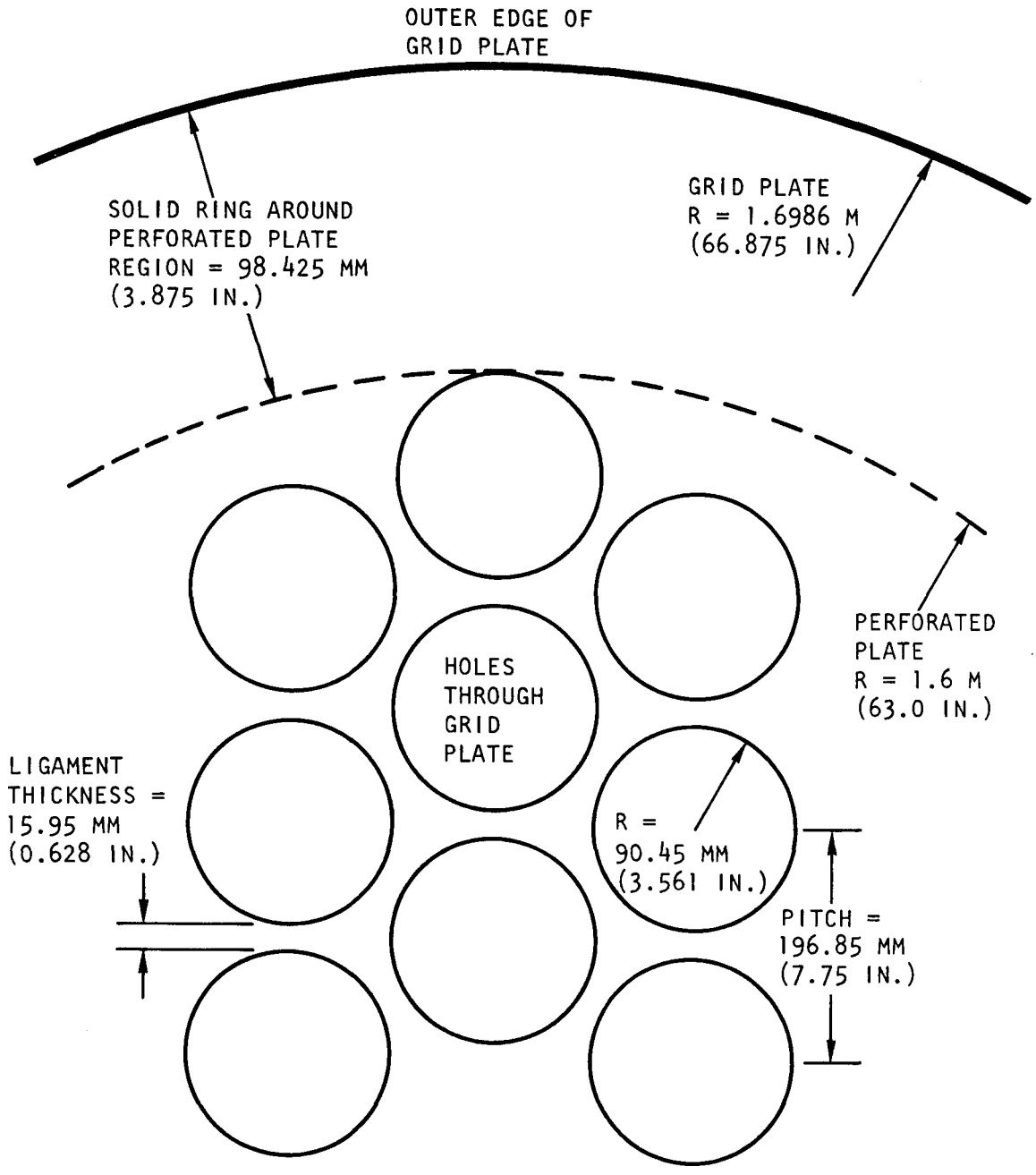

Fig. 3. Geometric considerations for grid plate deflection

the parameters. The computer results show that the reactivity of the core is sensitive to the change of grid plate thickness and ligament efficiency, but is virtually unaffected by variation of the grid plate radius in the range of interest. In Fig. 4, the ligament efficiency is plotted against the thickness of the grid plate for a particular radius size [1.6986 m (66.875 in.)] and a reactivity of $0.10. This figure indicates the important effect of both parameters on reactivity.

Figure 1 is a plot of deflection at the center of the grid plate versus grid plate thickness for different values of ligament efficiency in the range of interest. The computer results for stress and deflection of the thin plate solution are shown in Figs. 5 through 7. Figure 5 gives radial stress distribution versus radial coordinate of the grid plate; Fig. 6 shows tangential stress distribution versus radial coordinate of the grid plate; and Fig. 7 gives the axial displacement versus radial coordinate of the grid plate.

3.2.3. Transverse Shear and Normal Stress Effect on a Thick Plate

3.2.3.1. Discussion. In previous calculations of grid plate deflections (Section 3.2), the assumption was made that linear thin plate theory is applicable to the equivalent solid plate of the grid plate. This is true only when the plate thickness is small compared with the other lateral dimensions, in this case the diameter of the equivalent solid plate. Based on this assumption, the effect of the normal stress and shear stress in the transverse direction was neglected. For the GCFR 300-MW(e) demonstration plant, the grid plate diameter-to-thickness ratio is approximately 5.5. In general, a plate is considered to be thin when the ratio of the smallest lateral dimension to the thickness is greater than 10. For a plate as thick as the grid plate, the transverse shear effect cannot be ignored.

3.2.3.2. Analysis. For a simply supported plate which has a radius R and a thickness h and is subjected to a uniformly distributed load p

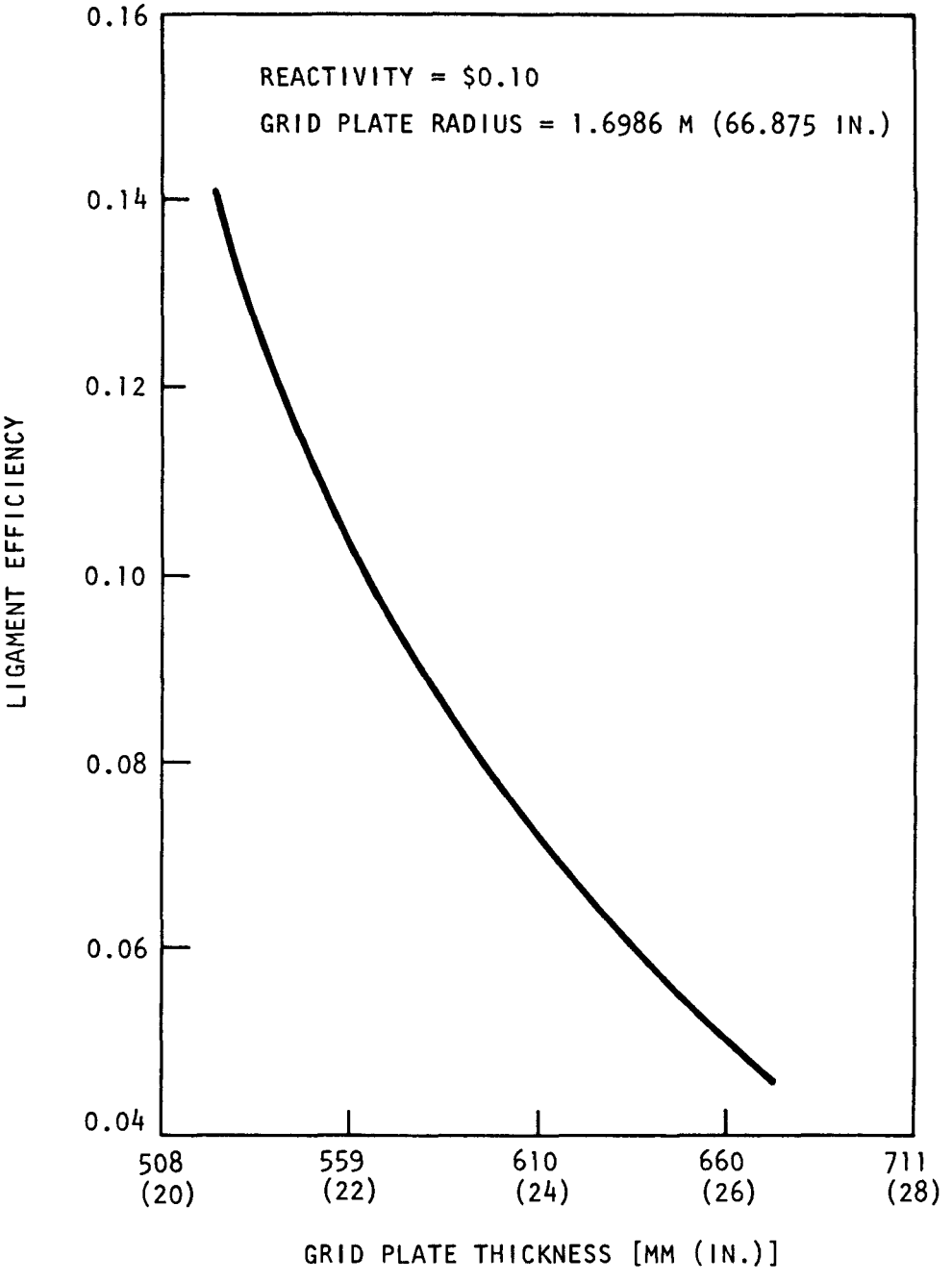

Fig. 4. Grid plate thickness vs ligament efficiency

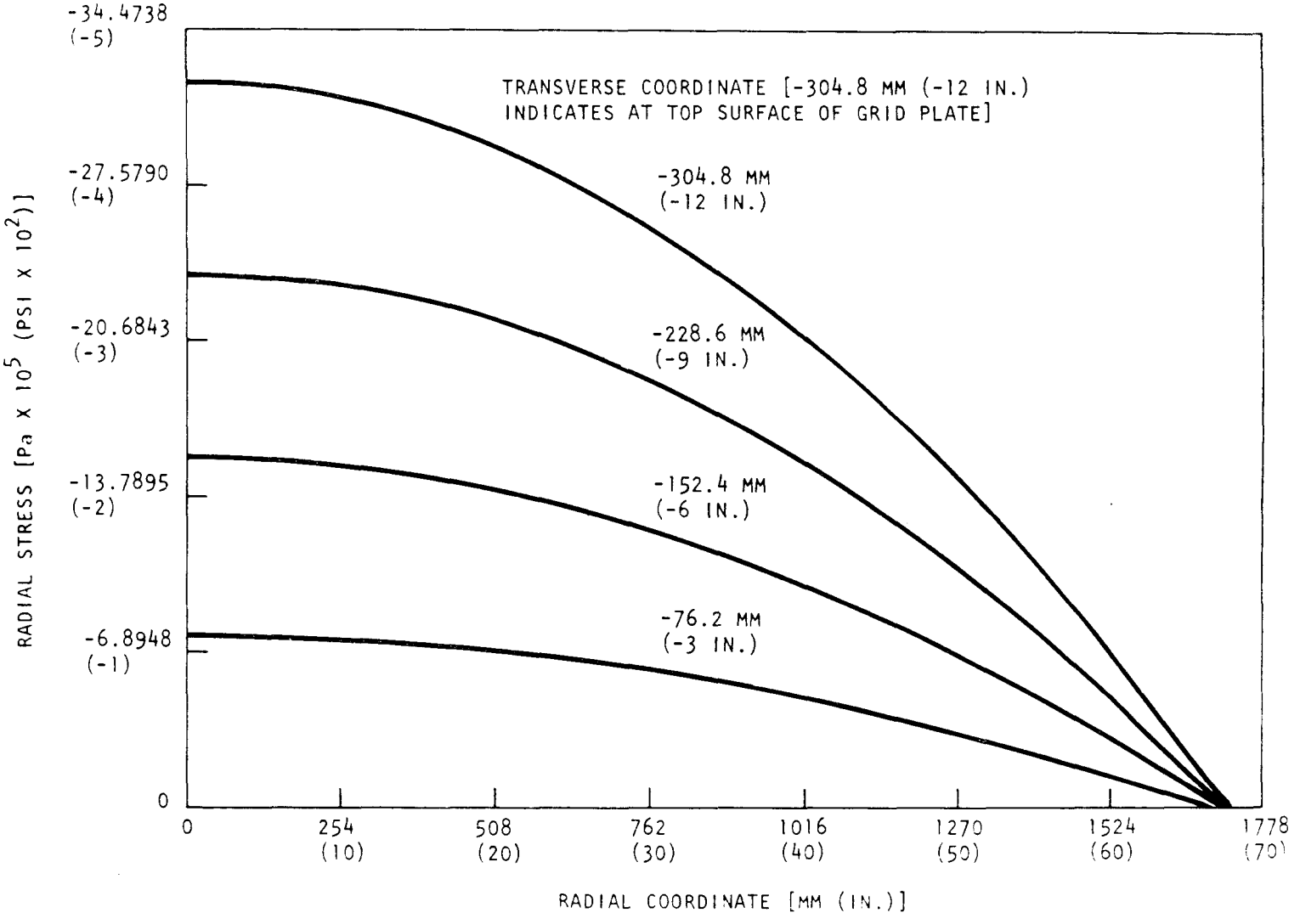

Fig. 5. Thin plate solution, radial stress distribution vs radial coordinate of grid plate

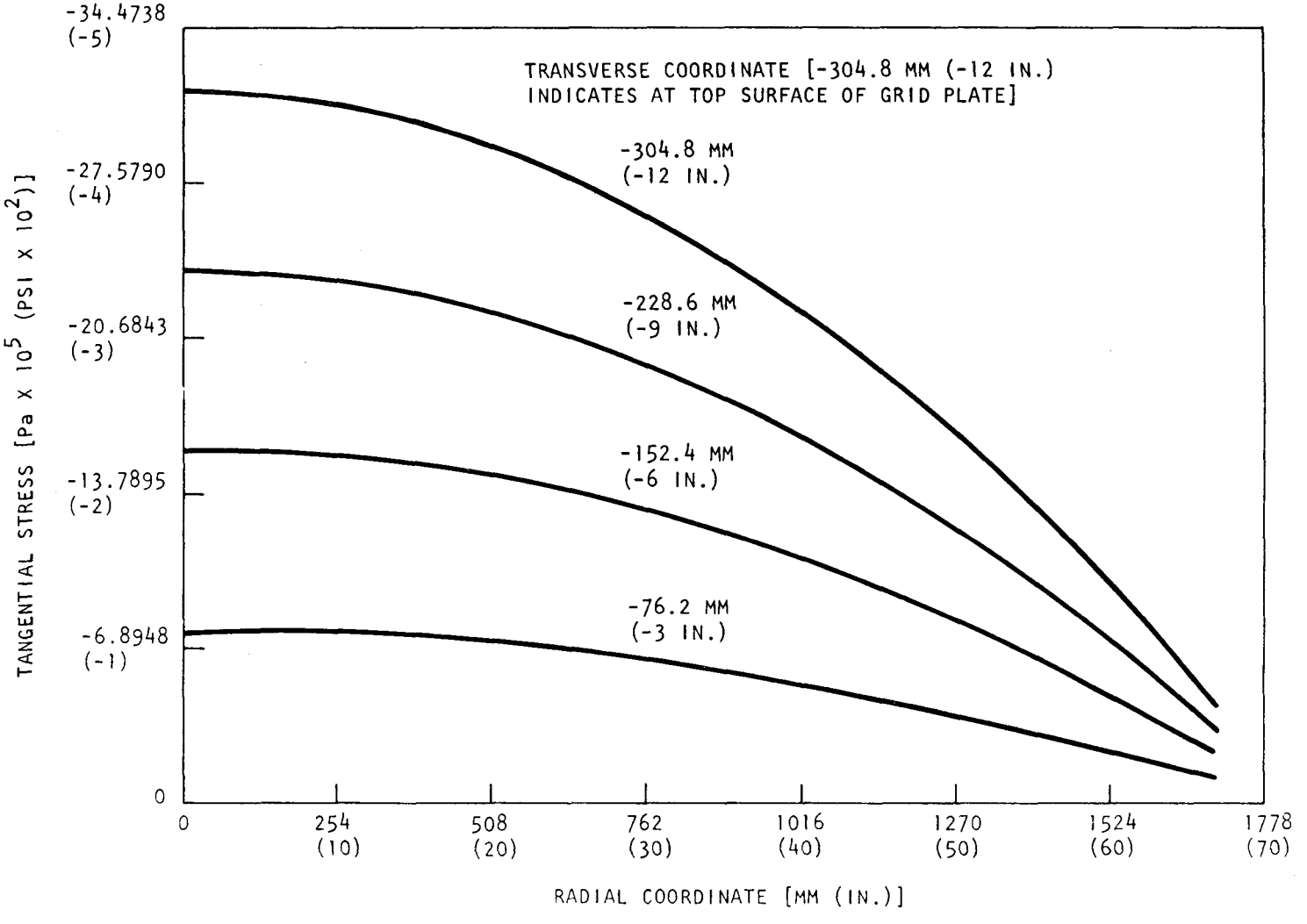

Fig. 6. Thin plate solution, tangential stress distribution vs radial coordinate of grid plate

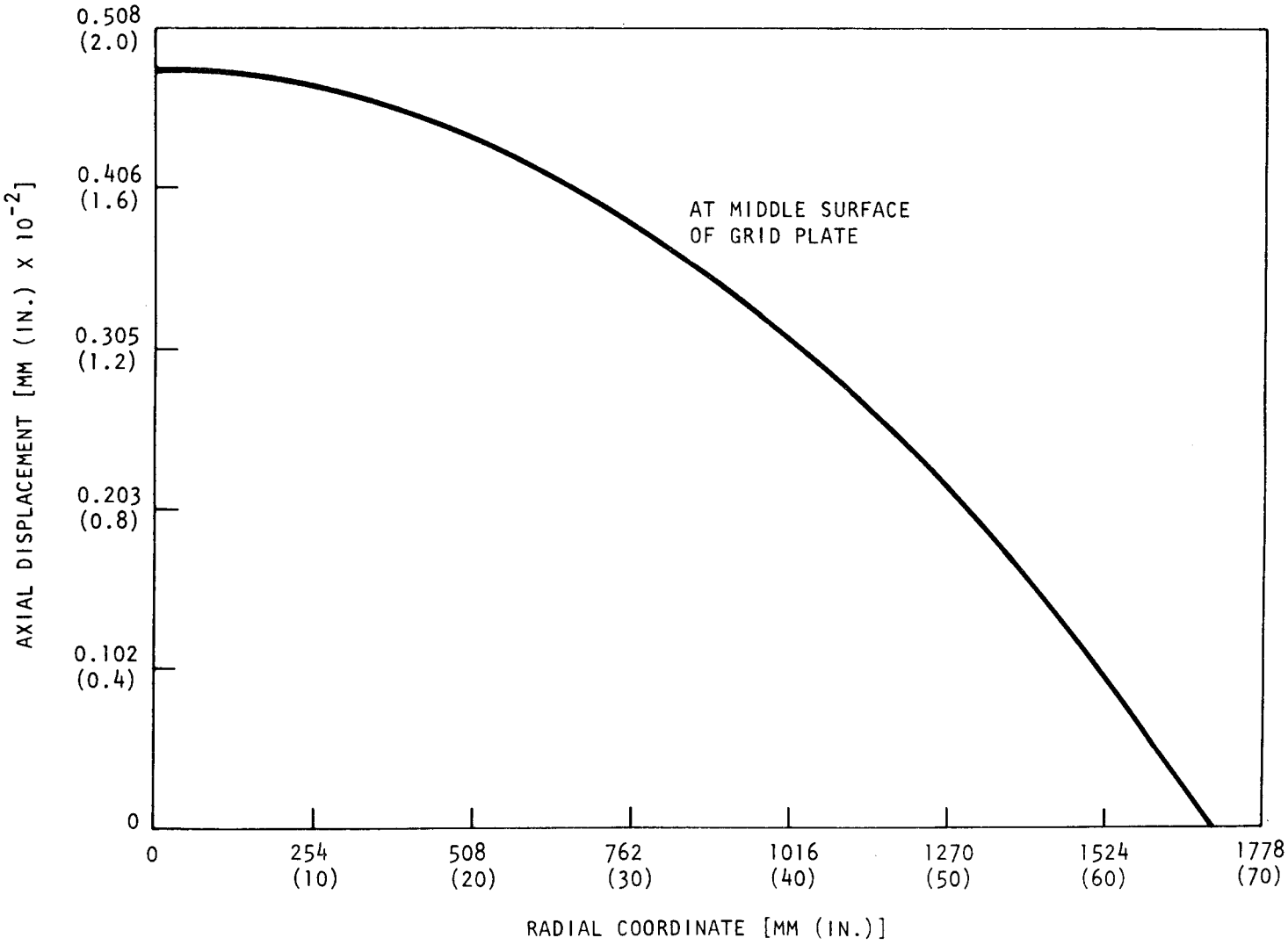

Fig. 7. Thin plate solution, axial displacement vs radial coordinate of grid plate

[Pa (lb/in.^{2})], the solution of deflection using linear elastic thin plate theory can be obtained as follows (Ref. 13):

$$W(r) = \frac{(R^2 - r^2)}{64D}\left(\frac{5 + \nu}{1 + \nu} R^2 - r^2\right) \quad . \tag{19}$$

For deflection due to the shear effect, the shear force Q per unit length of the circumference of a circle with a radius r is

$$Q = 1/2\ pr \quad . \tag{20}$$

The transverse shear τ_{rz} for plates whose thickness is not assumed to be small varies across the thickness of the plate according to the parabolic law in the same way as it varies in beams of narrow rectangular cross section (Ref. 13). Hence, the maximum shear stress is at the middle surface of the plate, and its magnitude is

$$(\tau_{rz})_{max} = \frac{3}{2}\frac{pr}{2h} \quad . \tag{21}$$

The corresponding shear strain is

$$\frac{dw_1}{dr} = \frac{3}{2}\frac{pr}{2Gh} \quad , \tag{22}$$

where w_1 is the additional deflection of the middle surface of the plate due to shear stress. By integration, the deflections produced by shear stresses are found to be

$$w_1 = \frac{3}{2}\frac{p}{4Gh}(R^2 - r^2) \quad . \tag{23}$$

At the center of the plate, the deflections are

$$(w_1)_{max} = \frac{3}{2}\frac{pR^2}{4Gh} \quad . \tag{24}$$

For deflection due to the effect of normal stress for a plate subject to a uniformly distributed load, axial stress σ_z varies from compressive stress p at the upper surface to zero at the lower surface. This compressive stress produces a radial elongation of $\nu p/2E$ at the upper surface and zero at the bottom of the plate, assuming a straight line relationship. The radius elongation at the middle surface of the plate is $\nu p/2E$, and the radius of curvature can be found from the equation

$$\frac{\nu p}{2E} = \frac{h}{2R_c} \quad , \tag{25}$$

where R_c is the radius of curvature.

Since

$$\frac{d^2 w_3}{dr^2} = \frac{1}{R_c} \quad ,$$

the deflection w_3 is obtained by integrating

$$\frac{d^2 w_3}{dr^2} = \frac{\nu p}{hE} \quad ,$$

which yields

$$w_3 = \frac{\nu p}{2hE}\left(r^2 + C_1 r + C_2\right) \quad . \tag{26}$$

The arbitrary constants C_1 and C_2 are then determined by the following boundary conditions:

$$\left.\begin{aligned} w_3 &= 0 \text{ at } r = R \quad , \\ \frac{dw_3}{dr} &= 0 \text{ at } r = 0 \quad . \end{aligned}\right\} \tag{27}$$

Consequently,

$$w_3 = -\frac{\nu p}{2hE}(R^2 - r^2) = -\frac{p\nu h^2}{24D(1 - \nu^2)}(R^2 - r^2) \quad . \tag{28}$$

If Eqs. 19 and 23 are added to Eq. 28, a more exact expression for deflection can be found:

$$w = \frac{p(R^2 - r^2)}{64D}\left(\frac{5 + \nu}{1 + \nu}R^2 - r^2\right) + \frac{ph^2}{8D}\frac{3 + \nu}{6(1 - \nu^2)}(R^2 - r^2) \quad . \tag{29}$$

At the center of the plate this becomes

$$w_{max} = \frac{pR^4}{64D}\left(\frac{5 + \nu}{1 + \nu} + \frac{4}{3}\frac{3 + \nu}{1 - \nu^2}\frac{h^2}{R^2}\right) \quad . \tag{30}$$

The second term in Eq. 30, $\frac{pR^4}{64D}\left(\frac{4}{3}\frac{3 + \nu}{1 + \nu^2}\frac{h^2}{R^2}\right)$, represents the correction for shear stresses and lateral pressure. This correction is small when the ratio of the thickness of the plate to the radius is small. The values of this correction given by the exact solution are

$$\frac{pR^4}{64D}\left(\frac{2}{5}\right)\frac{8 + \nu + \nu^2}{1 - \nu^2}\left(\frac{h^2}{R^2}\right) \quad . \tag{31}$$

3.2.3.3. Comparison of Results. Numerical calculations were made for the 300-MW(e) grid plate to demonstrate the contribution of σ_z and τ_{rz} to grid

plate deflection and the associated reactivity change. The grid plate dimensions and effective elastic constants are

$$
\begin{aligned}
R &= 1.7018 \text{ m (67 in.)}, \\
R_c &= 995.68 \text{ mm (39.2 in.)}, \\
h &= 609.6 \text{ mm (24 in.)}, \\
E^* &= 3.537 \times 10^3 \text{ MPa } (5.13 \times 10^5 \text{ psi}), \\
\nu^* &= 0.76.
\end{aligned}
$$

The increase in the deflection at the center due to σ_z and τ_{rz} expressed in percentage of deflection from thin plate theory is

$$
\Delta w_c = \frac{\text{deflection at center due to } \sigma_z \text{ and } \tau_{rz}}{\text{deflection at center from thin plate theory}} \cdot 100\%
$$

$$
= \frac{4(3 + \nu^*)}{3(1 - \nu^{*2})} \frac{h^2}{R^2} \Bigg/ \frac{5 + \nu^*}{1 + \nu^*} \cdot 100\% = 47\% \quad .
$$

Note that the analysis in this report is based on the assumption that the deflection due to σ_z and τ_{rz} can be independently calculated and added to the deflection from thin plate theory. However, in general, these stress components are coupled with other stress components in equations of equilibrium, compatibility conditions, and material constitutive relations. The 47% deflection increase due to σ_z and τ_{rz} is overestimated owing to the approximation derivation. As indicated in Ref. 13, the center deflection given in Eq. 31 for $\nu = 0.3$ is the exact expression. The expression given in Eq. 31 is approximately 20% less than that given in Eq. 30.

3.3. ANISOTROPIC ELASTICITY THEORY

3.3.1. Background

When applying the concept of the equivalent solid plate to grid plate analysis, it should be recognized that, in general, the equivalent solid

material of the plate does not behave isotropically. In fact, for a triangular pattern of perforations, the elastic properties in the plate in-plane directions could be quite different from those in the direction perpendicular to the plane of the plate. As noted by Slot (Ref. 14), the effect of anisotropy on deflections of thick plates could be pronounced. In view of this and the effect of grid plate deflection on the reactivity response of the core, an investigation of the anisotropic effect on grid plate structural behavior was conducted.

3.3.2. Mathematical Formulation

3.3.2.1. Stress-Strain Relations for Transversely Isotropic Material. The grid plate problem was formulated in such a way that the grid plate was simply supported at the edge and uniformly loaded by the distributed forces p, as shown in the diagram accompanying Eq. 9. In addition, the plate was assumed to be made of a transversely isotropic material with the axis of symmetry coincident with the z coordinate axis.

For the axisymmetric problem, the stress-strain relationship can be written as

$$\left.\begin{aligned}
\varepsilon_r &= a_{11}\sigma_r + a_{12}\sigma_\theta + a_{13}\sigma_z \quad , \\
\varepsilon_\theta &= a_{12}\sigma_r + a_{11}\sigma_\theta + \sigma_{13}\sigma_z \quad , \\
\varepsilon_z &= a_{13}(\sigma_r + \sigma_\theta) + a_{33}\sigma_z \quad , \\
\gamma_{\theta z} &= a_{44}\tau_{\theta z} \quad , \\
\gamma_{rz} &= a_{44}\tau_{rz} \quad , \\
\gamma_{r\theta} &= 2(a_{11} - a_{12})\tau_{r\theta} \quad ,
\end{aligned}\right\} \qquad (32)$$

where a_{11}, a_{12}, a_{13}, a_{33}, and a_{44} are independent coefficients of deformation which are related to the technical constants in the following expressions:

$$
\left.
\begin{aligned}
a_{11} &= \frac{1}{E} \quad , \\
a_{12} &= -\frac{\nu}{E} \quad , \\
a_{33} &= \frac{1}{E'} \quad , \\
a_{13} &= -\frac{\nu'}{E'} \quad , \\
a_{44} &= \frac{1}{G'} \\
2(a_{11} - a_{21}) &= \frac{2(1+\nu)}{E} = \frac{1}{G} \quad ,
\end{aligned}
\right\} \tag{33}
$$

where E and E' are the Young's moduli in the plane of and perpendicular to the plane of isotropy, respectively; ν is the Poisson's ratio which characterizes the transverse reduction in the plane of isotropy for tension in the same plane; ν' is the Poisson's ratio which characterizes the transverse reduction in the plane of isotropy for tension in a direction normal to it; and G' and G are the shear moduli for the planes normal and parallel to the plane of isotropy, respectively.

3.3.2.2. Stress Function. In view of the symmetrical loading, it is reasonable to assume that the radial sections remain planar and the body is a body of revolution in the deformed state; i.e.,

$$
\left.
\begin{aligned}
u_r &= u_r(r,z) \quad , \\
u_\theta &= 0 \quad , \\
w &= w(r,z) \quad .
\end{aligned}
\right\} \tag{34}
$$

Hence, it follows that

$$
\gamma_{\theta z} = \frac{\partial u_\theta}{\partial z} + \frac{1}{r}\frac{\partial w}{\partial \theta} = 0 \quad , \tag{35}
$$

$$\left.\begin{aligned} \gamma_{r\theta} &= \frac{1}{r}\frac{\partial u_r}{\partial \theta} + \frac{\partial u_\theta}{\partial r} - \frac{u_\theta}{r} = 0 \quad , \\ \tau_{\theta z} &= 0 \quad , \\ \tau_{r\theta} &= 0 \quad . \end{aligned}\right\} \tag{35}$$

The remaining strain and stress components will not depend on θ; moreover,

$$\left.\begin{aligned} \varepsilon_r &= \frac{\partial u_r}{\partial r} \quad , \\ \varepsilon_\theta &= \frac{u_r}{r} \quad , \\ \varepsilon_z &= \frac{\partial w}{\partial z} \quad , \\ \gamma_{rz} &= \frac{\partial u_r}{\partial z} + \frac{\partial w}{\partial r} \quad . \end{aligned}\right\} \tag{36}$$

The four non-zero stress components satisfy the equations of equilibrium (with absence of body forces):

$$\left.\begin{aligned} \frac{\partial \sigma_r}{\partial r} + \frac{\partial \tau_{rz}}{\partial z} + \frac{\sigma_r - \sigma_\theta}{r} &= 0 \quad , \\ \frac{\partial \tau_{rz}}{\partial r} + \frac{\partial \sigma_z}{\partial z} + \frac{\tau_{rz}}{r} &= 0 \quad . \end{aligned}\right\} \tag{37}$$

Eliminating u_r and w from Eq. 36 yields

$$\left.\begin{aligned} \varepsilon_r - \frac{\partial}{\partial r}(r\varepsilon_\theta) &= 0 \quad , \\ \frac{\partial^2 \varepsilon_r}{\partial z^2} + \frac{\partial^2 \varepsilon_z}{\partial r^2} - \frac{\partial^2 \gamma_{rz}}{\partial r \partial z} &= 0 \quad . \end{aligned}\right\} \tag{38}$$

Or, in terms of stress using Eq. 32,

$$\left.\begin{aligned} & a_{11}\sigma_r + a_{12}\sigma_\theta + a_{13}\sigma_z - \frac{\partial}{\partial r}\left[r(a_{12}\sigma_r + a_{11}\sigma_\theta + a_{13}\sigma_z)\right] = 0 \\ & \frac{\partial^2}{\partial z^2}(a_{11}\sigma_r + a_{12}\sigma_\theta + a_{13}\sigma_z) - \frac{\partial^2}{\partial r^2}(a_{13}\sigma_r + a_{13}\sigma_\theta + a_{33}\sigma_z) \\ & \qquad - \frac{\partial^2}{\partial r \partial z} a_{44}\tau_{rz} = 0 \quad . \end{aligned}\right\} \tag{39}$$

Using the method of Lekhnitskii (Ref. 15), the problem can be solved by introducing a stress function ϕ defined by

$$\left.\begin{aligned} \sigma_r &= -\frac{\partial}{\partial z}\left(\frac{\partial^2\phi}{\partial r^2} + \frac{b}{r}\frac{\partial\phi}{\partial r} + a\frac{\partial^2\phi}{\partial z^2}\right) \quad , \\ \sigma_\theta &= -\frac{\partial}{\partial z}\left(b\frac{\partial^2\phi}{\partial r^2} + \frac{1}{r}\frac{\partial\phi}{\partial r} + a\frac{\partial^2\phi}{\partial z^2}\right) \quad , \\ \sigma_z &= \frac{\partial}{\partial z}\left(c\frac{\partial^2\phi}{\partial r^2} + \frac{c}{r}\frac{\partial\phi}{\partial r} + d\frac{\partial^2\phi}{\partial z^2}\right) \quad , \\ \tau_{rz} &= \frac{\partial}{\partial r}\left(\frac{\partial^2\phi}{\partial r^2} + \frac{1}{r}\frac{\partial\phi}{\partial r} + a\frac{\partial^2\phi}{\partial z^2}\right) \quad , \end{aligned}\right\} \tag{40}$$

where

$$\left.\begin{aligned} a &= \frac{a_{13}(a_{11} - a_{12})}{a_{11}a_{33} - a_{13}^2} \quad , \\ b &= \frac{a_{13}(a_{13} + a_{44}) - a_{12}a_{33}}{a_{11}a_{33} - a_{13}^2} \quad , \\ c &= \frac{a_{13}(a_{11} - a_{12}) + a_{11}a_{44}}{a_{11}a_{33} - a_{13}^2} \quad , \end{aligned}\right\} \tag{41}$$

$$d = \frac{a_{11}^2 - a_{12}^2}{a_{11}a_{33} - a_{13}^2} \quad . \tag{41}$$

Equation 40 satisfies the first equation of Eq. 37 and all the equations of Eq. 39, and the stress function is governed by the second equation of Eq. 37 in the following form:

$$\begin{aligned}
\frac{\partial \tau_{rz}}{\partial r} + \frac{\partial \sigma_z}{\partial z} + \frac{\tau_{rz}}{r} &= \frac{\partial^2}{\partial r^2}\left(\frac{\partial^2 \phi}{\partial r^2} + \frac{1}{r}\frac{\partial \phi}{\partial r} + a\frac{\partial^2 \phi}{\partial r}\right) \\
&+ \frac{\partial^2}{\partial z^2}\left(c\frac{\partial^2 \phi}{\partial r^2} + \frac{c}{r}\frac{\partial \phi}{\partial r} + d\frac{\partial^2 \phi}{\partial z^2}\right) + \frac{1}{r}\frac{\partial}{\partial r}\left(\frac{\partial^2 \phi}{\partial r^2} + \frac{1}{r}\frac{\partial \phi}{\partial r} + a\frac{\partial^2 \phi}{\partial r}\right) \\
&= \left(\frac{\partial^2}{\partial r^2} + \frac{1}{r}\frac{\partial}{\partial r}\right)\left(\frac{\partial^2 \phi}{\partial r^2} + \frac{1}{r}\frac{\partial \phi}{\partial r} + a\frac{\partial^2 \phi}{\partial z}\right) \\
&+ c\frac{\partial^2}{\partial z^2}\left(\frac{\partial^2 \phi}{\partial r^2} + \frac{1}{r}\frac{\partial \phi}{\partial r} + \frac{d}{c}\frac{\partial^2 \phi}{\partial z^2}\right) \\
&= 0 \quad ,
\end{aligned} \tag{42}$$

or

$$\begin{aligned}
&\left(\frac{\partial^2}{\partial r^2} + \frac{1}{r}\frac{\partial}{\partial r}\right)\left(\frac{\partial^2 \phi}{\partial r^2} + \frac{1}{r}\frac{\partial \phi}{\partial r} + a\frac{\partial^2 \phi}{\partial z^2}\right) + \frac{\partial^2}{\partial z^2}\left(c\frac{\partial^2 \phi}{\partial z^2} + \frac{c}{r}\frac{\partial \phi}{\partial r} + d\frac{\partial^2 \phi}{\partial z^2}\right) \\
&\qquad = 0 \quad .
\end{aligned} \tag{43}$$

In the case of an isotropic body,

$$a = b = -\frac{\nu}{1 - \nu} \quad ,$$

$$c = \frac{2 - \nu}{1 - \nu} \quad ,$$

$$d = 1 \quad .$$

Introducing the new function

$$\chi = \frac{\phi}{1 - \nu}$$

yields the following known formulas from Eq. 40:

$$\left.\begin{aligned}
\sigma_r &= \frac{\partial}{\partial z}\left(\nu\nabla^2\chi - \frac{\partial^2\chi}{\partial r^2}\right) \quad , \\
\sigma_o &= \frac{\partial}{\partial z}\left(\nu\nabla^2\chi - \frac{1}{r}\frac{\partial\chi}{\partial r}\right) \quad , \\
\sigma_z &= \frac{\partial}{\partial z}\left[(2 - \nu)\nabla^2\chi - \frac{\partial^2\chi}{\partial z^2}\right] \quad , \\
\tau_{rz} &= \frac{\partial}{\partial r}\left[(1 - \nu)\nabla^2\chi - \frac{\partial^2\chi}{\partial z^2}\right] \quad ,
\end{aligned}\right\} \tag{44}$$

where χ is a biharmonic function; i.e.,

$$\left.\begin{aligned}
\nabla^2\nabla^2\chi &= 0 \quad , \\
\nabla^2 &\equiv \frac{\partial^2}{\partial r^2} + \frac{1}{r}\frac{\partial}{\partial r} + \frac{\partial^2}{\partial z^2} \quad .
\end{aligned}\right\} \tag{45}$$

The solution of this problem is obtained with the aid of a stress function in the form of homogeneous polynomials of the third, fourth, and sixth degrees:

$$\begin{aligned}
\phi = {} & A_{30}z^3 \\
& + A_{32}zr^2 \\
& + A_{40}\left(z^4 - \frac{3}{8}\,dr^4\right)
\end{aligned} \tag{46}$$

$$+ A_{42}\left(z^2r^2 - \frac{a+c}{8}r^4\right)$$

$$+ A_{60}\left[z^6 - \frac{45}{8}dz^2r^4 + \frac{5}{16}(a+c)dr^6\right]$$

$$+ A_{62}\left[z^4r^2 - \frac{3}{4}(a+c)z^2r^4 + \frac{(a+c)^2 - d}{24}r^6\right] \quad , \tag{46}$$

where A_{30}, A_{32}, A_{40}, A_{42}, A_{60}, and A_{62} are arbitrary constants to be determined by boundary conditions.

Substituting Eq. 46 into Eq. 40 allows the stress expressions to be found:

$$\left.\begin{aligned}
\sigma_r &= -\frac{\partial}{\partial z}\left(\frac{\partial^2\phi}{\partial r^2} + \frac{b\partial\phi}{r\partial r} + a\frac{\partial^2\phi}{\partial z^2}\right) \\
&= Az + B - 8[15A_{60}a + A_{62}(1+b)]z^3 \\
&\quad + 3\{15A_{60}(3+b)d + 2A_{62}[(a+c)(3+b) - 4a]\}zr^2 \quad , \\
\sigma_\theta &= \frac{\partial}{\partial z}\left(b\frac{\partial^2\phi}{\partial r^2} + \frac{1}{r}\frac{\partial\phi}{\partial r} + a\frac{\partial^2\phi}{\partial z^2}\right) \\
&= Az + B - 8[15A_{60}a + A_{62}(1+b)]z^3 \\
&\quad + 3\{15A_{60}(1+3b)d + 2A_{62}[(1+3b) - 4a]\}zr^2 \quad , \\
\sigma_z &= \frac{\partial}{\partial z}\left(c\frac{\partial^2\phi}{\partial r^2} + \frac{c}{r}\frac{\partial\phi}{\partial r} + d\frac{\partial^2\phi}{\partial z^2}\right) \\
&= 2Cz + D + 8(15A_{60}d + 2A_{62}c)z^3 \\
&\quad - 12\{15A_{60}cd + 2A_{62}[c(a+c) - d]\}2r^2 \quad ,
\end{aligned}\right\} \tag{47}$$

$$\left.\begin{aligned}
\tau_{rz} &= \frac{\partial}{\partial r}\left(\frac{\partial^2\phi}{\partial r^2} + \frac{1}{r}\frac{\partial\phi}{\partial r} + a\frac{\partial^2\phi}{\partial z^2}\right) \\
&= -Cr - 12(15A_{60}d + 2A_{62}C)zr^2 \\
&\quad + 3\{15A_{60}cd + 2A_{62}[c(a+c) - d]r^3 \quad ,
\end{aligned}\right\} \tag{47}$$

where $A = -4[6A_{40}a + A_{42}(b+1)]$,

$B = -2[3A_{30}a + A_{32}(b+1)]$,

$C = 4(3A_{40}d + A_{42}c)$,

$D = 2(3A_{30}d + 2A_{32}c)$.

3.3.2.3. Boundary Conditions. For a simply supported plate with uniform pressure load p, the boundary conditions are

$$\left.\begin{aligned}
&\sigma_z = \tau_{rz} = 0 \qquad \text{at} \qquad z = \frac{h}{2} \quad ; \\
&\sigma_z = -p \quad , \quad \tau_{rz} = 0 \qquad \text{at} \qquad z = -\frac{h}{2} \quad ; \\
&\int_{-\frac{h}{2}}^{\frac{h}{2}} \sigma_r dz = 0 \qquad \text{at} \qquad r = R \quad ; \\
&\int_{-\frac{h}{2}}^{\frac{h}{2}} \sigma_r dz = 0 \qquad \text{at} \qquad r = R \quad .
\end{aligned}\right\} \tag{48}$$

The first two equations which specify the conditions on the plate surfaces are exactly satisfied, and the last two equations approximately describe the conditions on the edge. However, according to the St. Venant Principle,

the solution is exact away from the boundary. Applying the first two equations of Eqs. 3-47 and 3-48, the following formulas are obtained:

$$\left.\begin{aligned}
\sigma_z\Big|_{z=\frac{h}{2}} &= 2C\left(\frac{h}{2}\right) + D + 8(15A_{60}d + 2A_{62}c)\left(\frac{h}{2}\right)^3 - 12\{15A_{60}cd \\
&\quad + 2A_{62}[c(a+c) - d]\}\left(\frac{h}{2}\right)r^2 = 0 \quad , \\
\sigma_z\Big|_{z=-\frac{h}{2}} &= 2C\left(-\frac{h}{2}\right) + D + 8(15A_{60}d + 2A_{62}c)\left(-\frac{h}{2}\right)^3 - 12\{15A_{60}cd \\
&\quad + 2A_{62}[c(a+c) - d]\}\left(-\frac{h}{2}\right)r^2 = -p \quad , \\
\tau_{rz} &= -Cr - 12(15A_{60}d + 2A_{62}c)r\left(\frac{h}{2}\right)^2 \\
&\quad + 3\{15A_{60}cd + 2A_{62}[c(a+c) - d]\}r^3 = 0 \quad .
\end{aligned}\right\} \tag{49}$$

From the above expressions, the constants can be determined to be

$$\left.\begin{aligned}
A &= -\frac{3p}{20h}\left[\frac{2(a+c)}{d} + \frac{c(1-b)}{ac-d}\right] + \frac{3pR^2}{4h^3}\left[4 + \frac{d(1-b)}{ac-d}\right] \quad , \\
B &= 0 \quad , \\
C &= \frac{3p}{4h} \quad , \\
D &= -\frac{p}{2} \quad , \\
A_{60} &= -\frac{p[c(a+c) - d]}{60h^3(ac-d)d} \quad , \\
A_{62} &= \frac{cp}{8h^3(ac-d)} \quad .
\end{aligned}\right\} \tag{50}$$

3.3.2.4. Expressions for Stresses. The expressions for stresses can be obtained by combining Eqs. 47 and 50. However, it is convenient to express

the stresses in terms of technical constants, and the final expressions for the stresses in terms of technical constants can be written as

$$\left.\begin{aligned}
\sigma_r &= \frac{3p}{4h^3}(3+\nu)(R^2 - r^2)z + pm\left[\left(\frac{z}{h}\right)^3 - \frac{3}{20}\left(\frac{z}{h}\right)\right] \quad , \\
\sigma_\theta &= \frac{3p}{4h^3}\left[(3+\nu)R^2 - (1+3\nu)r^2\right]z \\
&\quad + pm\left[\left(\frac{z}{h}\right)^3 - \frac{3}{20}\left(\frac{z}{h}\right)\right] \quad , \\
\sigma_z &= \frac{p}{2}\left[-1 + 3\left(\frac{z}{h}\right) - 4\left(\frac{z}{h}\right)^3\right] \quad , \\
\tau_{rz} &= \frac{3pr}{4h}\left[1 - 4\left(\frac{z}{h}\right)^2\right] \quad ,
\end{aligned}\right\} \qquad (51)$$

where

$$m = \frac{E}{1-\nu}\left[\frac{1}{G'} - \frac{\nu'(3+\nu)}{E'}\right] \quad .$$

3.3.2.5. Expressions for Displacement. Using the stress-strain relationship equation (Eq. 32) and the final stress expressions (Eq. 51), strains can be derived in the following form:

$$\left.\begin{aligned}
\varepsilon_r &= \frac{1}{E}\sigma_r - \frac{\nu}{E}\sigma_\theta - \frac{\nu'}{E'}\sigma_z \\
&= \frac{3p}{4Eh^3}\left[(3+\nu)(1-\nu)R^2 - 3(1-\nu^2)r^2\right]z \\
&\quad + \frac{pm}{E}(1-\nu)\left[\left(\frac{z}{h}\right)^3 - \frac{3}{20}\left(\frac{z}{h}\right)\right] \\
&\quad - \frac{\nu' p}{E'2}\left[-1 + 3\left(\frac{z}{h}\right) - 4\left(\frac{z}{h}\right)^3\right] \quad ,
\end{aligned}\right\} \qquad (52)$$

$$
\left.
\begin{aligned}
\varepsilon_\theta &= -\frac{\nu}{E}\sigma_r + \frac{1}{E}\sigma_\theta - \frac{\nu'}{E'}\sigma_z \\
&= \frac{3p}{4Eh^3}\left[(3+\nu)(1-\nu)R^2 - (1-\nu^2)r^2\right]z \\
&\quad + \frac{pm(1-\nu)}{E}\left[\left(\frac{z}{h}\right)^3 - \frac{3}{20}\left(\frac{z}{h}\right)\right] \\
&\quad - \frac{\nu' p}{E'2}\left[-1 + 3\left(\frac{z}{h}\right) - 4\left(\frac{z}{h}\right)^3\right] \quad , \\
\varepsilon_z &= -\frac{\nu'}{E'}\sigma_r - \frac{\nu'}{E'}\sigma_\theta + \frac{1}{E'}\sigma_z \\
&= -\frac{3p}{4E'h^3}\left[2\nu'(3+\nu)R^2 - 4\nu'(1+\nu)r^2\right]z \\
&\quad - \frac{2pm\nu'}{E'}\left[\left(\frac{z}{h}\right)^3 - \frac{3}{20}\left(\frac{z}{R}\right)\right] \\
&\quad + \frac{p}{2E'}\left[-1 + 3\left(\frac{z}{h}\right) - 4\left(\frac{z}{h}\right)^3\right] \quad .
\end{aligned}
\right\} \tag{52}
$$

If Eqs. 36 and 52 are incorporated, the displacements can be derived:

$$
\begin{aligned}
\frac{\partial u_r}{\partial r} &= \frac{3p}{4Eh^3}\left[(3+\nu)(1-\nu)R^2 - 3(1-\nu^2)r^2\right]z \\
&\quad + \frac{pm(1-\nu)}{E}\left[\left(\frac{z}{h}\right)^3 - \frac{3}{20}\left(\frac{z}{h}\right)\right] \\
&\quad - \frac{\nu' p}{E'2}\left[-1 + 3\left(\frac{z}{h}\right) - 4\left(\frac{z}{h}\right)^3\right] \quad .
\end{aligned} \tag{53}
$$

Then

$$
\begin{aligned}
u_r &= \frac{3p}{4Eh^3}\left[(3+\nu)(1-\nu)R^2 r - (1-\nu^2)r^3\right]z \\
&\quad + \frac{pm(1-\nu)}{E}\left[\left(\frac{z}{h}\right)^3 - \frac{3}{20}\left(\frac{z}{h}\right)\right] \\
&\quad - \frac{\nu' p}{E'2}\left[-1 + 3\left(\frac{z}{h}\right) - 4\left(\frac{z}{h}\right)^3\right] r + f(z) \quad ,
\end{aligned} \tag{54}
$$

where f(z) is an arbitrary function of z due to integration.

The circumferential strain ε_θ can be written as

$$\varepsilon_\theta = \frac{u_r}{r} = \frac{3p}{4Eh^3}\left[(3+\nu)(1-\nu)R^2 - (1-\nu^2)r^2\right]z + \frac{pm(1-\nu)}{E}\left[\left(\frac{z}{h}\right)^3 - \frac{3}{20}\left(\frac{z}{h}\right)\right] - \frac{\nu' p}{2E'}\left[-1 + 3\left(\frac{z}{h}\right) - 4\left(\frac{z}{h}\right)^3\right] \quad . \tag{55}$$

Comparing Eqs. 54 and 55, in order to have $f(z) \equiv 0$, the radial displacement u_r should be

$$u_r = \frac{pr}{E}\left\{\frac{E\nu'}{2E'} + \frac{3(1-\nu)}{\Delta h^3}\left[(3+\nu)R^2 - (1+\nu)r^2\right]z - \frac{3z}{20h}\left[m(1-\nu) + 10\frac{E}{E'}\nu'\right] + \frac{z^3}{h^3}\left[m(1-\nu) - 2\frac{E}{E'}\nu'\right]\right\} \quad . \tag{56}$$

The axial displacement w can also be derived in the same fashion:

$$\varepsilon_z = \frac{\partial w}{\partial z} = -\frac{3p}{4E'h^3}\left[2\nu'(3+\nu)R^2 - 4\nu'(1+\nu)r^2\right]z - \frac{2pm\nu'}{E'}\left[\left(\frac{z}{h}\right)^3 - \frac{3}{20}\left(\frac{z}{h}\right)\right] + \frac{p}{2E'}\left[-1 + 3\left(\frac{z}{h}\right) - 4\left(\frac{z}{h}\right)^3\right] \quad . \tag{57}$$

Integrating the equation with respect to z,

$$w = -\frac{3p}{8E'h^3}\left[2\nu'(3+\nu)R^2 - 4\nu'(1+\nu)r^2\right]z^2$$

$$-\frac{2pm\nu'}{E'}\left[\frac{z^4}{4h^3} - \frac{3z^2}{40h}\right] + \frac{p}{2E'}\left[-z + \frac{3z^2}{2h} - \frac{z^4}{h^3}\right] + g(r) \quad , \tag{58}$$

where g(r) is an arbitrary function of r by integration which may be evaluated using the relationship between shear strain and shear stress:

$$\gamma_{rz} = \frac{\partial u_r}{\partial z} + \frac{\partial w}{\partial r} = \frac{1}{G'}\tau_{rz}$$

or

$$\frac{3p}{4Eh^3}\left[(3+\nu)(1-\nu)R^2 - (1-\nu^2)r^2\right]r$$

$$+\frac{pm(1-\nu)}{E}\left[\frac{3z^2}{h^3} - \frac{3}{20h}\right]r$$

$$-\frac{p\nu'}{2E'}\left[\frac{3}{h} - \frac{12z^2}{h^3}\right]r - \frac{3p}{8E'h^3}\left[-8\nu'(1+\nu)r\right]z^2 + \frac{dg}{dr}$$

$$= -\frac{3p}{4G'h}r\left[1 - 4\left(\frac{z}{h}\right)^2\right] \quad . \tag{59}$$

Therefore,

$$\frac{dg}{dr} = -\frac{3p}{4Eh^3}\left[(3+\nu)(1-\nu)R^2 - (1-\nu^2)r^2\right]r$$

$$+\left[-\frac{3p}{5G'h} + \frac{3\nu'(7-\nu)p}{20E'h}\right]r \tag{60}$$

The function g(r) can be obtained by integrating the above expression with respect to r:

$$g(r) = -\frac{3p}{16Eh^3}\left[2(3+\nu)(1-\nu)R^2r^2 - (1-\nu^2)r^4\right] + \frac{3p}{10h}\left[\frac{\nu'(7-\nu)}{4E'} - \frac{1}{G'}\right]r^2 + C \quad , \tag{61}$$

where C is an arbitrary constant by integration.

The axial displacement of the plate can be written as

$$w = -\frac{3p}{4E'h^3}\left[\nu'(3+\nu)R^2 - 2\nu'(1+\nu)r^2\right]z^2 - \frac{2pm\nu'}{E'}\left[\frac{z^4}{4h^3} - \frac{3z^2}{40h}\right] + \frac{p}{2E'}\left[-z + \frac{3z^2}{2h} - \frac{z^4}{h^3}\right] - \frac{3p}{16Eh^3}\left[2(3+\nu)(1-\nu)R^2r^2 - (1-\nu^2)r^4\right] + \frac{3p}{10h}\left[\frac{\nu'(7-\nu)}{4E'} - \frac{1}{G'}\right]r^2 + C \quad . \tag{62}$$

The constant C can be determined by the boundary condition

$$w\Big|_{\substack{r=R\\z=0}} = 0 \quad .$$

However, the exact boundary condition should be

$$w\Big|_{\substack{r=R\\z=h/2}} = 0 \quad .$$

Thus,

$$C = \frac{3p}{16Eh^3}\left[2(3 + \nu)(1 - \nu)R^4 - (1 - \nu^2)R^4\right]$$
$$- \frac{3p}{10h}\left[\frac{\nu'(7 - \nu)}{4E'} - \frac{1}{G'}\right]R^2 \quad . \tag{63}$$

Subsequently,

$$w = \frac{3p(1 - \nu^2)}{16Eh^3}\left[\frac{5 + \nu}{1 + \nu}R^4 - \frac{2(3 + \nu)R^2r^2}{1 + \nu} + r^4\right]$$
$$- \frac{3p}{10h}\left[\frac{\nu'(7 - \nu)}{4E'} - \frac{1}{G'}\right](R^2 - r^2)$$
$$- \frac{3p}{4E'h^3}\left[\nu'(3 + \nu)R^2 - 2\nu'(1 + \nu)r^2\right]z^2$$
$$- \frac{2pm\nu'}{E'}\left[\frac{z^4}{4h^3} - \frac{3z^2}{40h}\right] + \frac{p}{2E'}\left[-z + \frac{3z^2}{2h} - \frac{z^4}{h^3}\right] \quad , \tag{64}$$

or

$$w = \frac{p}{64D}(R^2 - r^2)\left[\frac{5 + \nu}{1 + \nu}R^2 - r^2\right]$$
$$+ \frac{3p}{10h}\left[\frac{1}{G'} - \frac{\nu'(7 - \nu)}{4E'}\right](R^2 - r^2)$$
$$+ \frac{pz}{E'}\left\{-\frac{1}{2} - \frac{3\nu'z}{4E'h^3}\left[(3 + \nu)R^2 - 2(1 + \nu)r^2\right]\right.$$
$$\left. + \frac{3z}{20h}\left[m\nu' + 5\right] - \frac{z^3}{2h^3}\left[m\nu' + 1\right]\right\} \quad , \tag{65}$$

where

$$D = \frac{Eh^3}{12(1 - \nu^2)}$$

is the flexural rigidity of the plate.

3.3.2.6. Isotropic Solution. The derivation of the expressions for stresses and displacements of the anisotropic plate is rather lengthy and complex. Hence, it is desirable to analytically reduce the results to the form for isotropic material which can be compared with the known solution. If the material of the plate is isotropic, then

$$\left.\begin{aligned} E &= E' \quad , \\ \nu &= \nu' \quad , \\ G &= G' = \frac{E}{2(1 + \nu)} \quad , \\ m &= \frac{E}{1 - \nu}\left[\frac{1}{G'} - \frac{\nu'(3 + \nu)}{E'}\right] \\ &= \frac{E}{1 - \nu}\left[\frac{2(1 + \nu)}{E} - \frac{\nu(3 + \nu)}{E}\right] \\ &= \frac{1}{1 - \nu}\left[2 + 2\nu - 3\nu - \nu^2\right] \\ &= \frac{1}{1 - \nu}\left[(2 + \nu)(1 - \nu)\right] \\ &= 2 + \nu \quad . \end{aligned}\right\} \qquad (66)$$

This subsequently reduces the expression for the stresses (Eq. 51) to

$$\sigma_r = \frac{3p}{4h^3}(3 + \nu)(R^2 - r^2)z + p(2 + \nu)\left[\left(\frac{z}{h}\right)^3 - \frac{3}{20}\left(\frac{z}{h}\right)\right] \quad , \qquad (67)$$

$$
\left.
\begin{aligned}
\sigma_\theta &= \frac{3p}{4h^3}\left[(3+\nu)R^2 - (1+3\nu)r^2\right]z \\
&\quad + p(2+\nu)\left[\left(\frac{z}{h}\right)^3 - \frac{3}{20}\left(\frac{z}{h}\right)\right] \quad , \\
\sigma_z &= \frac{p}{2}\left[-1 + 3\left(\frac{z}{h}\right) - 4\left(\frac{z}{h}\right)^3\right] \quad , \\
\tau_{rz} &= -\frac{3pr}{4h}\left[1 - 4\left(\frac{z}{h}\right)^2\right] \quad , \\
\tau_{r\theta} &= \tau_{z\theta} = 0 \quad .
\end{aligned}
\right\} \tag{67}
$$

This set of stress solutions is identical to that derived by Timoshenko (Ref. 16).

In the same manner, the radial and transverse displacements of the plate can be reduced to the isotropic solution and the expressions written as

$$
\left.
\begin{aligned}
u_r &= \frac{pr}{E}\left\{\frac{\nu}{2} + \frac{3(1-\nu)}{4h^3}\left[(3+\nu)R^2 - (1+\nu)r^2\right]z\right. \\
&\quad \left. - \frac{3z}{20h}(2 + 9\nu - \nu^2) + \frac{z^3}{h^3}(2 + \nu - \nu^2)\right\} \quad , \\
w &= \frac{p}{64D}(R^2 - r^2)\left[\frac{5+\nu}{1+\nu}R^2 - r^2\right] \\
&\quad + \frac{3p(8 + \nu + \nu^2)}{40Eh}(R^2 - r^2) \\
&\quad + \frac{pz}{E}\left\{-\frac{1}{2} - \frac{3\nu z}{4Eh^3}\left[(3+\nu)R^2 - 2(1+\nu)r^2\right]\right. \\
&\quad \left. + \frac{3z}{20h}(5 + 2\nu + \nu^2) - \frac{z^3}{2h^3}(1+\nu)^2\right\} \quad , \\
u_\theta &= 0 \quad .
\end{aligned}
\right\} \tag{68}
$$

These displacements agree with Love's results (Ref. 17).

3.3.3. Analysis of the Effect of the Solid Outer Ring on Displacement of the Grid Plate

The free-body diagram of the perforated plate and the solid outer ring is shown below. In this diagram, H is the discontinuity membrane force [N/m (lb/in.)] and M is the discontinuity bending moment [N·m/m (lb·in./in.)].

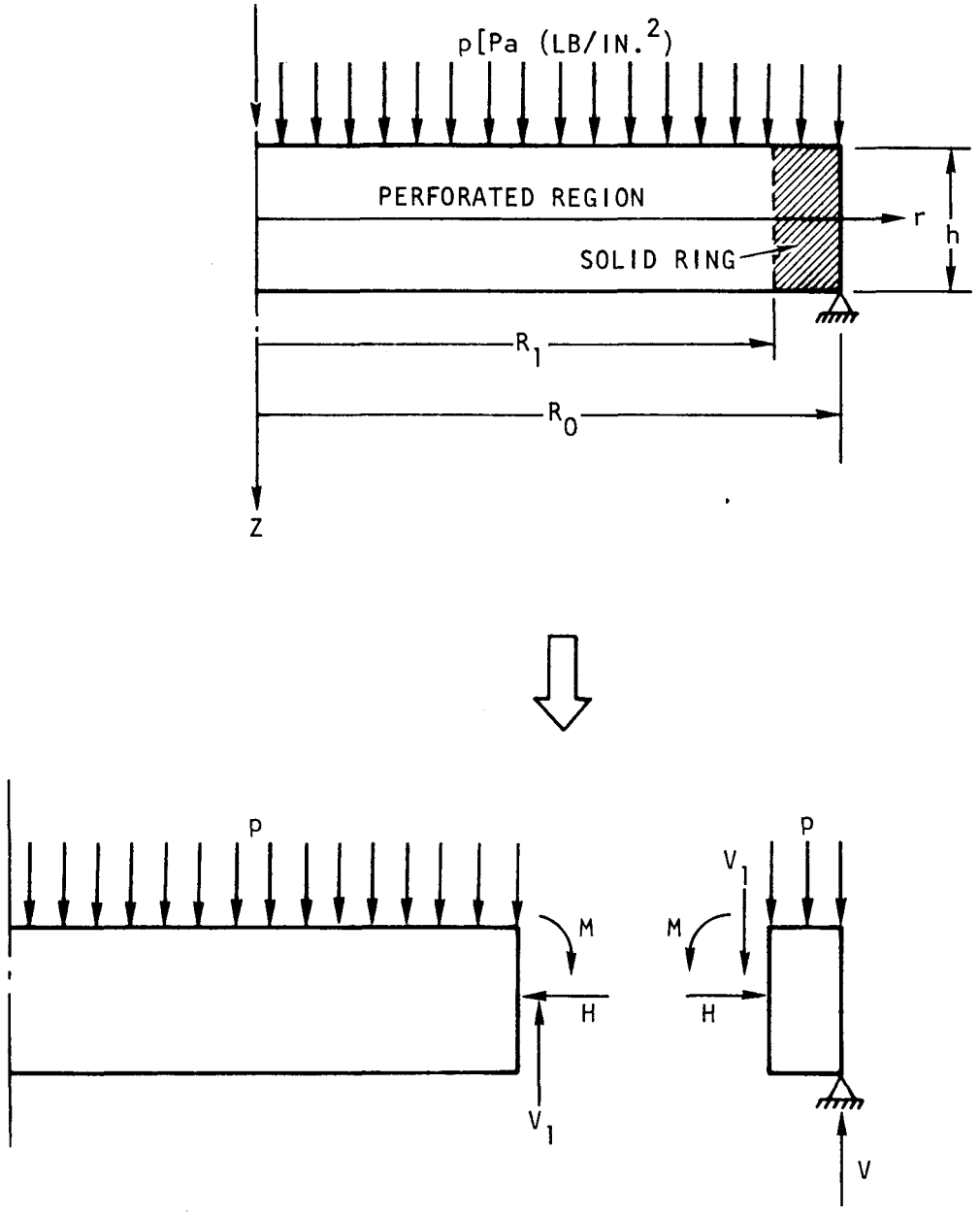

The expressions for the radial and axial displacements of an equivalent solid plate of the perforated portion of the grid plate subjected to pressure load are derived in Section 3.3.1 as follows:

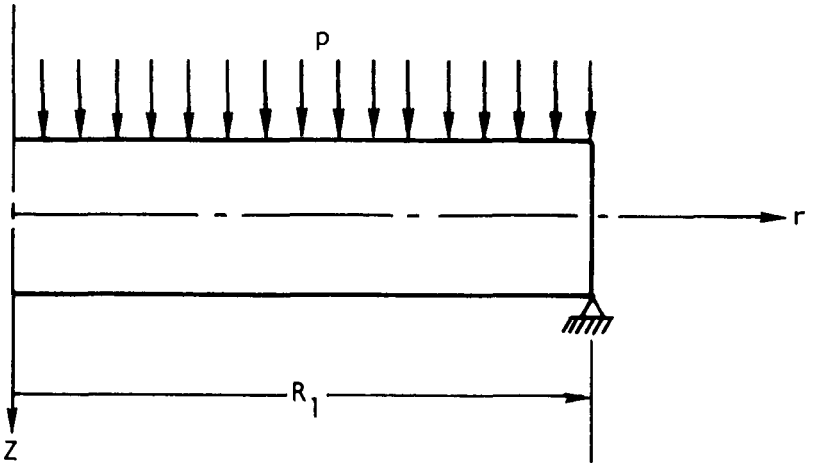

$$
\left.
\begin{aligned}
u_1^p = \frac{pr}{E^*}\Bigg\{ & \frac{E^*\nu'}{2E'} + \frac{3(1-\nu^*)}{4h^3}\left[(3+\nu^*)R_1^2 - (1+\nu^*)r^2\right]z \\
& - \frac{3z}{20h}\left[m(1-\nu^*) + 10\frac{E^*}{E'}\nu'\right] \\
& + \frac{z^3}{h^3}\left[m(1-\nu^*) - 2\frac{E^*}{E'}\nu'\right]\Bigg\} \quad , \\
w_1^p = \frac{p}{64D}\,(R_1^2 - r^2)\left[\frac{5+\nu^*}{1+\nu^*}R_1^2 - r^2\right] & \\
+ \frac{3p}{10h}\left[\frac{1}{G'} - \frac{\nu'(7-\nu^*)}{4E'}\right](R_1^2 - r^2) & \\
+ \frac{pz}{E'}\Bigg\{ & -\frac{1}{2} - \frac{3\nu' z}{4E'h^3}\left[3+\nu^*)R_1^2 - 2(1+\nu^*)r^2\right] \\
& + \frac{3z}{20h}\,(m\nu' + 5) - \frac{z^3}{2h^3}\,(m\nu' + 1)\Bigg\} \quad .
\end{aligned}
\right\} \qquad (69)
$$

Displacement due to the discontinuity bending moment for an equivalent solid circular plate with a thickness h and a radius R and the edge subjected to a moment M is expressed by

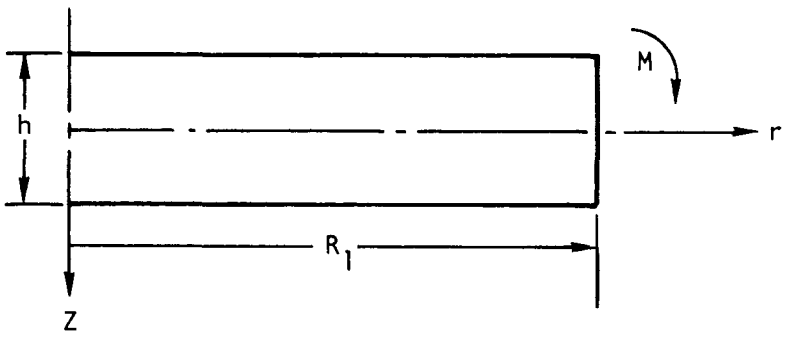

$$u_2^p = \frac{-12(1 - \nu^*)rz}{E^* h^3} M \quad ,$$

$$w_2^p = \frac{-6}{h^3} \left[\frac{(1 - \nu^*)}{E^*} (R_1^2 - r^2) - \frac{2\nu'}{E'} z^2 \right] M \quad . \qquad (70)$$

Displacement due to the discontinuity membrane force for an equivalent solid circular plate with a thickness h and a radius R_1 and the edge subjected to an edge compression force H can be characterized by

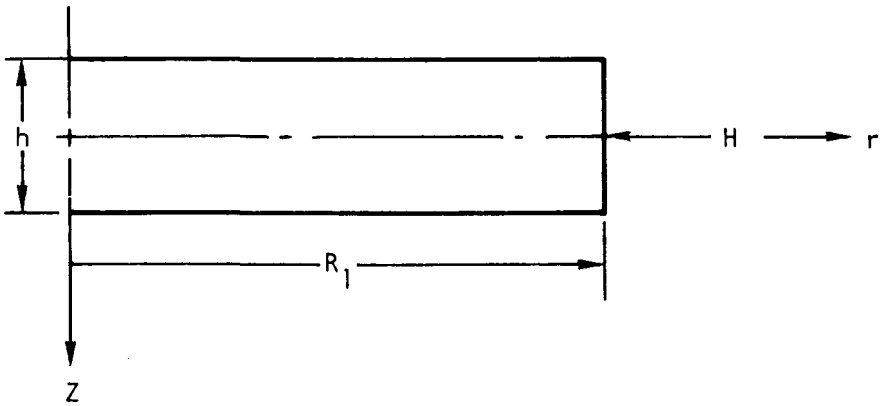

$$u_3^p = \frac{-(1 - \nu^*)r}{E^* h} H \quad ,$$

$$w_3^p = \frac{2\nu'}{E'} \frac{z}{h} H \quad . \tag{71}$$

The total displacement of the equivalent solid plate is the sum of the displacement due to pressure plus the displacement due to the discontinuity moment and the displacement due to the discontinuity membrane force:

$$\left.\begin{aligned}
u^p &= u_1^p + u_2^p + u_3^p \\
&= \frac{pr}{E^*}\left\{\frac{E^*\nu'}{2E'} + \frac{3(1 - \nu^*)}{4h^3}[(3 + \nu^*)R_1^2 - (1 + \nu^*)r^2]z\right. \\
&\quad - \frac{3z}{20h}\left[m(1 - \nu^*) + 10\frac{E^*}{E'}\nu'\right] \\
&\quad \left. + \frac{z^3}{h^3}\left[m(1 - \nu^*) - 2\frac{E^*}{E'}\nu'\right]\right\} \\
&\quad - \frac{12(1 - \nu^*)rz}{E^* h^3} M - \frac{(1 - \nu^*)r}{E^* h} H \quad , \\
w^p &= w_1^p + w_2^p + w_3^p \\
&= \frac{p}{64D}(R_1^2 - r^2)\left[\frac{5 + \nu^*}{1 + \nu^*} R_1^2 - r^2\right] \\
&\quad + \frac{3p}{10h}\left[\frac{1}{G'} - \frac{\nu'(7 - \nu')}{4E'}\right](R^2 - r^2) \\
&\quad + \frac{pz}{E'}\left\{-\frac{1}{2} - \frac{3\nu' z}{4E' h^3}[(3 + \nu^*)R_1^2 - 2(1 + \nu^*)r^2]\right. \\
&\quad \left. + \frac{3z}{20h}(m\nu' + 5) - \frac{z^3}{2h^3}(m\nu' + 1)\right\}
\end{aligned}\right\} \tag{72}$$

$$- \frac{6}{h^3}\left[\frac{(1-\nu^*)}{E^*}(R_1^2 - r^2) - \frac{2\nu'}{E^*} z^2\right] M + \frac{2\nu' z}{E' h} H \quad . \tag{72}$$

The free-body diagram of the cross section of a solid ring is shown below, and the displacement due to each force or moment is derived as follows:

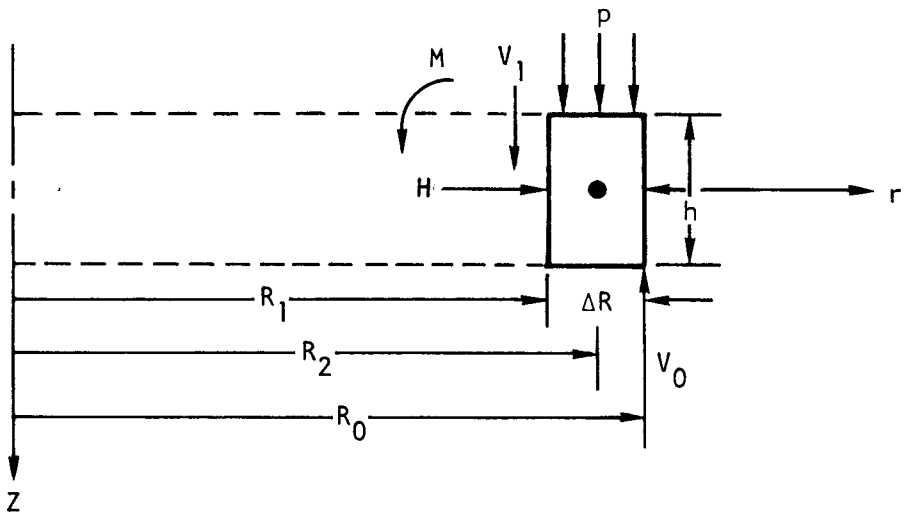

For displacement due to the discontinuity moment,

$$\theta_1^r = \frac{MR_1R_2^2}{R_2EI} = \frac{MR_1R_2}{EI} \quad ; \qquad I = \frac{\Delta R h^3}{12} \quad . \tag{73}$$

For displacement due to vertical forces, the rotation about the centroid is

$$\theta_2^r = \left[\frac{V_1(2\pi R_1)}{2\pi R_2} + \frac{V(2\pi R_0)}{2\pi R_2}\right]\frac{\Delta R}{2} R_2^2 \Big/ EI$$

$$= [V_1R_1 + V_0R_0]R_2\Delta R/2EI \quad , \tag{74}$$

where

$$V_1 = \frac{p(\pi R_1^2)}{2\pi R_1} = \frac{pR_1}{2} \quad ,$$

$$V_0 = \frac{p(\pi R_1^2)}{2\pi R_0} = \frac{pR_0}{2} \quad .$$

Hence,

$$\theta_2^r = \left[\frac{pR_1}{2} R_1 + \frac{pR_0}{2} R_0\right] R_2 \Delta R/2EI$$

$$= \frac{pR_2 \Delta R(R_1^2 + R_0^2)}{4EI} \quad . \tag{75}$$

For displacement due to the discontinuity membrane force H,

$$\left.\begin{aligned} \theta_3^r &= 0 \quad , \\ \sigma_\theta &= \frac{HR_1}{h\Delta R} \quad , \\ \varepsilon_\theta &= \frac{\Delta R}{R_2} = \frac{\sigma_\theta}{E} \quad , \\ u_3^r &= \Delta R = R_2 \frac{\sigma_\theta}{E} = \frac{HR_1R_2}{E\Delta Rh} \quad . \end{aligned}\right\} \tag{76}$$

For total displacement of the solid ring, the total rotation about the centroid is

$$\theta^r = \theta_1^r + \theta_2^r + \theta_3^r$$

$$= \frac{MR_1R_2}{EI} + \frac{pR_2 \Delta R(R_1^2 + R_0^2)}{4EI} \quad . \tag{77}$$

The total radial displacement of the ring due to the discontinuity membrane force H is

$$\left.\begin{aligned} u^r &= u_1^r + u_2^r + u_3^r \quad ; \\ u_1^r &= u_2^r \sim 0 \quad ; \qquad \theta << 1 \quad ; \\ u^r &= u_3^r = \frac{HR_1R_2}{hE\Delta R} \quad . \end{aligned}\right\} \tag{78}$$

The axial deflection of the ring at the junction of the plate and the ring can be written and shown as

$$w^r = 2\,\frac{\Delta R}{2}\,\theta^r = \frac{pR_2\Delta R^2(R_1^2 + R_0^2)}{4EI} \quad . \tag{79}$$

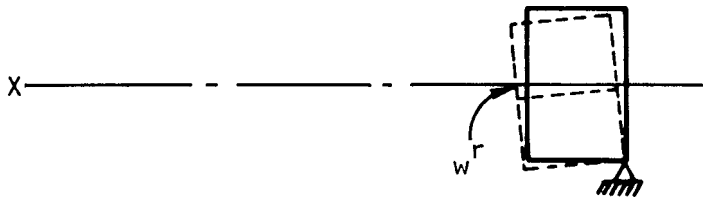

At the junction of the plate and the outer ring, the deflection and rotation of the plate and the ring should be the same; thus,

$$\left.\begin{aligned} u^p\Big|_{\substack{Z=0\\ r=R_1}} &= u^r\Big|_{\substack{Z=0\\ r=R_1}} \quad , \\ -\theta^p\Big|_{\substack{Z=0\\ r=R_1}} &= \theta^r\Big|_{\substack{Z=0\\ r=R_1}} \quad . \end{aligned}\right\} \tag{80}$$

It is known that

$$u^p\Big|_{\substack{Z=0\\R=R_1}} = \frac{pR_1}{E^*}\frac{E^*\nu'}{2E'} - \frac{(1-\nu^*)R_1}{E^*h}H \quad ,$$

$$u^r\Big|_{\substack{Z=0\\R=R_1}} = \frac{HR_1R_2}{E\Delta R} \quad .$$

Applying the compatibility condition,

$$\frac{pR_1\nu'}{2E'} - \frac{(1-\nu^*)R_1}{E^*h}H = \frac{R_1R_2}{E\Delta Rh}H \quad .$$

Therefore, the discontinuity membrane force H can be solved by

$$H = \frac{pR_1\nu'/2E'}{(R_1R_2/E\Delta Rh) + [(1-\nu^*)R_1/E^*h]}$$

$$= \frac{pEE^*\nu'h\Delta R}{2E'[E^*R_2 + (1-\nu^*)E\Delta R]} \quad . \tag{81}$$

The rotation at the edge of the plate can be expressed as

$$\theta^p\Big|_{\substack{Z=0\\r=R_1}} = \frac{\partial w^p}{\partial r}\Bigg|_{\substack{Z=0\\r=R_1}} \quad . \tag{82}$$

Differentiating the expression of the displacement of the plate with respect to r yields

$$\frac{\partial w^p}{\partial r} = \frac{p}{64D}(-2r)\left[\frac{5+\nu^*}{1+\nu^*}R_1^2 - r^2\right] + \frac{p}{64D}(R_1^2 - r^2)(-2r)$$

$$+ \frac{3p}{10h}\left[\frac{1}{G'} - \frac{\nu'(7-\nu^*)}{4E'}\right](-2r) + \frac{pz}{E'}\left\{-\frac{3\nu' z}{4E'h^3}[-4(1+\nu^*)r]\right\}$$

$$- \frac{6M}{h^3}\frac{(1-\nu^*)}{E^*}(-2r) \qquad (83)$$

or

$$\frac{\partial w^p}{\partial r} = -\frac{pr}{16D}\left(\frac{3+\nu^*}{1+\nu^*}R_1^2 - r^2\right) - \frac{3pr}{5h}\left[\frac{1}{G'} - \frac{\nu'(7-\nu')}{4E'}\right]$$

$$+ \frac{pz}{E'}\left[\frac{3\nu'(1+\nu^*)}{E'h^3}\right]r + \frac{12M}{h^3}\frac{(1-\nu^*)}{E^*}r \quad .$$

Substituting the boundary condition $r = R_1$ into the expression $\partial w^p/\partial r$ simplifies θ^p such that

$$\theta^p\Big|_{\substack{Z=0\\ r=R_1}} = \frac{-pR_1^3}{8D(1+\nu^*)} - \frac{3pR_1}{5h}\left[\frac{1}{G'} - \frac{\nu'(7-\nu')}{4E'}\right]$$

$$+ \frac{12MR_1(1-\nu^*)}{E^*h^3} \quad . \qquad (84)$$

Since the rotation of the ring is known, the compatibility condition of the joint of the plate and the ring can be applied:

$$\frac{pR_1^3}{8D(1+\nu^*)} + \frac{3pR_1}{5h}\left[\frac{1}{G'} - \frac{\nu'(7-\nu^*)}{4E'}\right] - \frac{12MR_1(1-\nu^*)}{E^*h^3}$$

$$= \frac{MR_1R_2}{EI} + \frac{pR_2\Delta R(R_1^2 + R_0^2)}{4EI} \quad .$$

Thus, the discontinuity moment between the plate and the ring can be solved:

$$M = \frac{\frac{pR_1^3}{8D(1+\nu^*)} - \frac{pR_2(R_1^2+R_0^2)\Delta R}{4EI} + \frac{3pR_1}{5h}\left[\frac{1}{G'} - \frac{\nu'(7-\nu^*)}{4E'}\right]}{\frac{R_1R_2}{EI} + \frac{12R_1(1-\nu^*)}{E^*h^3}} \quad . \tag{85}$$

The total displacement of the grid plate should be the displacement of the perforated plate plus the displacement of the solid outer ring; i.e., $w = w_1 + w_2$, where w_1 is the axial displacement of the solid ring, and w_2 is the axial displacement of the equivalent solid plate (perforated plate):

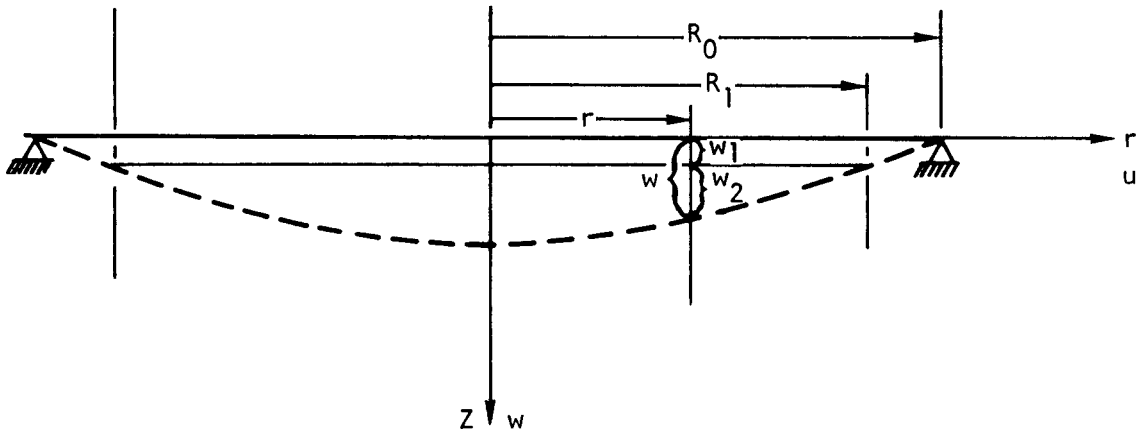

From the previous derivation, it can be shown that

$$\left.\begin{aligned} w_1 &= \Delta R\theta^r = \frac{pR_2(R_1^2+R_0^2)\Delta R^2}{4EI} \quad , \\ w_2 &= w_1^p + w_2^p + w_3^p \quad , \end{aligned}\right\} \tag{86}$$

where w_1^p = axial displacement of the equivalent solid plate due to pressure load,

w_2^p = axial displacement of the equivalent solid plate due to discontinuity bending moment,

w_3^p = axial displacement of the equivalent solid plate due to discontinuity membrane force.

The total axial displacement of the grid plate is

$$
\begin{aligned}
w = {} & \frac{p}{64D}\,(R_1^2 - r^2)\left[\frac{5 + \nu^*}{1 + \nu^*}\,R_1^2 - r^2\right] \\
& + \frac{3p}{10h}\left[\frac{1}{G'} - \frac{\nu'(7 - \nu^*)}{4E'}\right](R_1^2 - r^2) \\
& + \frac{pz}{E'}\left\{-\frac{1}{2} - \frac{3\nu' z}{4E'h^3}\left[(3 + \nu^*)R_1^2 - 2(1 + \nu^*)r^2\right]\right. \\
& \left. + \frac{3z}{20h}\,(m\nu' + 5) - \frac{z^3}{2h^3}\,(m\nu' + 1)\right\} \\
& - \frac{6}{h^3}\left[\frac{(1 - \nu^*)}{E^*}\,(R_1^2 - r^2) - \frac{2\nu'}{E^*}\,z^2\right]M + \frac{2\nu'}{E'}\,\frac{z}{h}\,H \\
& + \frac{pR_2(R_1^2 + R_0^2)\Delta R^2}{4EI} \quad . \qquad (87)
\end{aligned}
$$

The total radial displacement of the grid plate for $0 \le r \le R_1$ can be written as

$$u = u^p = u_1^p + u_2^p + u_3^p \quad ,$$

where u_1^p = radial displacement of the equivalent solid plate due to pressure load,

u_2^p = radial displacement of the equivalent solid plate due to discontinuity bending moment,

u_3^p = radial displacement of the equivalent solid plate due to discontinuity membrane force.

Therefore, the total radial displacement of the grid plate is

$$u = \frac{pr}{E^*}\left\{\frac{E^*\nu'}{2E'} + \frac{3(1-\nu^*)}{4h^3}\left[(3+\nu^*)R_1^2 - (1+\nu^*)r^2\right]z\right.$$

$$- \frac{3z}{20h}\left[m(1-\nu^*) + 10\frac{E^*}{E'}\nu'\right]$$

$$\left. + \frac{z^3}{h^3}\left[m(1-\nu^*) - 2\frac{E^*}{E'}\nu'\right]\right\}$$

$$- \frac{12(1-\nu^*)rz}{E^*h^3}M - \frac{(1-\nu^*)}{E^*h}H \quad ; \qquad 0 \le r \le R_1 \quad . \quad (88)$$

3.3.4. Numerical Results

A computer program GRIPLAT has been developed based on the expressions of stress and displacement derived in Section 3.3. The input to the program includes geometric dimensions of the plate, loadings, in-plane effective elastic constants of the equivalent plate, and elastic constants of the plate in the perpendicular direction. The output of GRIPLAT consists of the stresses and displacements at any radius and thickness specified.

The geometric dimensions, elastic constants, and loadings for a transversely isotropic elastic body analysis of the grid plate are

Outside radius R_o = 1.6986 m (66.875 in.),
Thickness h = 609.6 mm (24.00 in.),
Pressure load p = 289.58 KPa (42.00 psi),
In-plane Young's modulus E = 6.102×10^3 MPa (0.885×10^6 psi),
Axial Young's modulus E' = 39.851×10^3 MPa (0.578×10^7 psi),

Axial shear modulus G' = 7.943×10^3 MPa (0.1152×10^7 psi),

In-plane Poisson's ratio ν = 0.743,

Axial Poisson's ratio ν' = 0.3.

All the elastic constants are the effective elastic constants calculated according to Refs. 10 and 14.

The output of GRIPLAT for the 300-MW(e) plane is specified at the following locations along the radius:

R_1 = 0 mm (0 in.),
R_2 = 187.96 mm (7.4 in.),
R_3 = 375.92 mm (14.8 in.),
R_4 = 563.88 mm (22.2 in.),
R_5 = 751.84 mm (29.6 in.),
R_6 = 939.80 mm (37.0 in.),
R_7 = 1.1278 m (44.4 in.),
R_8 = 1.3157 m (51.8 in.),
R_9 = 1.5037 m (59.2 in.),
R_{10} = 1.6986 m (66.875 in.),

and at the following thicknesses:

Z_1 = 0 mm (0 in.),
Z_2 = 33.782 mm (1.33 in.),
Z_3 = 67.564 mm (2.66 in.),
Z_4 = 101.346 mm (3.99 in.),
Z_5 = 135.128 mm (5.32 in.),
Z_6 = 168.91 mm (6.65 in.),
Z_7 = 202.692 mm (7.98 in.),
Z_8 = 236.474 mm (9.31 in.),
Z_9 = 270.256 mm (10.64 in.),
Z_{10} = 304.80 mm (12.0 in.).

The isotropic elastic body behavior can be obtained from the transversely isotropic model by letting all the elastic constants be the same as those in the in-plane direction; i.e., $E = E' = 6.102 \times 10^3$ MPa (0.885×10^6 psi), $G = G' = 7.943 \times 10^3$ MPa (0.1152×10^7 psi), and $\nu = \nu' = 0.743$. The other parameters remain unchanged.

The computer output of the transversely isotropic solution is plotted in Figs. 8 through 13, and the computer output of the isotropic solution is plotted in Figs. 14 through 19; the results are discussed in Section 6.

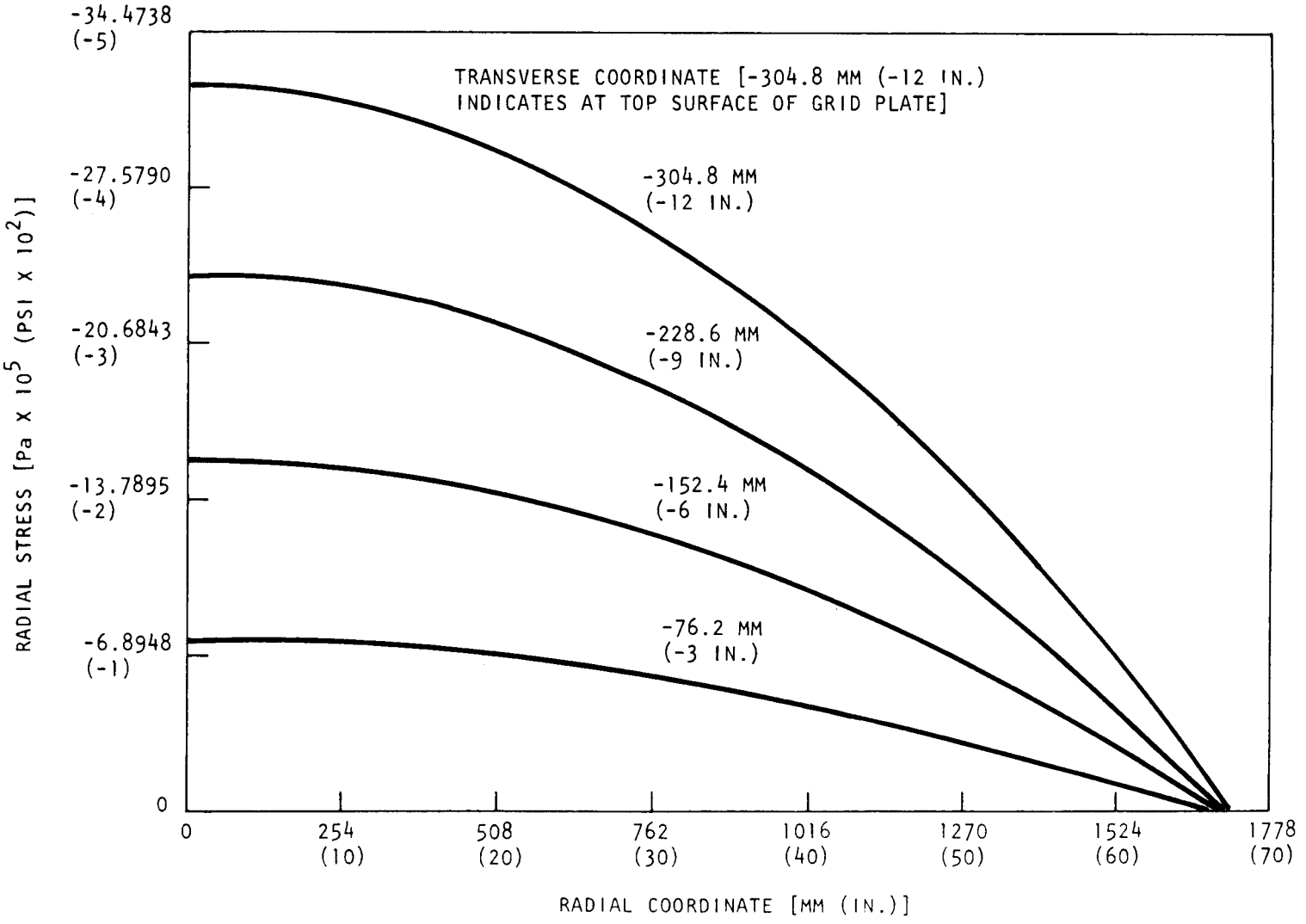

Fig. 8. Transversely isotropic solution, radial stress distribution vs radial coordinate of grid plate

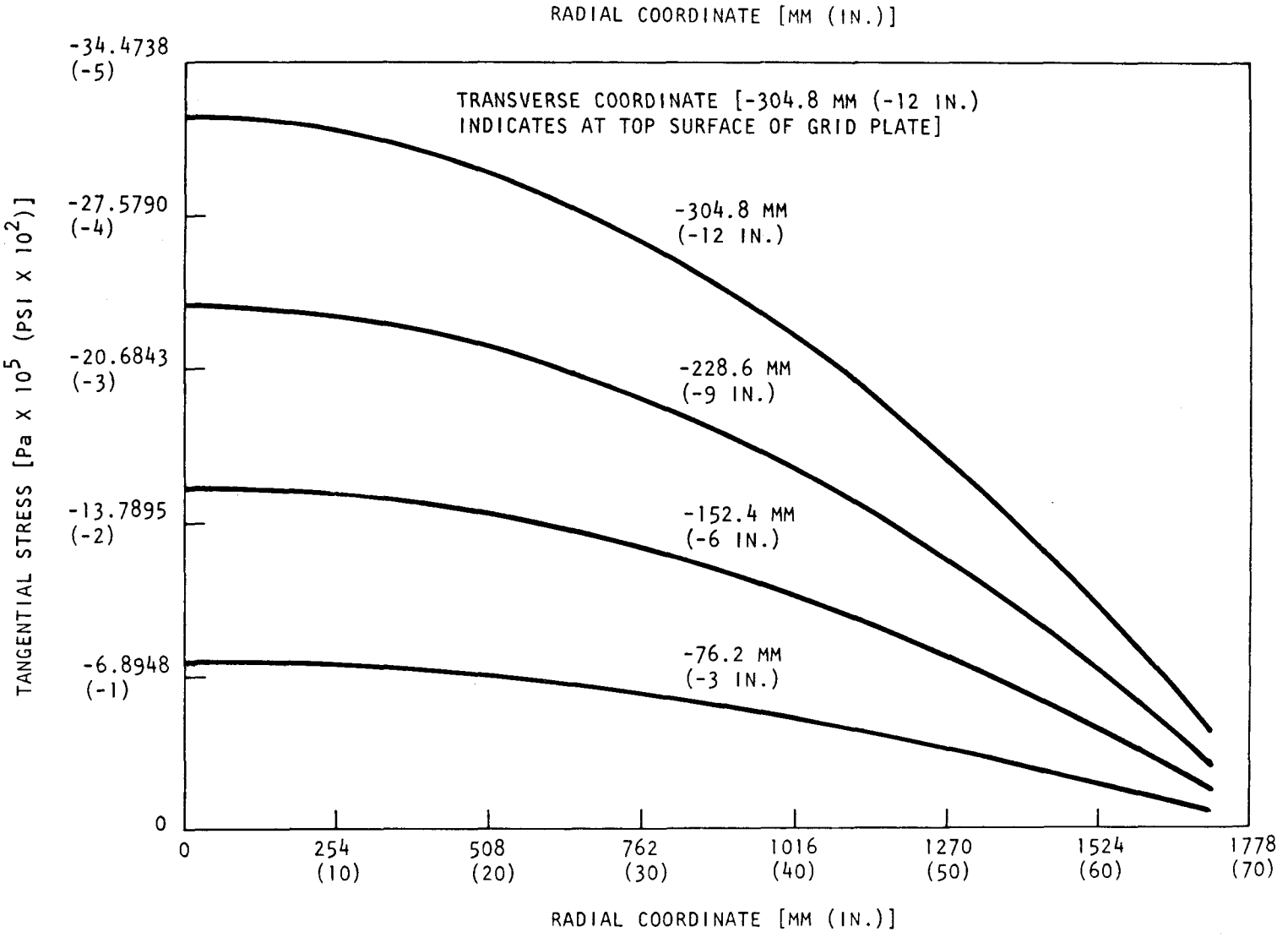

Fig. 9. Transversely isotropic solution, tangential stress distribution vs radial coordinate of grid plate

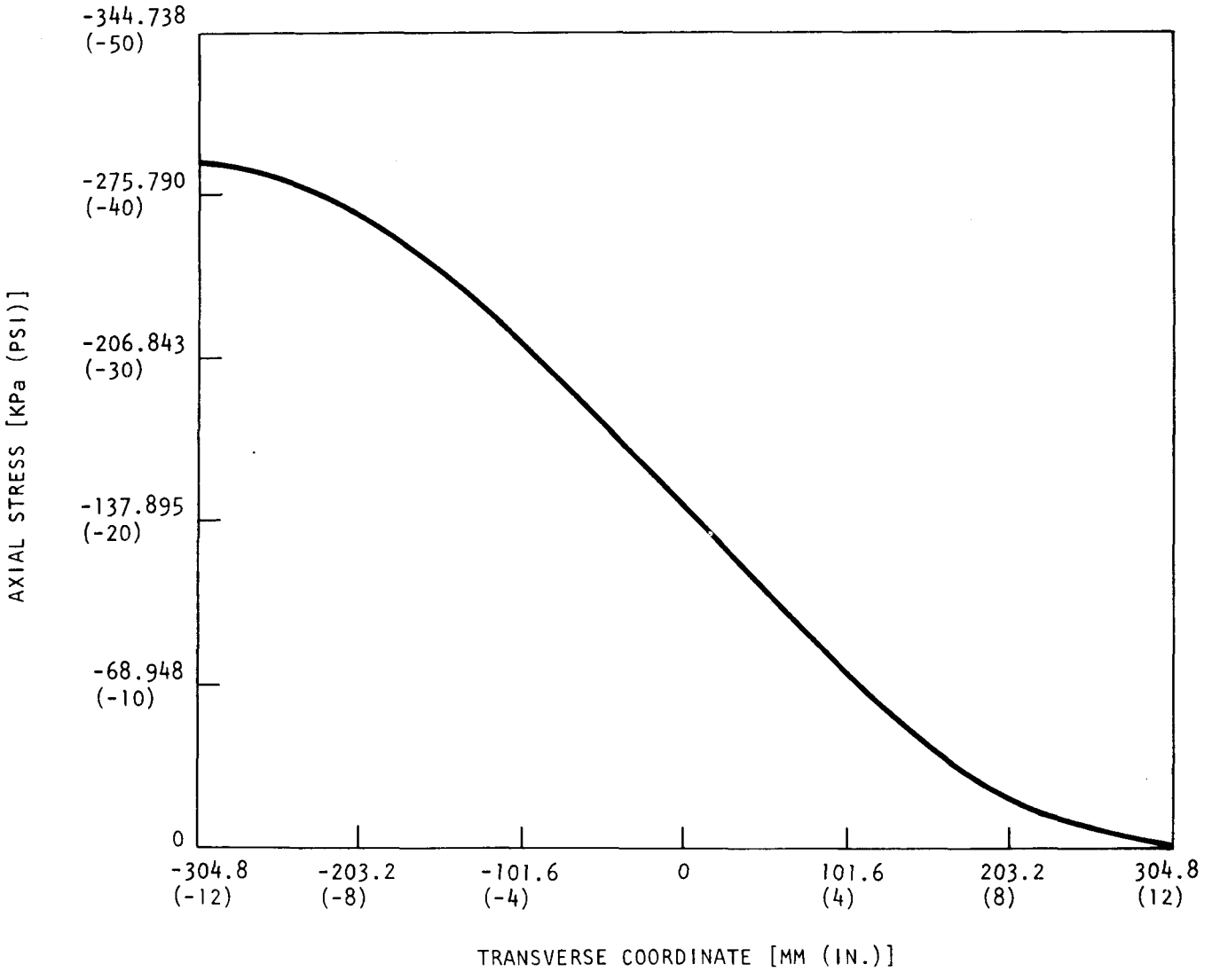

Fig. 10. Transversely isotropic solution, axial stress distribution vs transverse coordinate of grid plate

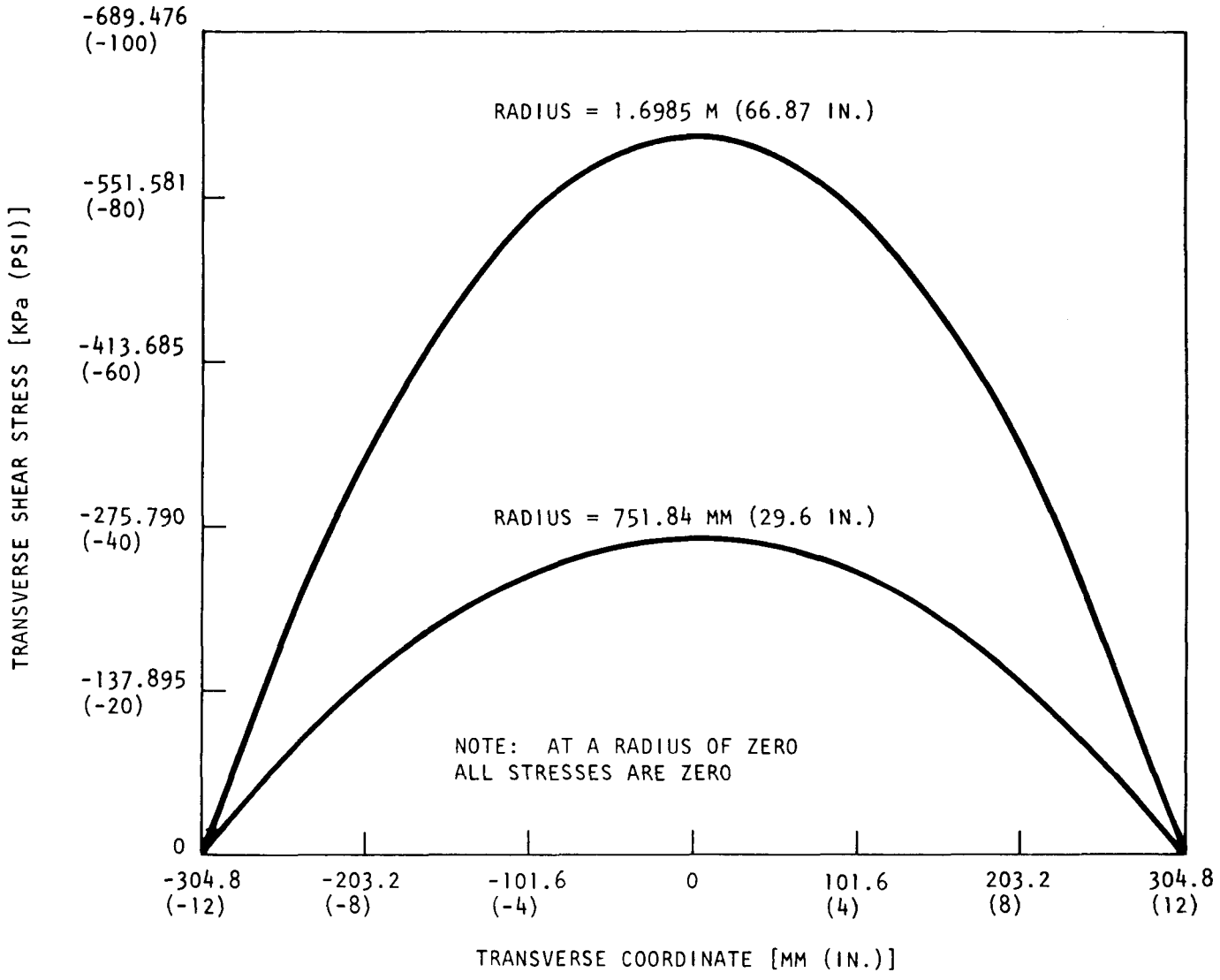

Fig. 11. Transversely isotropic solution, transverse shear stress vs transverse coordinate of grid plate

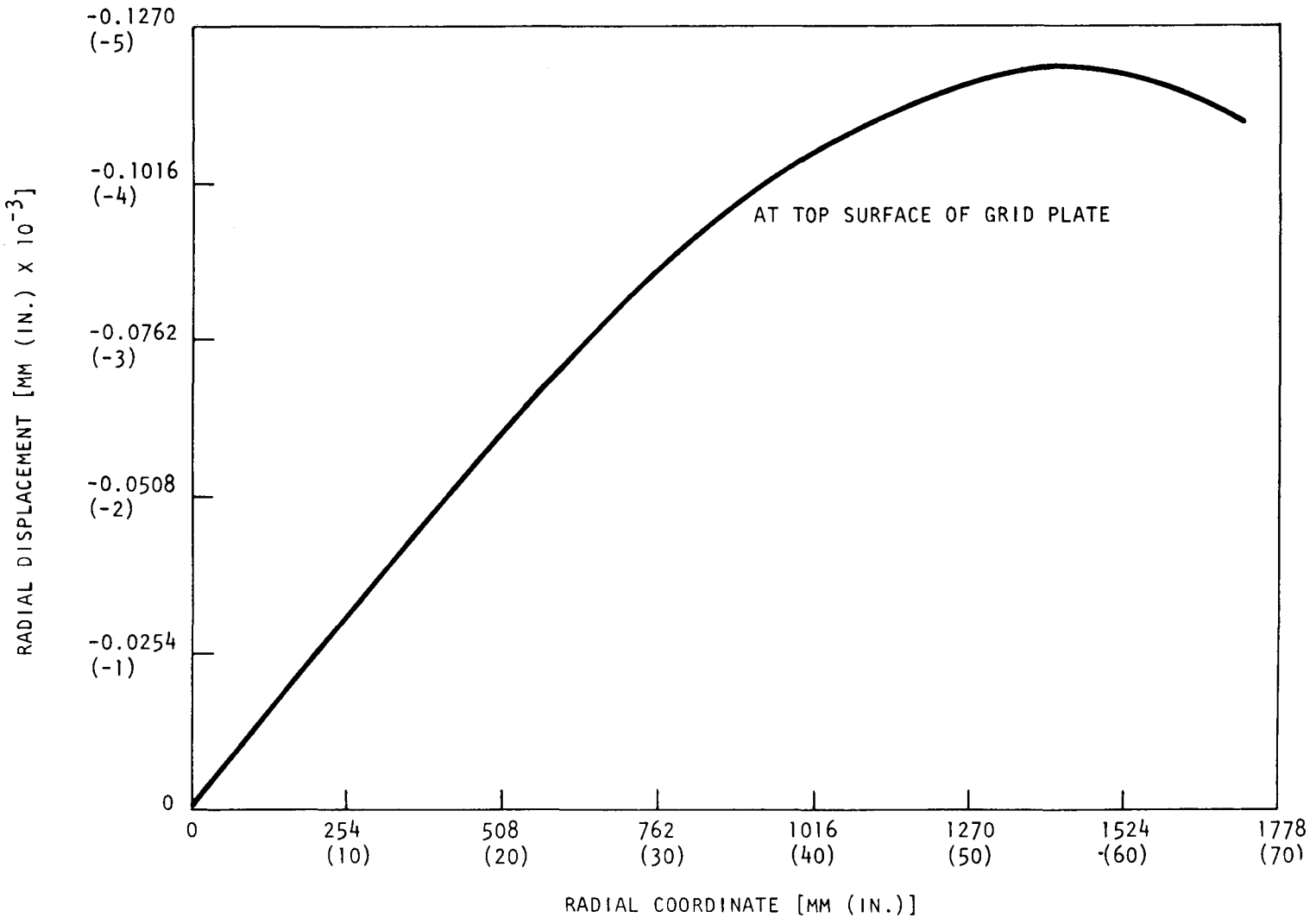

Fig. 12. Transversely isotropic solution, radial displacement vs radial coordinate of grid plate

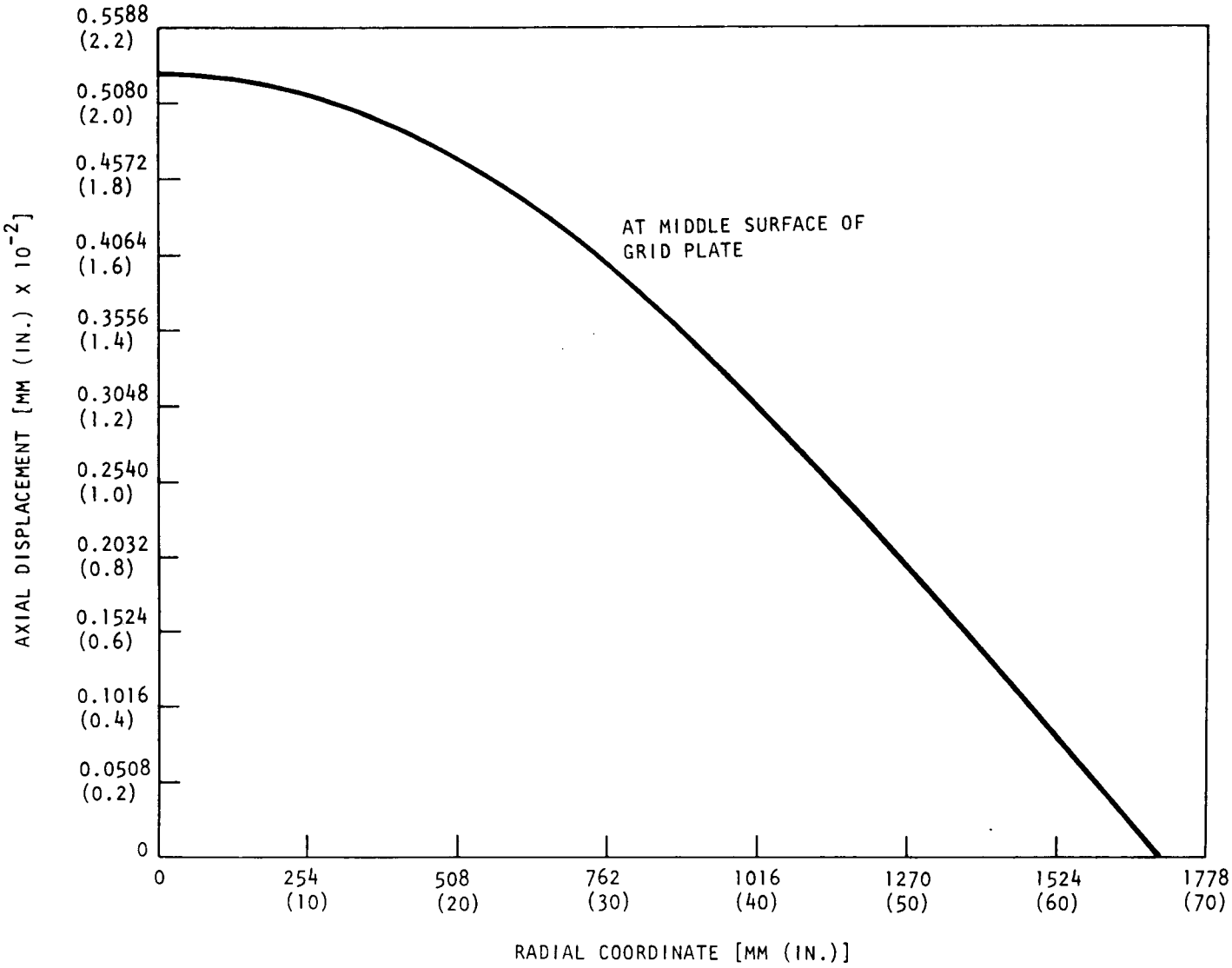

Fig. 13. Transversely isotropic solution, axial displacement vs radial coordinate of grid plate

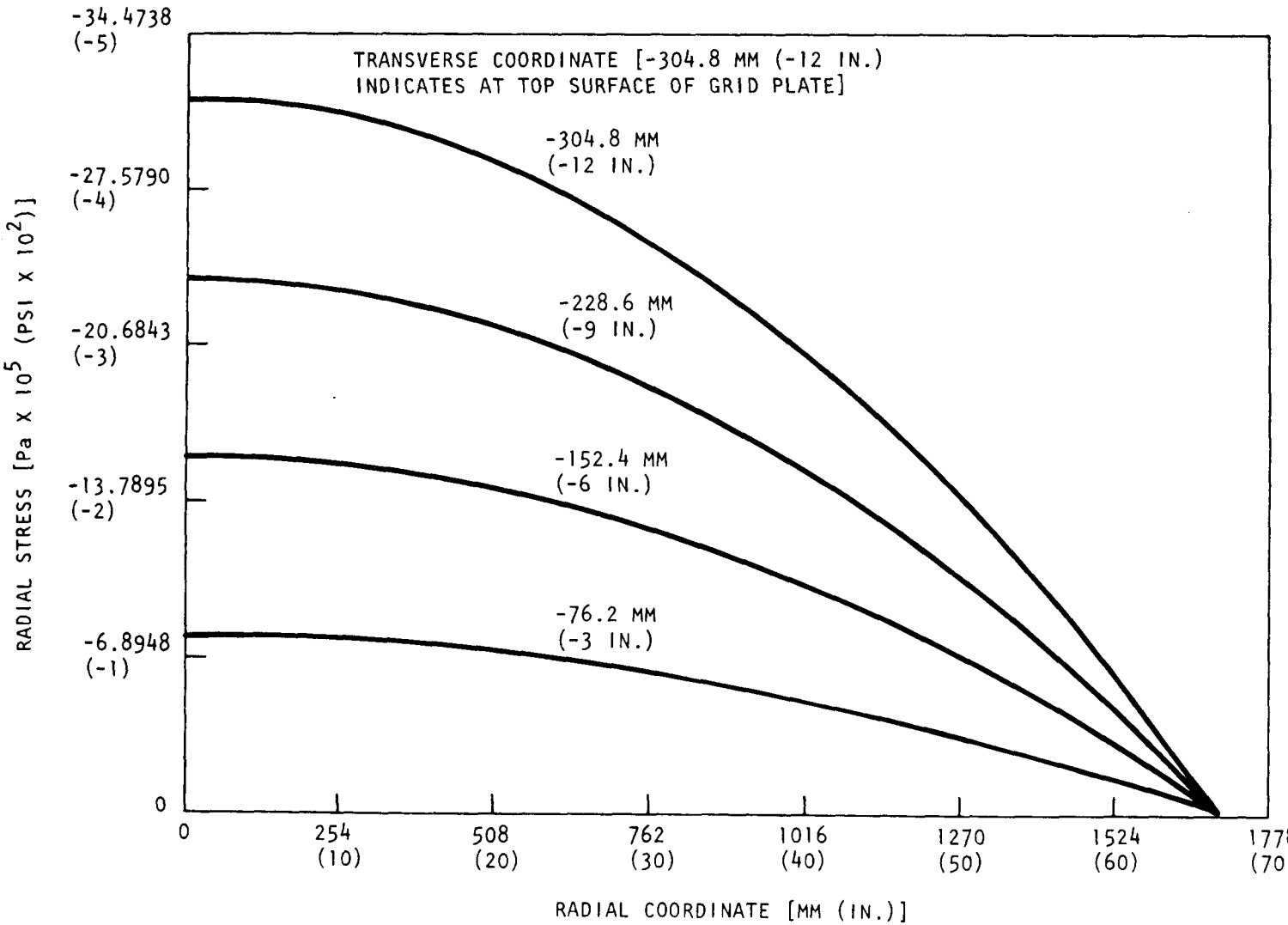

Fig. 14. Isotropic solution, radial stress distribution vs radial coordinate of grid plate

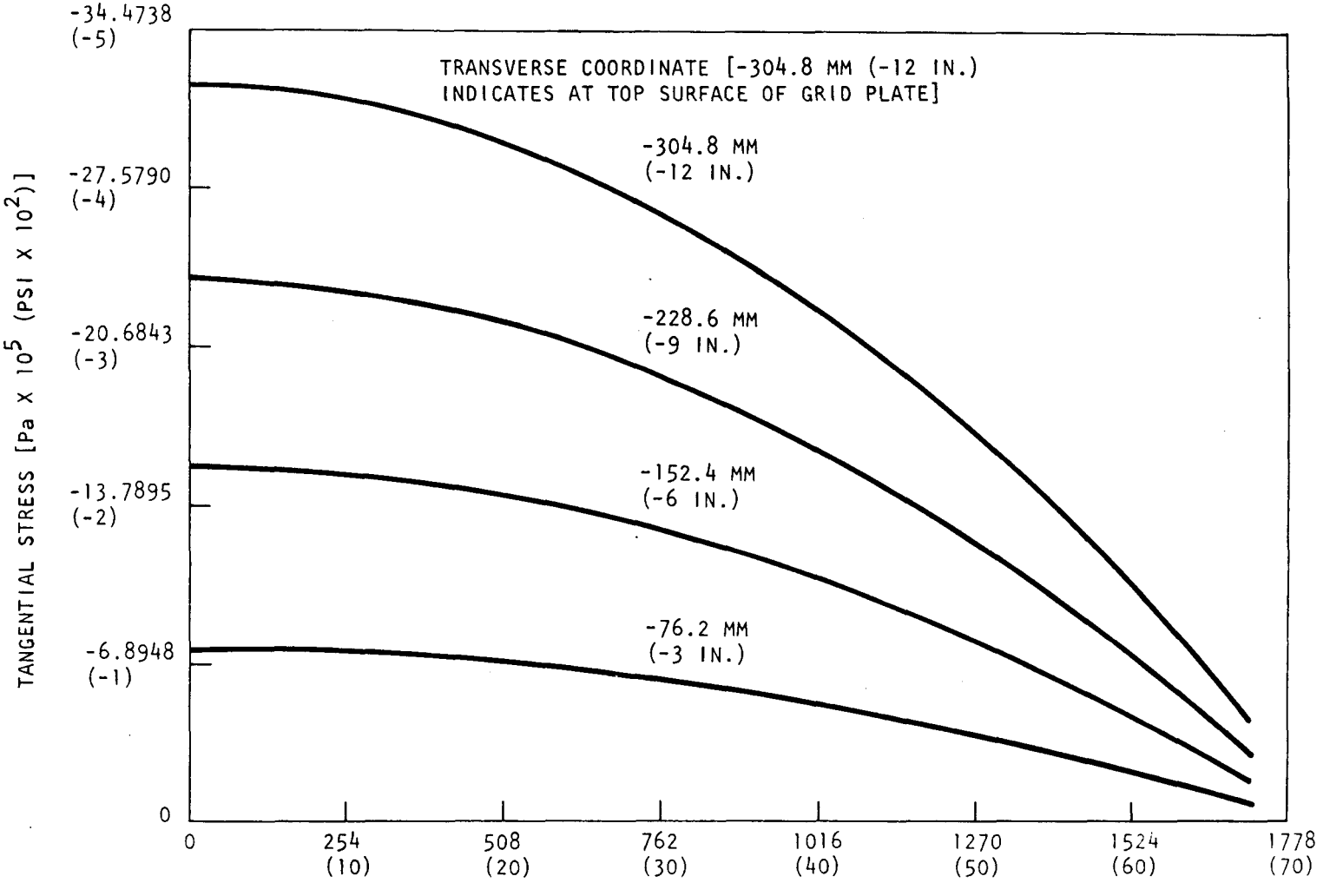

Fig. 15. Isotropic solution, tangential stress distribution vs radial coordinate of grid plate

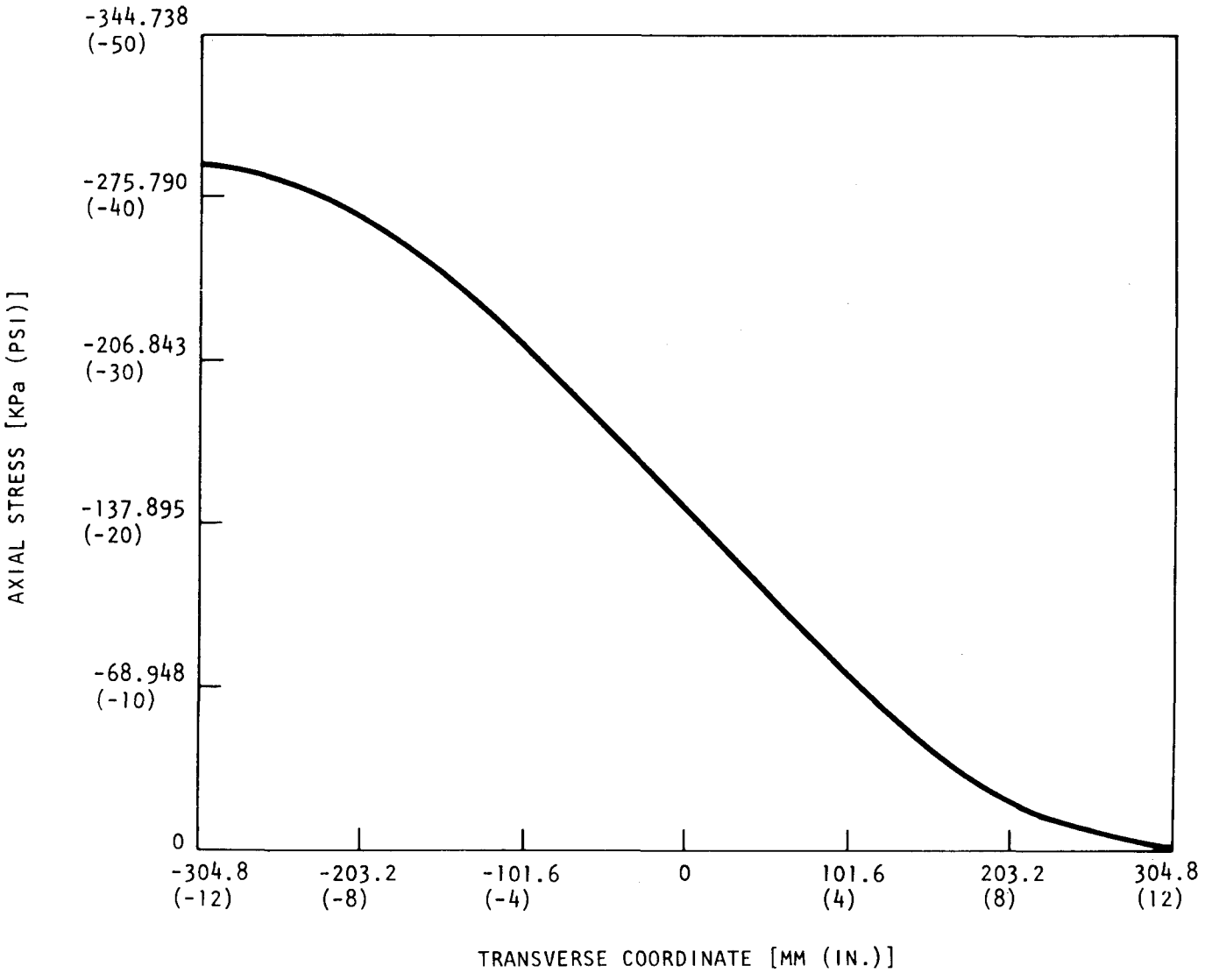

Fig. 16. Isotropic solution, axial stress distribution vs transverse coordinate of grid plate

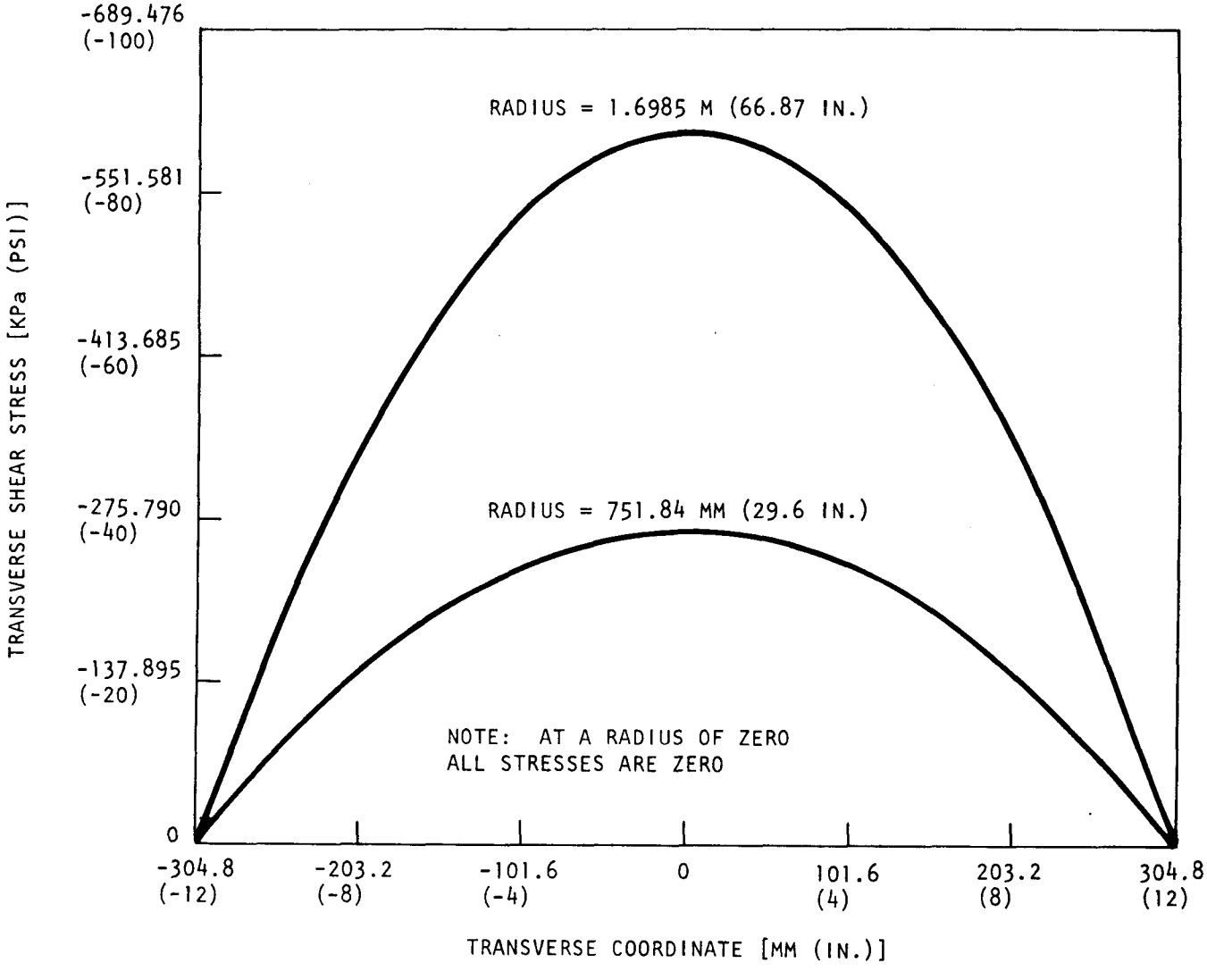

Fig. 17. Isotropic solution, transverse shear stress vs transverse coordinate of grid plate

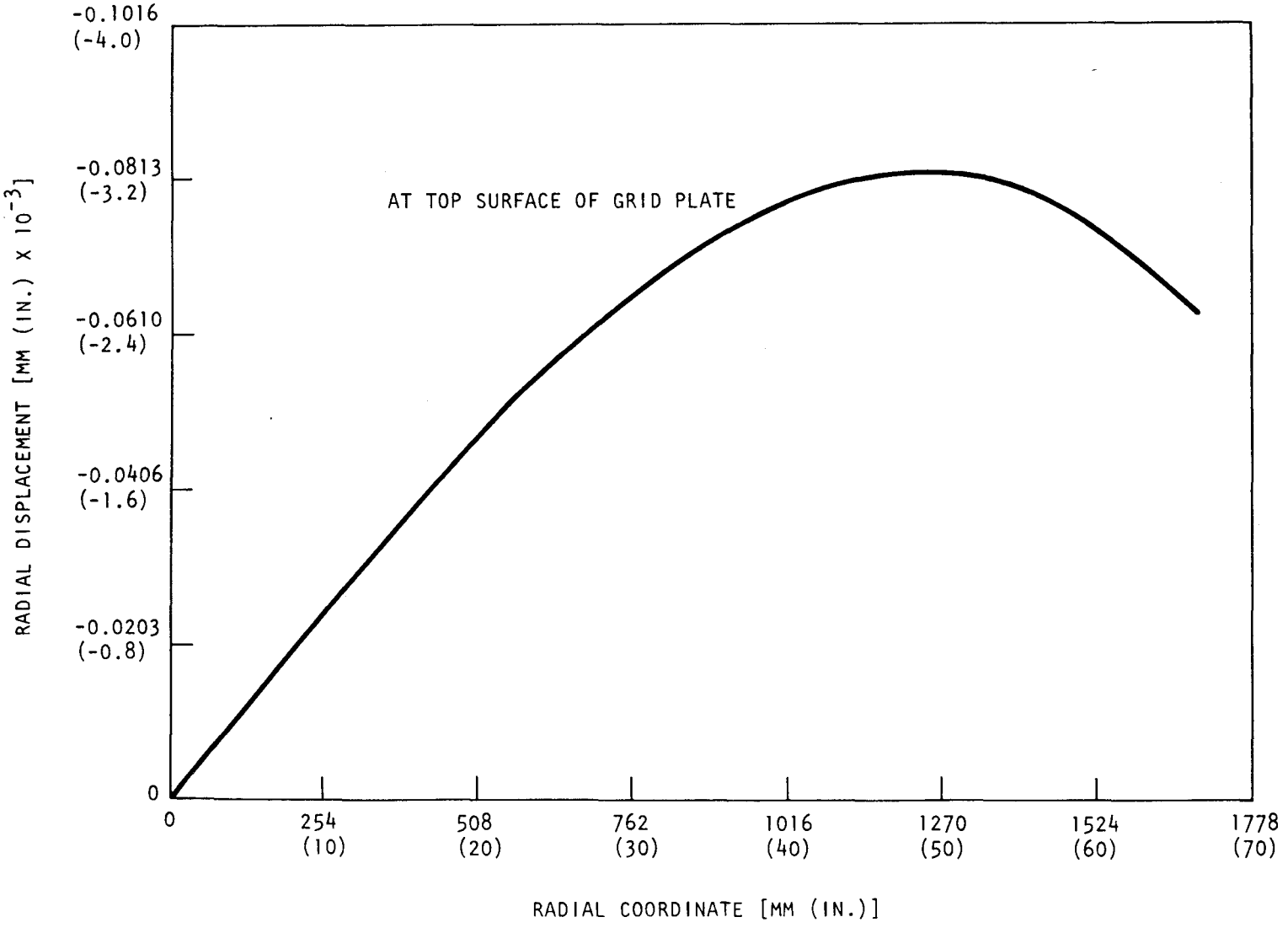

Fig. 18. Isotropic solution, radial displacement vs radial coordinate of grid plate

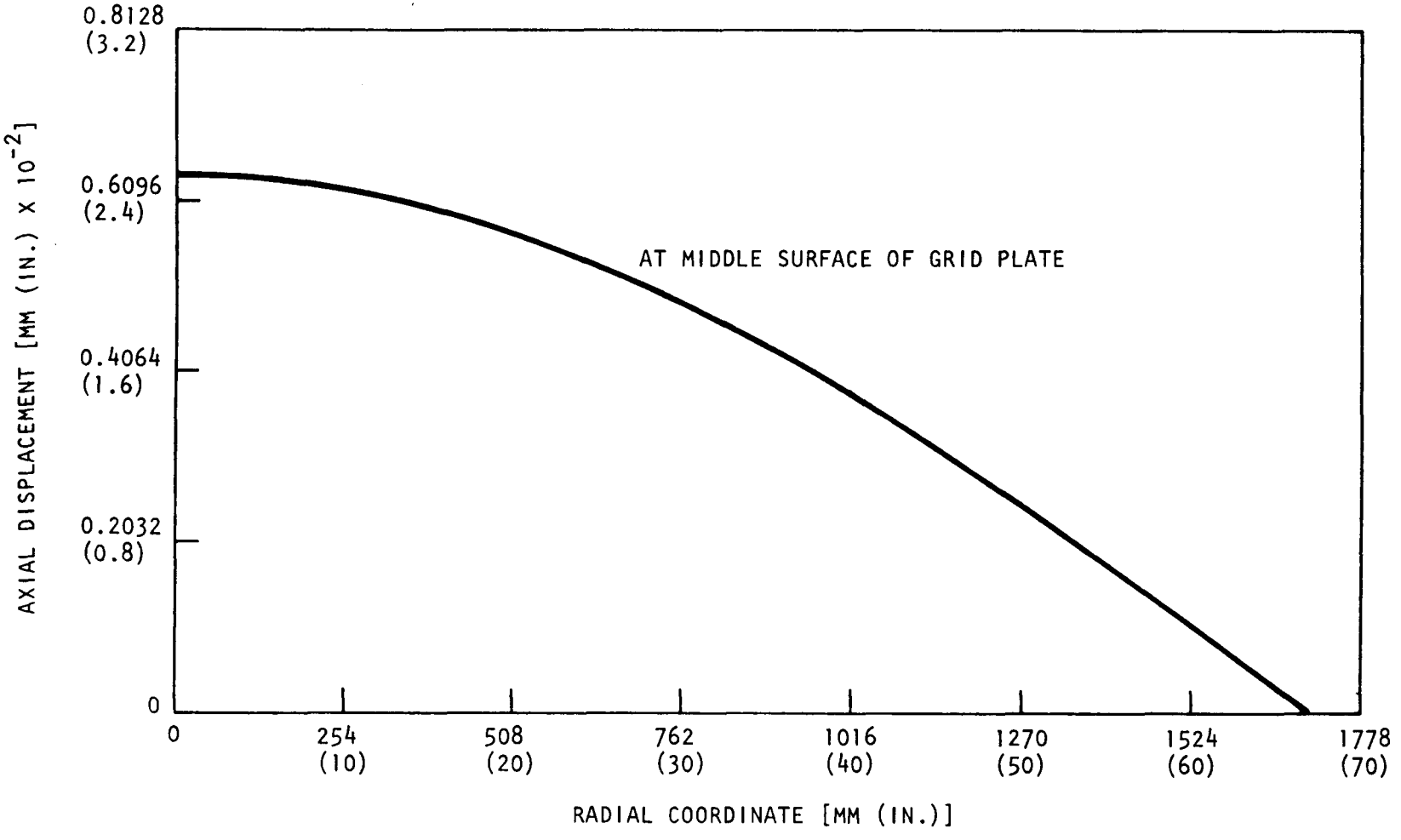

Fig. 19. Isotropic solution, axial displacement vs radial coordinate of grid plate

4. GRID PLATE SUPPORT STRUCTURE

4.1. STRUCTURAL MODEL AND METHOD OF ANALYSIS

The grid support structure is a thin-walled cylinder with a flange at the bottom end to support the grid plate and a flange at the upper end to transfer the loads to the penetration liner of the PCRV. The structure is modeled as shown in Fig. 20, where it is simply supported at the upper flange and circumferentially loaded on the lower flange. The cylinder and the lower flange are analyzed by the elastic thin shell theory, and the upper flange is treated as a ring. Compatibility conditions are used to find the redundant forces and moments at the geometrical discontinuity.

4.2. STRUCTURAL ANALYSIS

4.2.1. Stress Analysis at the Joint of the Cylinder and Upper Flange

4.2.1.1. Cylinder and Upper Flange. As shown below, a section cuts through A-A, separating the upper flange and the cylinder at their junction.

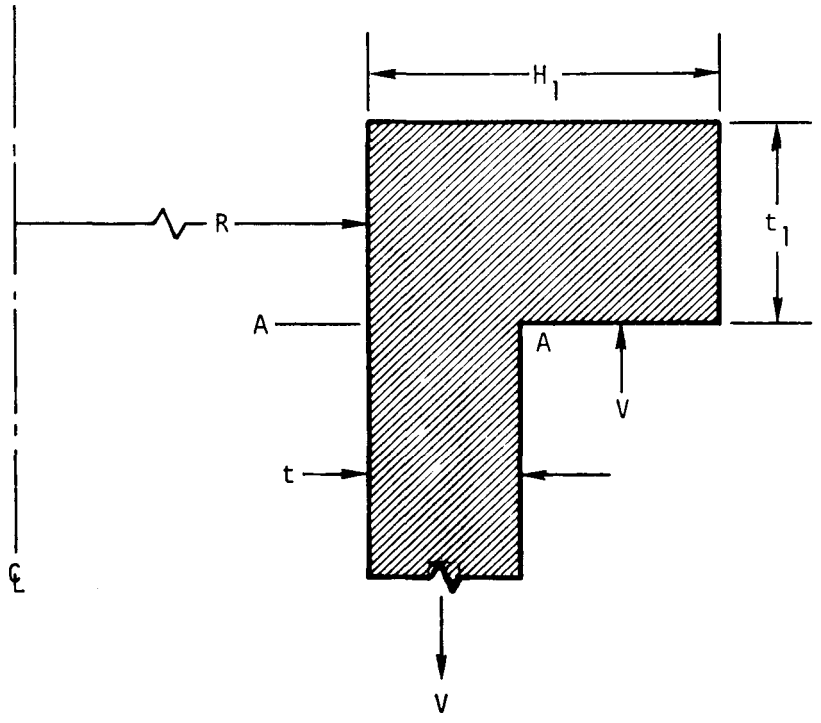

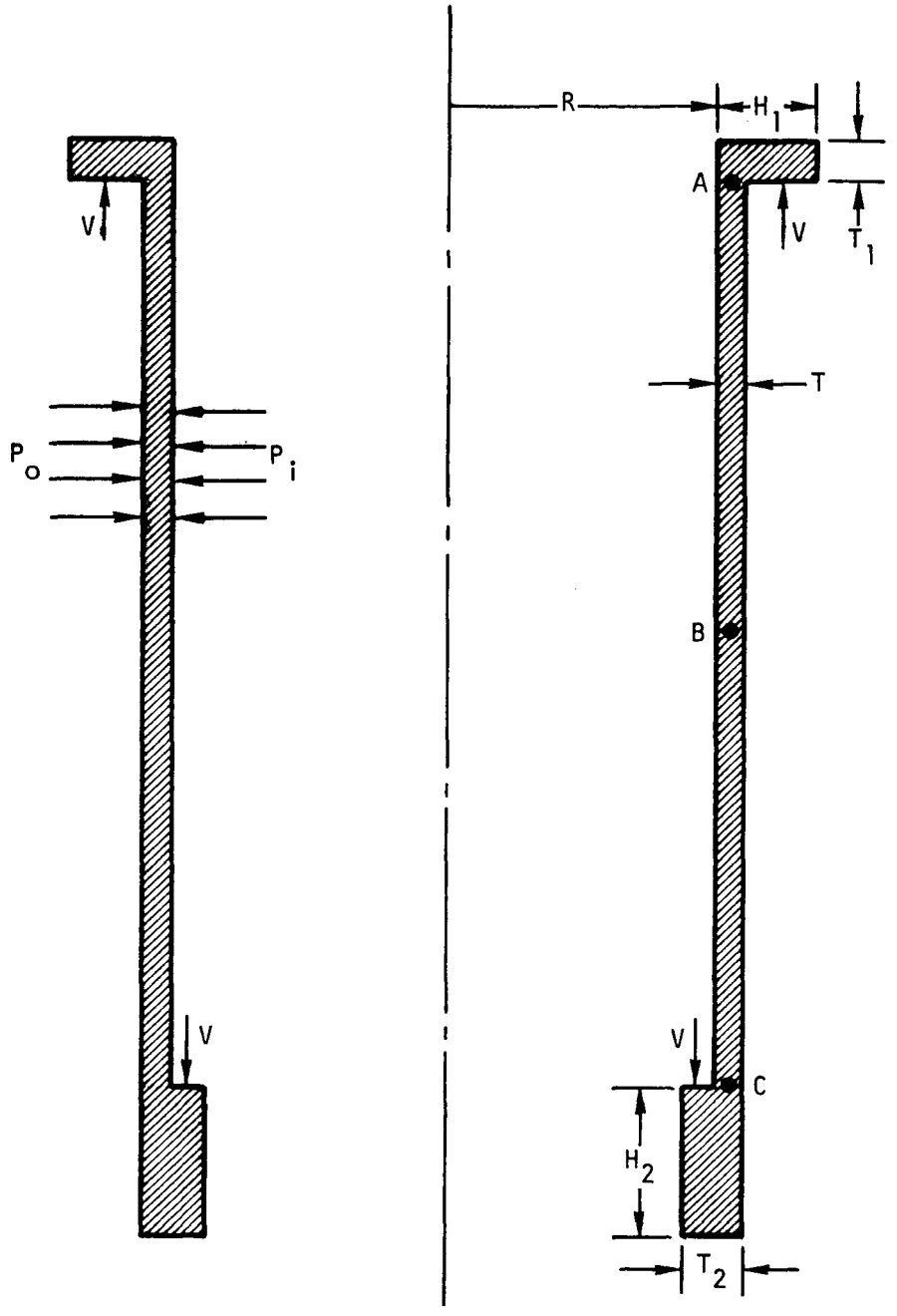

Fig. 20. Mechanical model of grid plate support structure

The free-body diagram is shown below. In this diagram, M_A and S_A are discontinuity moment and shear, respectively, a function of the cylinder and the upper flange.

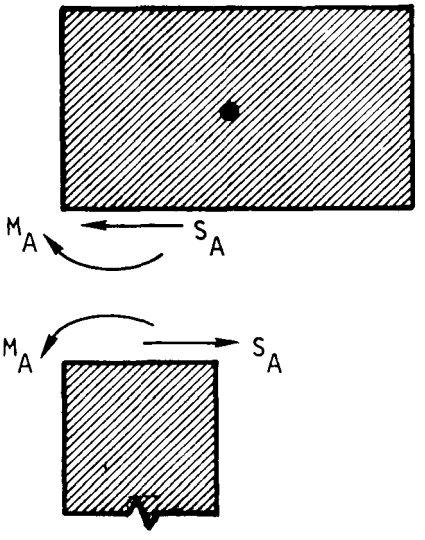

4.2.1.2. Deformation Due to Redundant Moment and Redundant Shear. In considering the cylindrical section, the length of the cylinder is assumed to be $L \geq 3/\beta$, where

$$\beta \equiv [3(1 - \nu^2)/(R + t/2)^2 t^2]^{1/4} \quad . \tag{89}$$

Using equations (a) and (b) of Section III of the ASME Code (1971 edition) for $\beta L >> 1$, the approximate values for the coefficients β_{11}, β_{12}, β_{22}, G_{11}, G_{12}, and G_{22} can be shown as

$$\left.\begin{aligned} \beta_{11} &\equiv \frac{\sinh 2\beta L - \sin 2\beta L}{2(\sinh^2 \beta L - \sin^2 \beta L)} \sim \frac{\sinh 2\beta L}{2 \sinh^2 \beta L} \sim 1 \quad , \\ \beta_{12} &\equiv \frac{\cosh 2\beta L - \cos 2\beta L}{2(\sinh^2 \beta L - \sin^2 \beta L)} \sim \frac{\cosh 2\beta L}{2 \sinh^2 \beta L} \sim 1 \quad , \end{aligned}\right\} \tag{90}$$

$$\left.\begin{aligned}
\beta_{22} &\equiv \frac{\sinh 2\beta L + \sin 2\beta L}{\sinh^2 \beta L - \sin 2\beta L} \sim \frac{\sinh 2\beta L}{\sinh^2 \beta L} \sim 2 \quad , \\
G_{11} &\equiv \frac{-(\cosh \beta L \sin \beta L - \sinh \beta L \cos \beta L)}{\sinh^2 \beta L - \sin^2 \beta L} \sim 0 \quad , \\
G_{12} &\equiv \frac{-2 \sinh \beta L \sin \beta L}{\sinh^2 \beta L - \sin^2 \beta L} \sim 0 \quad , \\
G_{22} &= \frac{-2(\cosh \beta L \sin \beta L + \sinh \beta L \cos \beta L)}{\sinh^2 \beta L - \sin^2 \beta L} \sim 0 \quad .
\end{aligned}\right\} \tag{90}$$

At junction A, the radial displacement w_{A1} and the rotation of the cylinder wall θ_{A1} are

$$\left.\begin{aligned}
w_{A1} &= w_{C1} = \frac{1}{2\beta^3 D} S_A - \frac{1}{2\beta^2 D} M_A \quad , \\
\theta_{A1} &= \theta_{C1} - \frac{1}{2\beta^2 D} S_A + \frac{1}{\beta D} M_A \quad ,
\end{aligned}\right\} \tag{91}$$

where w_{C1} and θ_{C1} are radial displacement and wall rotation, respectively, for the cylinder at the junction, and D is the stiffness of the shell and is equal to $Et^3/12(1 - \nu^2)$. There is a discrepancy in the formulation for the radial displacement w_{A1}. As indicated by Roark (Ref. 12) and Timoshenko (Ref. 13), the second term of the expression should be $1/2\beta^2 D$. However, as used in the example in the ASME code, the second term of the formula is $1/\beta^2 D$. Thus, there is an error in the ASME code (this error was corrected in the 1974 edition of the code). The sign convention for the moment is such that a positive sign indicates a counterclockwise moment.

The upper flange is considered to be a ring, and redundant moment M_A and redundant shear S_A are shown in the free-body diagram below.

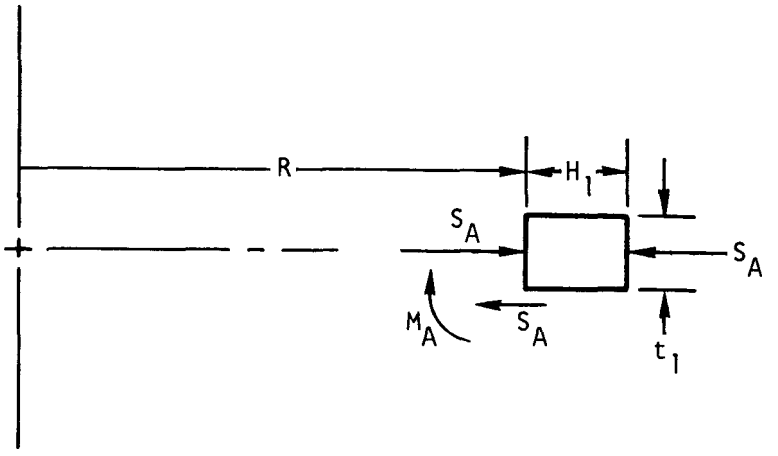

The rotation of the cross section about its centroid is

$$\theta_{R1} = \left[\frac{2\pi(R + t/2)M_A}{2\pi(R + H_1/2)} + \frac{2\pi(R + t/2)}{2\pi(R + H_1/2)} S_A \cdot \frac{t_1}{2} \right] \frac{(R + H_1/2)^2}{E \frac{H_1 t_1^3}{12}}$$

$$= \frac{(2R + t)}{(2R + H_1)} \left(M_A + \frac{S_A t_1}{2} \right) \frac{3(2R + H_1)^2}{E H_1 t_1^3}$$

$$= \frac{3(2R + t)(2M_A + S_A t_1)(2R + H_1)}{2E H_1 t_1^3} \quad . \qquad (92)$$

The clockwise rotation is considered positive.

The radial deflection of the upper flange can be calculated by combining the deflection due to rotation and the deflection due to shear. The cross section for calculation is shown below.

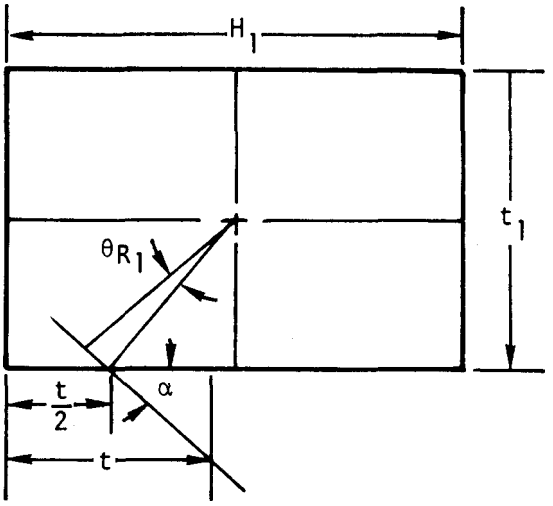

Radial deflection due to rotation θ_{R1} is

$$w'_{R1} = \sqrt{\left(\frac{t_1}{2}\right)^2 + \left(\frac{H_1}{2} - \frac{t}{2}\right)^2}\ \theta_{R1} \cos\alpha$$

$$= \frac{1}{2}\sqrt{t_1^2 + (H_1 - t)^2}\theta_{R1}\ \frac{t_1/2}{\sqrt{\left(\frac{t_1}{2}\right)^2 + \left(\frac{H_1}{2} - \frac{t}{2}\right)^2}}$$

$$= \frac{t_1}{2}\theta_{R1} \quad , \tag{93}$$

and the deflection due to the redundant shear S_A can be shown as

$$w''_{R1} = \frac{(R + t/2)S_A}{Et_1H_1}\left(R + \frac{H_1}{2}\right) \quad , \tag{94}$$

where H_1 = width of flange,

t = thickness of cylinder,

t_1 = vertical thickness of flange,

α = angle (defined in the above figure of the cross section for calculation).

Therefore, the total deflection of the ring is

$$w_{R1} = w'_{R1} + w''_{R1} = \frac{t_1}{2}\theta_{R1} + \frac{(R + t/2)(R + H_1/2)}{Et_1H_1} S_A$$

$$= \frac{1.5(2R + t)(2R + H_1)(2M_A + S_A t_1)t_1}{2EH_1 t_1^3}$$

$$+ \frac{(2R + t)(2R + H_1)}{4Et_1H_1} S_A$$

$$= \frac{3(2R + t)(2R + H_1)M_A}{2EH_1 t_1^2} + \frac{(2R + t)(2R + H_1)S_A}{EH_1 t_1} \quad . \qquad (95)$$

4.2.1.3. Deformation Due to Loads Other Than Redundant Loads. Deformation due to loads other than redundant loads can be expressed as follows:

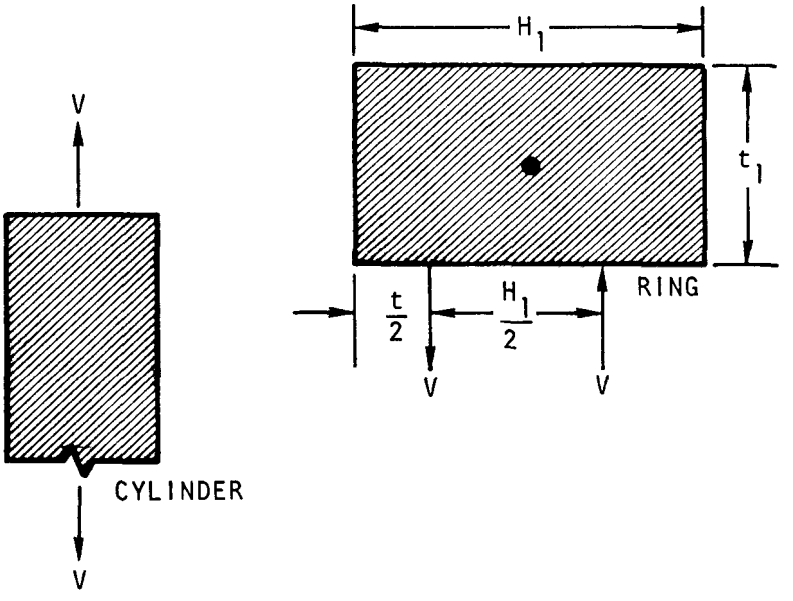

For the cylinder,

$$\left.\begin{aligned} \theta'_{C2} &= w'_{C2} = 0 \quad , \quad \text{due to V} \quad , \\ \theta''_{C2} &= 0 \quad , \\ w'_{C2} &= \frac{(Pi - Po)(R + t/2)^2}{Et} = w_{C2} \quad , \quad \text{due to pressure} \quad . \end{aligned}\right\} \tag{96}$$

Upper flange rotation of the cross section about its centroid can be expressed as

$$\begin{aligned} \theta_{R2} &= \frac{2\pi(R + t/2)}{2\pi(R + H_1/2)} V \cdot \frac{H_1}{2} \cdot \frac{(R + H_1/2)^2}{EH_1 t_1^3/12} \\ &= \frac{3(2R + t)(2R + H_1)V}{2Et_1^3} \quad . \end{aligned} \tag{97}$$

Radial deflection can be expressed as

$$w_{R2} = \frac{t_1}{2} \theta_{R2} = \frac{3(2R + t)(2R + H_1)V}{4Et_1^2} \quad . \tag{98}$$

4.2.1.4. Compatibility Conditions. At the junction of the cylinder and the upper flange, the rotation θ_C and radial displacement w_C of the cylinder must be equal to the rotation and radial displacement of the upper flange. Thus,

$$\left.\begin{aligned} \theta_C &= \theta_{C1} + \theta_{C2} = -\theta_{R1} + \theta_{R2} = \theta_R \quad , \\ w_C &= w_{C1} + w_{C2} = -w_{R1} + w_{R2} = w_R \quad . \end{aligned}\right\} \tag{99}$$

Using Eqs. 96 through 98, these two compatibility equations can be written as

$$-\frac{1}{2\beta^2 D}S_A + \frac{1}{\beta D}M_A = \frac{-3(2R+t)(2R+H_1)(2M_A + S_A t_1)}{2EH_1 t_1^3} + \frac{3(2R+t)(2R+H_1)V}{2Et_1^3} ,$$

$$\frac{1}{2\beta^3 D}S_A - \frac{1}{2\beta^2 D}M_A + \frac{(p_i - p_o)(R+t/2)^2}{Et} = \frac{-3(2R+t)(2R+H_1)M_A}{2EH_1 t_1^2} - \frac{(2R+t)(2R+H_1)S_A}{EH_1 t_1} + \frac{3(2R+t)(2R+H_1)V}{4Et_1^2} ,$$

or

$$\left.\begin{aligned} \left[\frac{1}{\beta D} + \frac{3(2R+t)(2R+H_1)}{EH_1 t_1^3}\right]M_A + \left[\frac{3(2R+t)(2R+H_1)}{2EH_1 t_1^2} - \frac{1}{2\beta^2 D}\right]S_A &= \frac{3(2R+t)(2R+H_1)V}{2Et_1^3} , \\ \left[\frac{3(2R+t)(2R+H_1)}{2EH_1 t_1^2} - \frac{1}{2\beta^2 D}\right]M_A + \frac{1}{2\beta^3 D} + \left[\frac{(2R+t)(2R+H_1)}{EH_1 t_1}\right]S_A &= \frac{3(2R+t)(2R+H_1)V}{4Et_1^2} - \frac{(Pi - Po)(R+t/2)^2}{Et} . \end{aligned}\right\} \quad (100)$$

Equation 100 can be simplified to be

$$\left.\begin{aligned} a_{11}M_A + a_{12}S_A &= b_1 \quad , \\ a_{21}M_A + a_{22}S_A &= b_2 \quad , \end{aligned}\right\} \tag{101}$$

where

$$a_{11} \equiv \frac{1}{\beta D} + \frac{3(2R + t)(2R + H_1)}{EH_1t_1^3} \quad ,$$

$$a_{12} \equiv \frac{3(2R + t)(2R + H_1)}{2EH_1t_1^2} - \frac{1}{2\beta^2 D} \quad ,$$

$$a_{21} \equiv \frac{3(2R + t)(2R + H_1)}{2EH_1t_1^2} - \frac{1}{2\beta^2 D} \quad ,$$

$$a_{22} \equiv \frac{1}{2\beta^3 D} + \frac{(2R + t)(2R + H_1)}{EH_1t_1} \quad ,$$

$$b_1 \equiv \frac{3(2R + t)(2R + H_1)V}{2Et_1^3} \quad ,$$

$$b_2 \equiv \frac{3(2R + t)(2R + H_1)V}{4Et_1^2} - \frac{(Pi - Po)(R + t/2)^2}{Et} \quad .$$

Hence,

$$\left.\begin{aligned} M_A &= (b_1a_{22} - b_2a_{12})/\Delta \quad , \\ S_A &= (a_{11}b_2 - a_{21}b_1)/\Delta \quad , \end{aligned}\right\} \tag{102}$$

where

$$\Delta \equiv a_{11}a_{22} - a_{21}a_{12} \quad .$$

4.2.1.5. Stresses in the Cylinder Wall at the Junction of the Cylinder and the Upper Flange. The stresses in the cylinder wall at the junction of the cylinder and the upper flange can be shown as

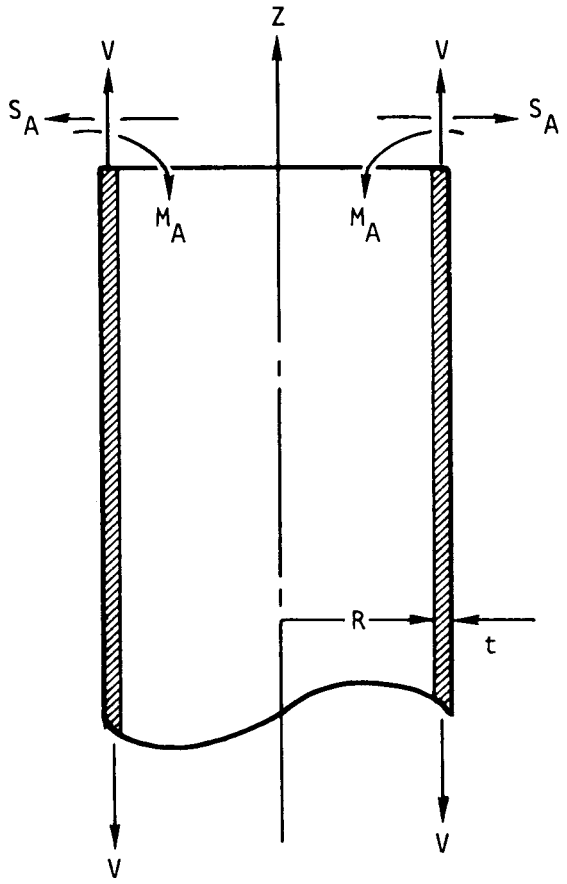

At the outer surface of the cylinder, the axial, circumferential, and radial stresses can be written as

$$\left.\begin{aligned}
\sigma_z^o &= \frac{V}{t} + \frac{6M_A}{t^2} \quad , \\
\sigma_\theta^o &= E \cdot \frac{\Delta R}{R + t/2} - \nu \frac{6M_A}{t^2} + \frac{(Pi - Po)(R + t/2)}{t} \\
&= E\frac{w_c}{R + t/2} - \nu \frac{6M_A}{t^2} + \frac{(Pi - Po)(R + t/2)}{t} \\
&= \frac{E}{R + t/2}\left(\frac{1}{2\beta^3 D} S_A - \frac{1}{2\beta^2 D} M_A\right) - \nu \frac{6M_A}{t^2} + \frac{(Pi - Po)(R + t/2)}{t} \quad , \\
\sigma_r^o &\simeq - \frac{Pi + Po}{2} \quad .
\end{aligned}\right\} \quad (103)$$

At the inner surface, the stresses are

$$\left.\begin{aligned}
\sigma_z^i &= \frac{V}{t} - \frac{6M_A}{t^2} \quad , \\
\sigma_\theta^i &= \frac{E}{R + t/2}\left(\frac{1}{2\beta^3 D} S_A - \frac{M_A}{2\beta^2 D}\right) + \nu \frac{6M_A}{t^2} + \frac{(Pi - Po)(R + t/2)}{2} \quad , \\
\sigma_r^i &\simeq - \frac{Pi + Po}{2} \quad .
\end{aligned}\right\} \quad (104)$$

4.2.2. Structural Analysis of the Middle Section of the Support Cylinder

A section is chosen at the middle of the cylinder so that the bending and shear effect from both ends is negligible. Therefore,

$$\left.\begin{aligned}
\sigma_z &= \frac{V}{t} \quad , \\
\sigma_\theta &= \frac{(Pi - Po)(R + t/2)}{t} \quad , \\
\sigma_r &= - \frac{Pi + Po}{2} \quad .
\end{aligned}\right\} \quad (105)$$

4.2.3. Structural Analysis at the Joint of the Cylinder and the Lower Flange

4.2.3.1. Cylinder and Lower Flange. The diagram below shows that a section cuts through C-C, separating the cylinder and the lower flange at their junction.

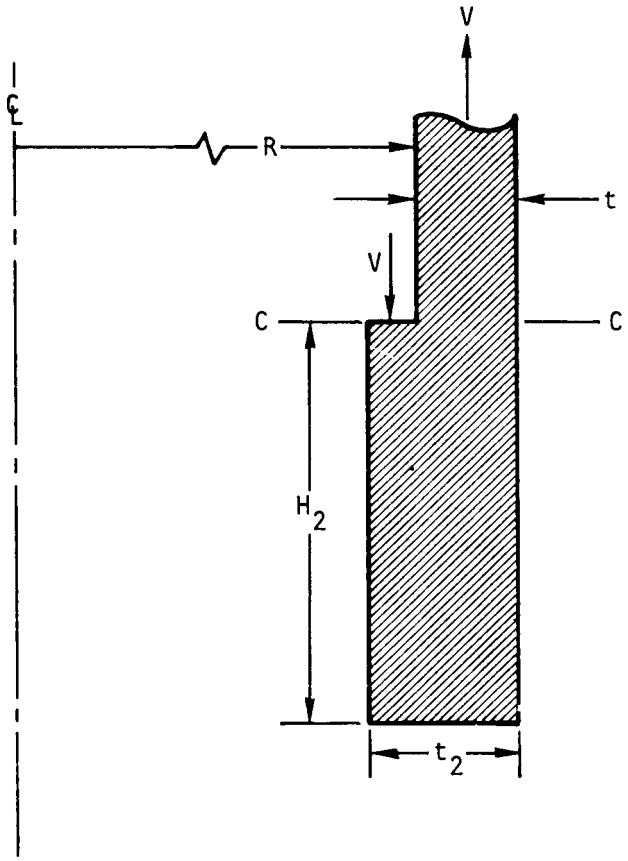

The free-body diagram of the cylinder and the lower flange as well as the redundant shear force S_c and the redundant moment M_c are shown in the figure below.

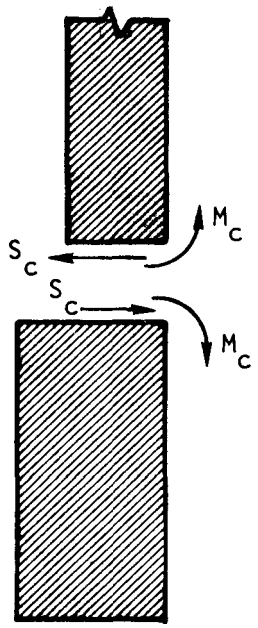

4.2.3.2. Deformation Due to Redundant Moment and Redundant Shear Force. The radial displacement of the cylinder due to redundant moment M_c and redundant shear S_c is

$$w_{c1} = \frac{1}{2\beta^2 D} M_c - \frac{1}{2\beta^3 D} S_c \quad , \tag{106}$$

and the rotation of the cylinder wall is

$$\theta_{c1} = \frac{1}{2\beta^2 D} S_c - \frac{1}{\beta D} M_c \quad . \tag{107}$$

The lower flange is considered to be a short cylinder; its radial displacement of the wall is

$$w_{f1} = \frac{B_{11}^f}{2\beta_f^3 D_f} S_c + \frac{B_{12}^f}{2\beta_f^2 D_f} M_c \quad , \tag{108}$$

and the rotation of the wall is

$$\theta_{f1} = -\frac{B_{12}^{f}}{2\beta_f^2 D_f} S_c - \frac{B_{22}^{f}}{\beta_f D_f} M_c \quad , \tag{109}$$

where

$$\beta_f \equiv \left[3(1 - \quad ^2)/(R + t - t_2/2)^2 t_2^2 \right]^{1/4} \quad ,$$

$$D_f \equiv Et_2^3/12(1 - \nu^2) \quad ,$$

$$B_{11}^{f} \equiv (\sinh 2\beta_f H_2 - \sin 2\beta_f H_2)/2\ (\sinh^2 \beta_f H_2 - \sin^2 \beta_f H_2) \quad ,$$

$$B_{12}^{f} = (\cosh 2\beta_f H_2 - \cos 2\beta_f H_2)/2\ (\sinh^2 \beta_f H_2 - \sin^2 \beta_f H_2) \quad ,$$

$$B_{22}^{f} = (\sinh 2\beta_f H_2 + \sin 2\beta_f H_2)/(\sinh^2 \beta_f H_2 - \sin^2 \beta_f H_2) \quad .$$

4.2.3.3. Deformations Due to Loads Other Than Redundant Loads. For the cylinder, radial deflection w'_{c2} and rotation of the wall θ'_{c2} are equal to zero owing to the vertical reaction V; i.e.,

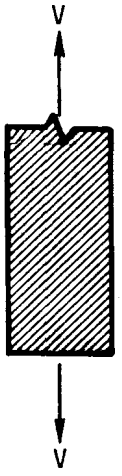

$$
\left.
\begin{aligned}
w'_{c2} &= \theta'_{c2} = 0 \quad , \\
\theta''_{c2} &= 0 \quad , \\
w''_{c2} &= \frac{(Pi - Po)(R + t/2)^2}{Et} = w_{c2} \quad ,
\end{aligned}
\right\} \tag{110}
$$

where, at the lower flange, the bending moment due to the vertical load V in a cross section is

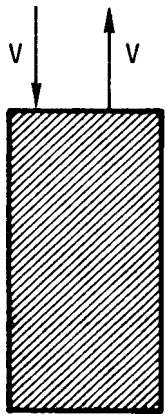

$$
\begin{aligned}
M &= V \cdot \left[t_2 - \frac{t}{2} - \frac{1}{2}(t_2 - t) \right] \\
&= Vt_2/2 \quad .
\end{aligned} \tag{111}
$$

The radial deflection and the rotation of the wall of the lower flange are

$$
\left.
\begin{aligned}
w_{f2} &= \frac{-B^f_{12}}{2\beta_f^2 D_f} \frac{Vt_2}{2} + \frac{(Pi - Po)(R + t - t_2/2)^2}{Et_2} \quad , \\
\theta_{f2} &= \frac{B^f_{22}}{2\beta_f D_f} \frac{Vt_2}{2} \quad .
\end{aligned}
\right\} \tag{112}
$$

4.2.3.4. Compatibility Conditions. At the junction of the cylinder and the lower flange, rotation of the cylinder wall θ_c and radial displacement of the cylinder wall w_c must equal rotation of the lower flange θ_F and radial displacement of the lower flange w_f:

$$\theta_c = \theta_{c1} + \theta_{c2} = -\theta_{F1} - \theta_{F2} = \theta_F \quad ,$$

$$w_c = w_{c1} + w_{c2} = w_{F1} + w_{F2} = w_F \quad .$$

Thus,

$$\left.\begin{aligned}
&\left[\frac{1}{\beta D} + \frac{B_{22}^f}{B_f D_f}\right] M_c + \left[\frac{-1}{2\beta^2 D} + \frac{B_{12}^f}{2\beta_f^2 D_f}\right] S_c = \frac{B_{22}^f Vt_2}{4\beta_f D_f} \quad , \\
&\left[-\frac{1}{2\beta^2 D} + \frac{B_{12}^f}{2\beta_f^2 D_f}\right] M_c + \left[\frac{1}{2\beta^3 D} + \frac{B_{11}^f}{2\beta_f^3 D_f}\right] S_c \\
&\qquad = \frac{B_{12}^f Vt_2}{4\beta_f^2 D_f} + \frac{(Pi - Po)(R + t/2)^2}{Et} \\
&\qquad - \frac{(Pi - Po)(R + t - t_2/2)^2}{Et_2} \quad .
\end{aligned}\right\} \qquad (113)$$

Equation 113 can be simplified to be

$$\left.\begin{aligned}
C_{11} M_c + C_{12} S_c &= d_1 \quad , \\
C_{21} M_c + C_{22} S_c &= d_2 \quad ,
\end{aligned}\right\} \qquad (114)$$

where

$$C_{11} \equiv \frac{1}{\beta D} + \frac{B_{22}^f}{\beta_f D_f} \quad ,$$

$$C_{12} \equiv -\frac{1}{2\beta^2 D} + \frac{B_{12}^f}{2\beta_f^2 D_f} = C_{21} \quad ,$$

$$C_{21} \equiv -\frac{1}{2\beta^2 D} + \frac{B_{12}^f}{2\beta_f^2 D_f} = C_{12} \quad ,$$

$$C_{22} \equiv \frac{1}{2\beta^3 D} + \frac{B_{11}^f}{2\beta_f^3 D_f} \quad ,$$

$$d_1 \equiv \frac{B_{22}^f t_2 V}{4\beta_f D_f} \quad ,$$

$$d_2 \equiv \frac{B_{12}^f t_2 V}{4\beta_f^2 D_f} + \frac{(Pi - Po)(R + t/2)^2}{Et} - \frac{(Pi - Po)(R + t - t_2/2)^2}{Et_2} \quad .$$

Hence,

$$\left.\begin{aligned} M_c &= (d_1 C_{22} - D_2 C_{12})/\Delta \quad , \\ S_c &= (C_{11} d_2 - C_{21} d_1)/\Delta \quad , \end{aligned}\right\} \tag{115}$$

where

$$\Delta \equiv C_{11} C_{22} - C_{12} C_{21} \quad .$$

4.2.3.5. Calculation of Stresses at Cross Section C-C. The stresses on cross section C-C can be calculated as follows:

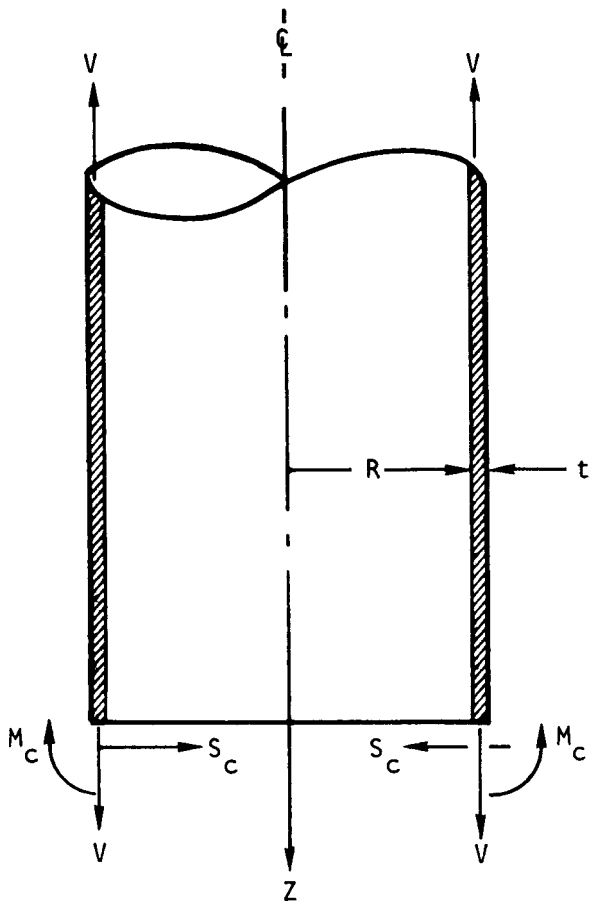

At the outer surface,

$$\left.\begin{aligned}
\sigma_Z^o &= \frac{V}{t} - \frac{M_c}{t^2} \quad , \\
\sigma_\theta^o &= E \cdot \frac{w_c}{(R + t/2)} + \nu \frac{6M_c}{t^2} + \frac{(Pi - Po)(R + t/2)}{t} \\
&= \frac{E}{R + t/2} \left[\frac{1}{2\beta^2 D} M_c - \frac{1}{2\beta^3 D} S_c \right] + \nu \frac{6M_c}{t^2} \\
&\quad + \frac{(Pi - Po)(R + t/2)}{t} \quad ,
\end{aligned}\right\} \qquad (116)$$

$$\sigma_r^o = -\frac{Pi - Po}{2} \quad . \tag{116}$$

At the inner surface,

$$\left.\begin{aligned}
\sigma_Z^i &= \frac{V}{t} + \frac{6M_c}{t^2} \quad , \\
\sigma_\theta^i &= \frac{E}{R + t/2}\left[\frac{1}{2\beta^2 D} M_c - \frac{1}{2\beta^3 D} S_c\right] - \nu \frac{6M_c}{t^2} \\
&\quad + \frac{(Pi - Po)(R + t/2)}{t} \quad , \\
\sigma_r^i &= -\frac{Pi + Po}{2} \quad .
\end{aligned}\right\} \tag{117}$$

4.3. NUMERICAL RESULTS

Three pertinent sections (A, B, and C in Fig. 20) were selected for analysis. Sections A and C, located at the junctions of the cylinder and the flanges, represent the local peak bending effect resulting from the geometrical discontinuity of the structure; section B is situated at the middle of the cylinder, where the membrane stresses prevail. The results of the analysis were written into the computer program GRISP in order to facilitate the parametric study. The computer results indicated that the stresses in the structure are quite low for the various dimensions in the range of design interest.

To provide an insight into the effect of the flanges on the stress distribution in the cylinder, stress intensities versus the dimensions of the flanges and the cylinder wall thickness were plotted in Figs. 21 through 26 for sections A and C. One interesting result is that the stress intensity at the outer surface of section A increases with an increase of upper flange width (Fig. 25); the stress intensity at the inner surface of section C also increases with an increase of lower flange thickness (Fig. 23). This

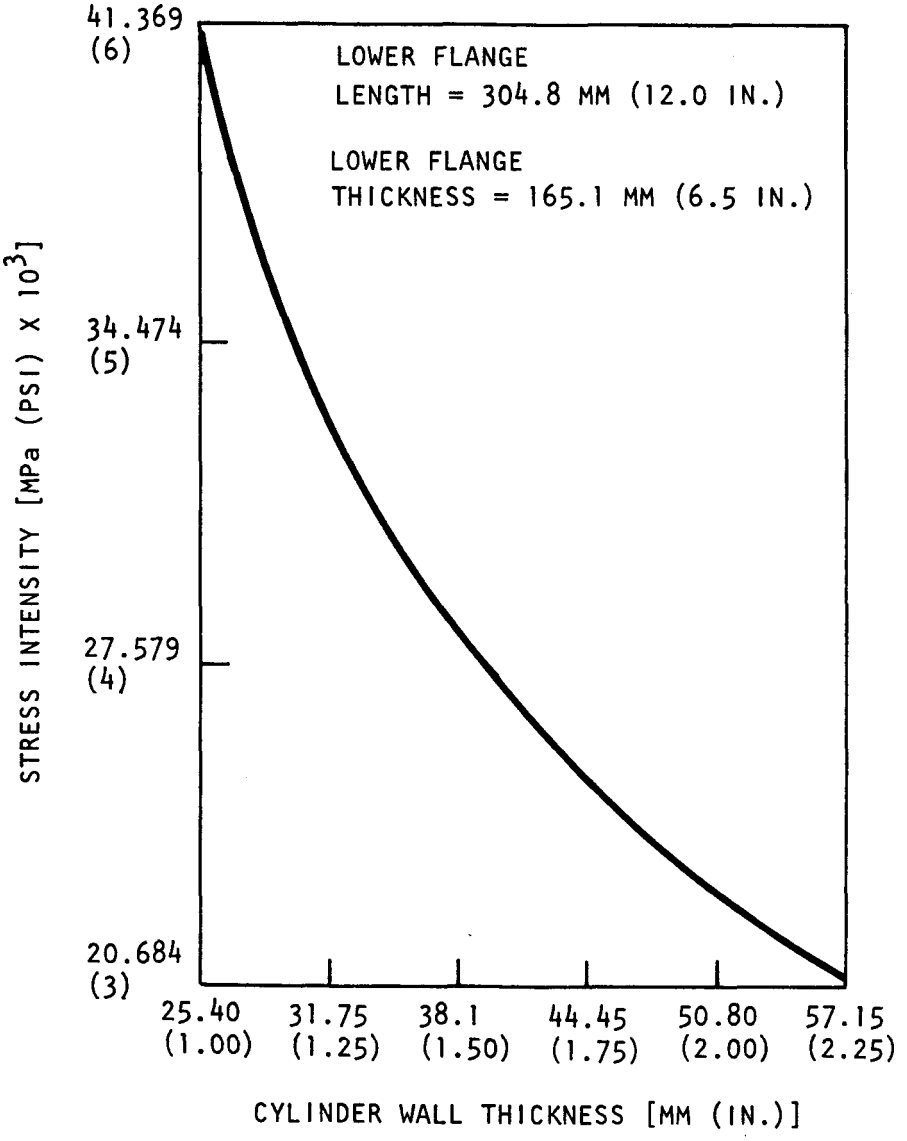

Fig. 21. Relationship of stress intensity at inner surface and cylinder wall thickness at joint of cylinder and lower flange

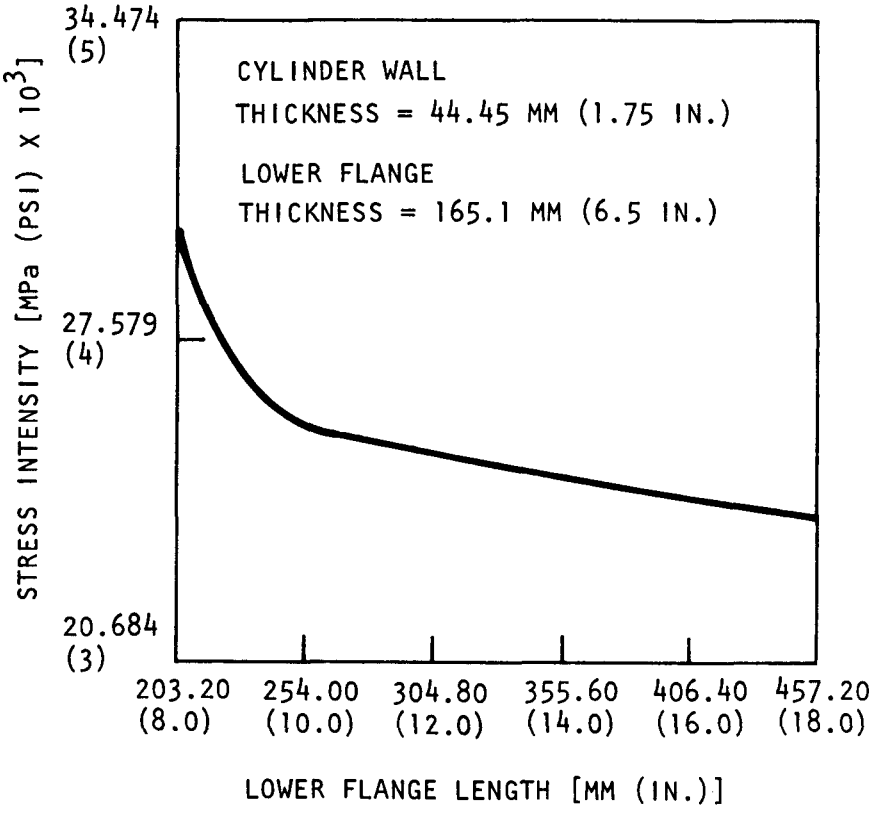

Fig. 22. Relationship of stress intensity at inner surface and lower flange length at joint of cylinder and lower flange

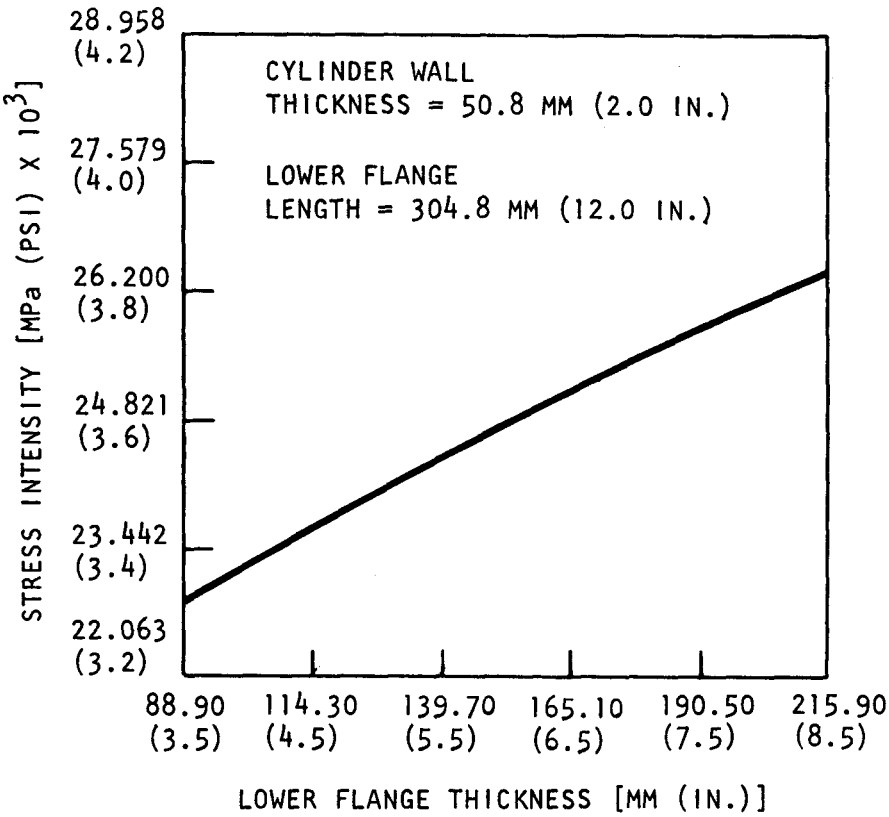

Fig. 23. Relationship of stress intensity at inner surface and lower flange thickness at joint of cylinder and lower flange

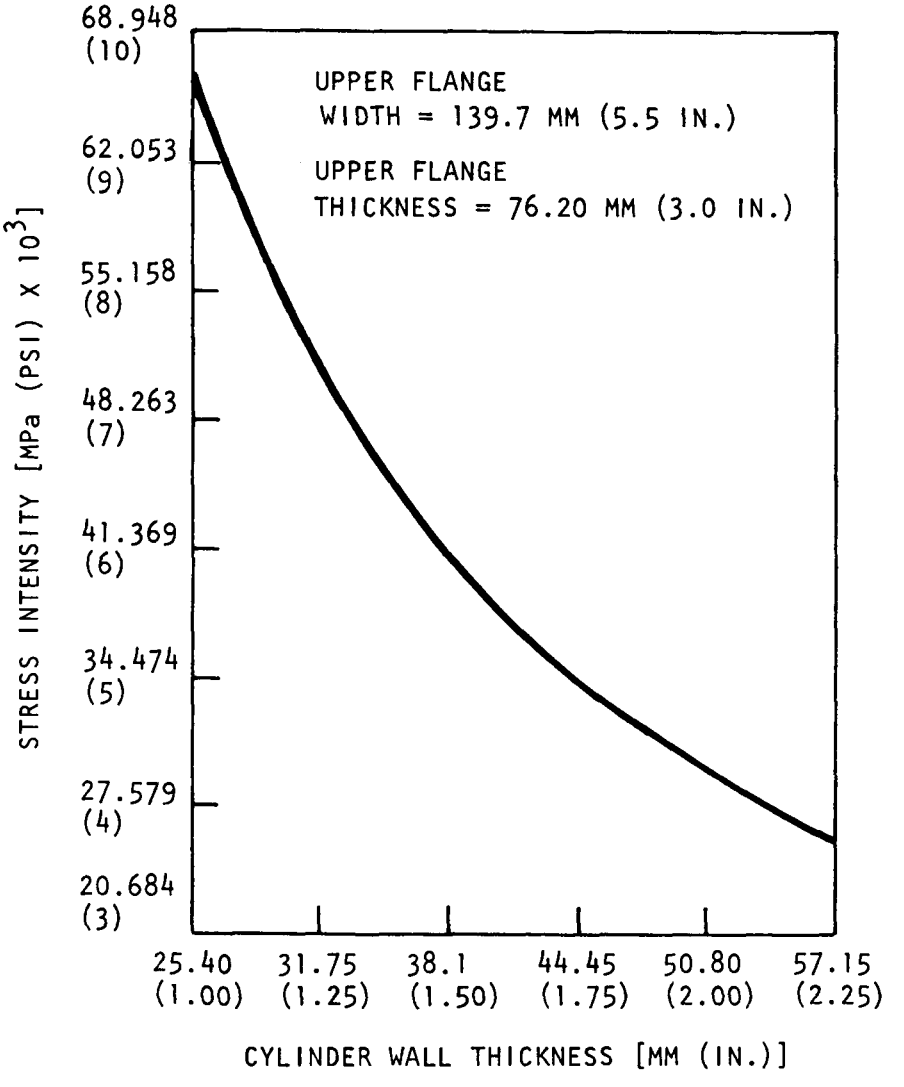

Fig. 24. Relationship of stress intensity at outer surface and cylinder wall thickness at joint of cylinder and upper flange

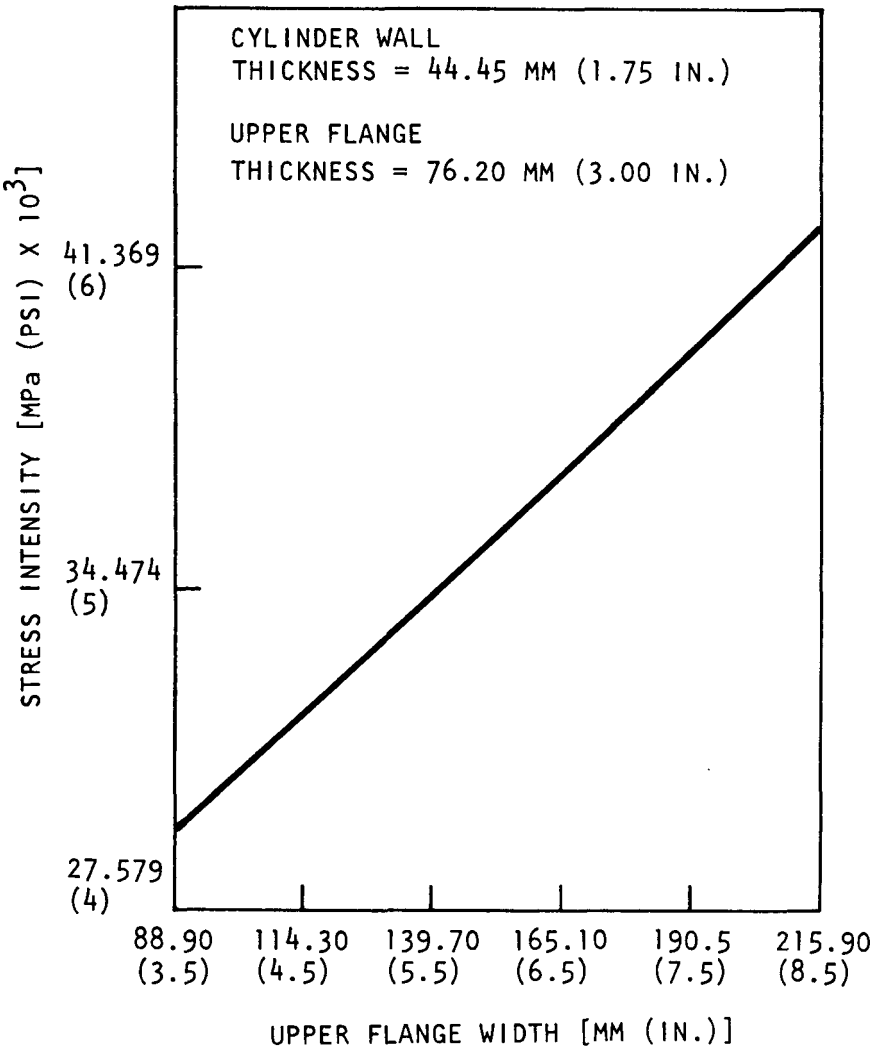

Fig. 25. Relationship of stress intensity at outer surface and upper flange width at joint of cylinder and upper flange

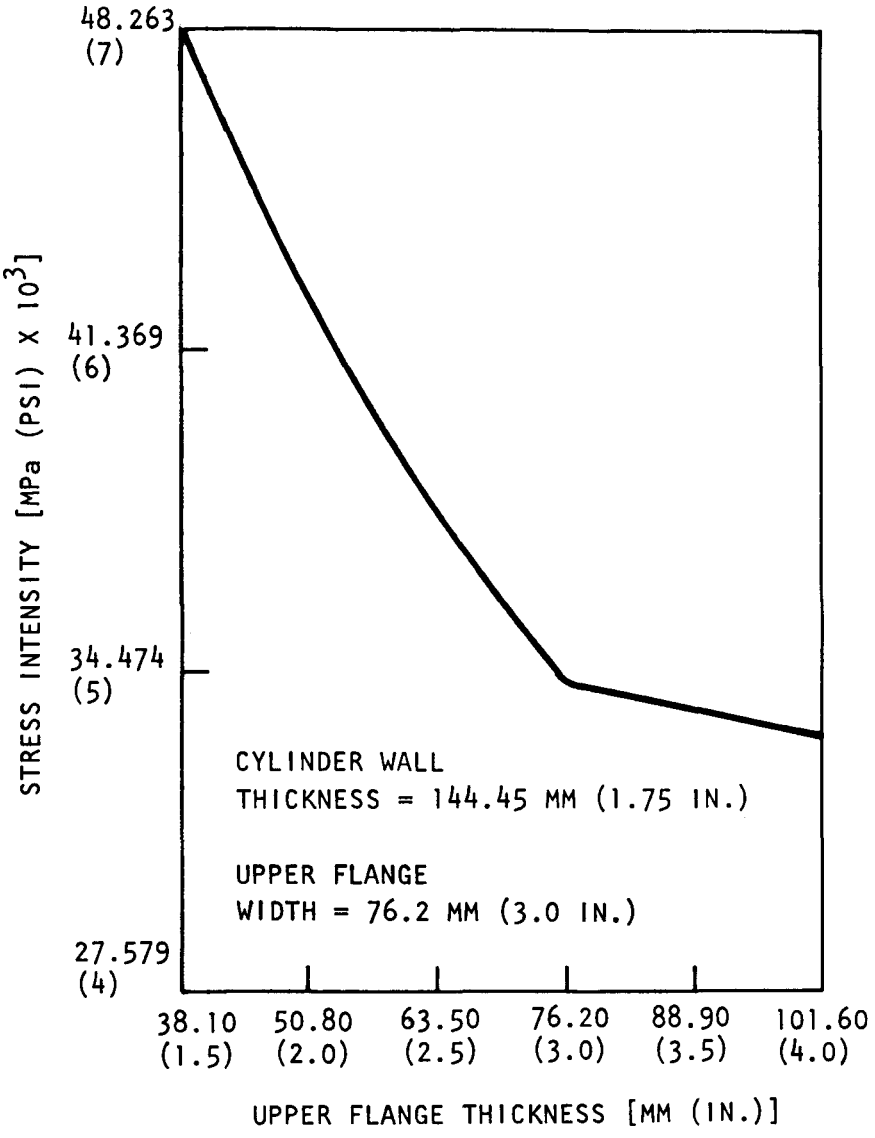

Fig. 26. Relationship of stress intensity at outer surface and upper flange thickness at joint of cylinder and upper flange

behavior is indicated by the fact that the magnitude of the redundant moments increases with an increase of flange thickness.

Figure 27 shows the current 300-MW(e) demonstration plant support cylinder.

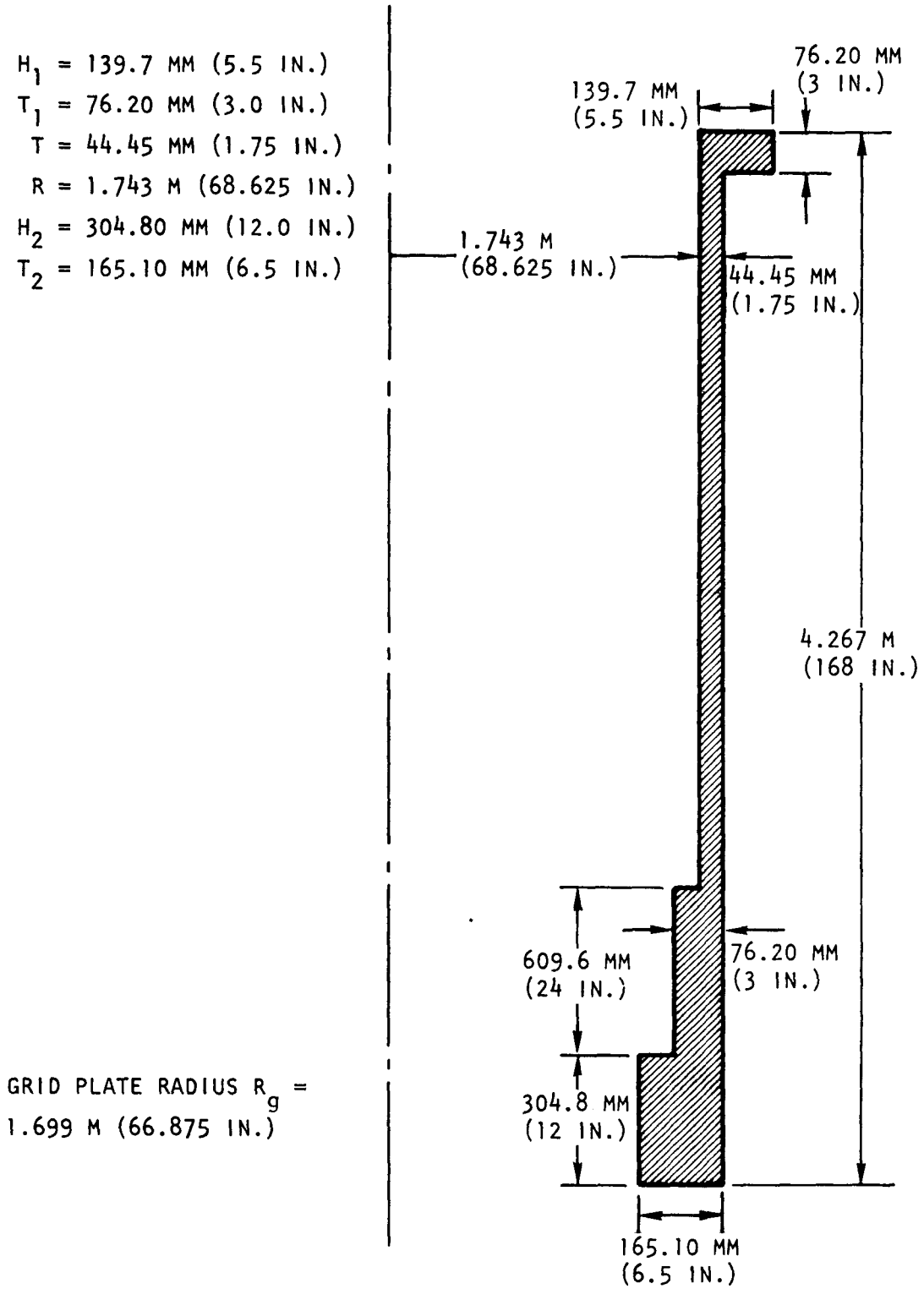

Fig. 27. 300-MW(e) demonstration plant grid plate support cylinder

5. STRUCTURAL INTERACTION BETWEEN THE GRID PLATE AND THE SUPPORT STRUCTURE

5.1. DISCUSSION

In the previous analyses, the grid plate is assumed to be simply supported along its edge by a rigid foundation. However, in actual construction, the grid plate is attached to the lower flange of the support cylinder, which is also a deformable structural member. As a result, the problem of structural coupling between the grid plate and the support cylinder should be investigated. The purpose of this study is to find the interactive moment between the grid plate and the support cylinder to determine the effect of local flexibility of the support cylinder on grid plate deflection. The problem is formulated in such a way that the grid plate is a part of the integrated core support structure so that when the grid plate is subjected to load, it, the support cylinder, and the lower flange rotate together. In the analysis, the support cylinder and lower flange are treated as a long and a short thin cylindrical shell, respectively. To simplify computation, thin plate theory was applied to the equivalent solid plate of the grid plate, and the solid rim effect was ignored.

As shown in Fig. 28, the core support structure is subjected to a uniformly distributed load P. The free-body diagram in Fig. 29 shows the interactive force and moment between the grid plate and the support cylinder due to clamping and the discontinuity shear force and bending moment at the joint section of the support cylinder and its lower flange. Figure 30 illustrates the discontinuity shear force and bending moment at the cylinder and flange joint section.

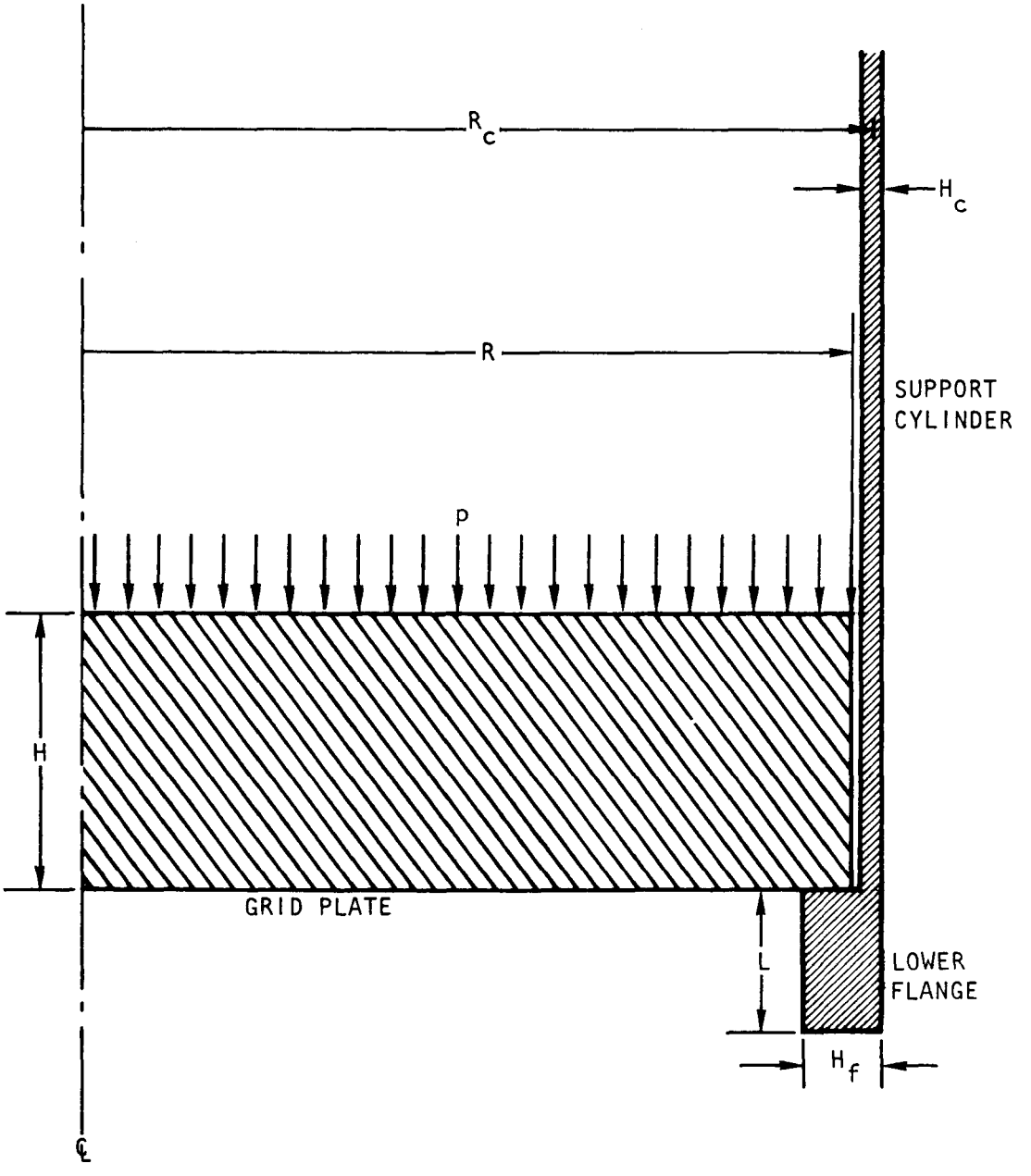

Fig. 28. Core support structure subjected to a uniform pressure load on the grid plate

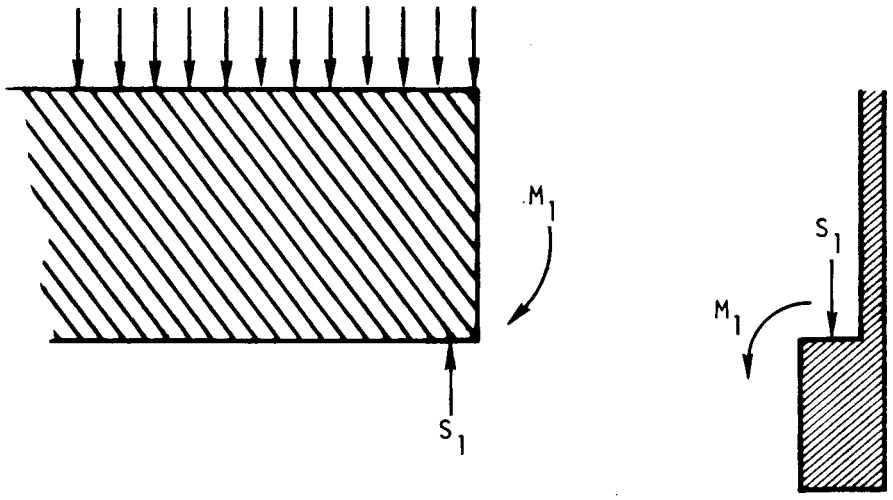

Fig. 29. Interactive force and moment between the grid plate and the support cylinder

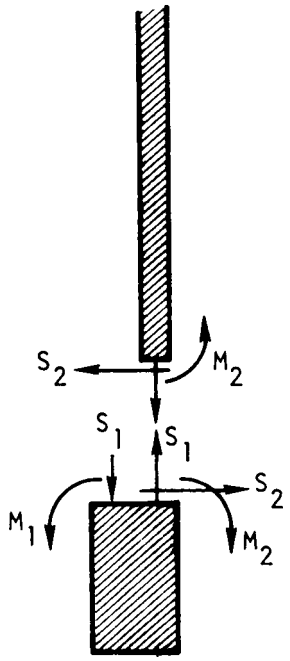

Fig. 30. Discontinuity shear force and bending moment at the cylinder and flange joint section

5.2. STRUCTURAL ANALYSIS

Based on the assumptions formulated for the grid plate problem, the equations for the rotations and displacements of the grid plate, the support cylinder, and the lower flange can be written as shown below.

Rotation at edge of grid plate

$$\theta_p = \frac{3(1 - \nu^*)PR^3}{2E^*H^3} - \frac{12(1 - \nu^*)RM_1}{E^*H^3} \quad . \tag{118}$$

Rotation at lower end of support cylinder

$$\theta_c = \frac{M_2}{\beta_c D_c} - \frac{S_2}{2\beta_c^2 D_c} \quad , \tag{119}$$

where

$$\beta_c = \left[\frac{3(1 - \nu^2)}{R_c^2 H_c^2}\right]^{1/4} \quad ,$$

$$D_c = \frac{EH_c^3}{12(1 - \nu^2)} \quad .$$

Radial displacement at lower end of support cylinder

$$w_c = \frac{M_2}{2\beta_c^2 D_c} - \frac{S_2}{2\beta_c^3 D_c} \quad . \tag{120}$$

Rotation at upper end of lower flange

$$\theta_f = \frac{A_1 S_2}{2\beta_f^2 D_f} + \frac{A_2(M_2 - M_1 - S_1 H_f/2)}{2\beta_f D_f} \quad , \tag{121}$$

where

$$\beta_f = \left[\frac{3(1 - \nu^2)}{R_f^2 H_f^2}\right]^{1/4} \quad ,$$

$$D_f = \frac{EH_f^3}{12(1 - \nu^2)} \quad ,$$

$$A_1 = (\cosh 2\beta_f L - \cos 2\beta_f L)/2(\sinh^2 \beta_f L - \sin^2 \beta_f L) \quad ,$$

$$A_2 = (\sinh 2\beta_f L + \sin 2\beta_f L)/(\sinh^2 \beta_f L - \sin^2 \beta_f L) \quad .$$

Radial displacement at upper end of lower flange

$$w_f = \frac{B_1 S_2}{2\beta_f^3 D_f} + \frac{B_2(M_2 - M_1 - S_1 H_f/2)}{2\beta_f^2 D_f} \quad , \tag{122}$$

where

$$B_1 = (\sinh 2\beta_f L - \sin 2\beta_f L)/2(\sinh^2 \beta_f L - \sin^2 \beta_f L) \quad ,$$

$$B_2 = A_1 \quad .$$

If the grid plate is rigidly clamped to the support cylinder, then

$$\theta_p = -\theta_f = \theta_c \quad . \tag{123}$$

Moreover,

$$w_c = w_f \quad . \tag{124}$$

Substituting Eqs. 118 to 122 into Eqs. 123 and 124 and performing a rearrangement gives

$$\frac{A_1}{2\beta_f^2 D_f} S_2 - \left[\frac{12(1-\nu^*)R}{E^* H^3} + \frac{A_2}{2\beta_f D_f}\right] M_1 + \frac{A_2}{2\beta_f D_f} M_2 = \frac{A_2 S_1 H_f}{4\beta_f D_f} - \frac{3(1-\nu^*)PR^3}{2E^* H^3} \quad , \tag{125}$$

$$\left[\frac{1}{2\beta_c^2 D_c} - \frac{A_1}{2\beta_f^2 D_f}\right] S_2 + \frac{A_2}{2\beta_f D_f} M_1 - \left[\frac{A_2}{2\beta_f D_f} + \frac{1}{\beta_c D_c}\right] M_2 = -\frac{A_1 S_1}{4\beta_f D_f} \quad , \tag{126}$$

$$\left[\frac{B_1}{2\beta_f^3 D_f} + \frac{1}{2\beta_c^3 D_c}\right] S_2 - \frac{B_2}{2\beta_f^2 D_f} M_1 + \left[\frac{B_2}{2\beta_f^2 D_f} - \frac{1}{2\beta_f^2 D_c}\right] M_2 = \frac{B_2 S_1}{4\beta_f^2 D_f} \quad , \tag{127}$$

where

$$S_1 = \frac{\pi R^2 P}{2\pi R} = \frac{PR}{2} \quad .$$

Consequently, the unknowns S_2, M_1, and M_2 can be determined.

5.3. NUMERICAL RESULTS

A computer program based on these analytical results was written, and numerical results were obtained for the core support structure of the 300-MW(e) plant. The following geometric and material constants were input to the program:

R = 1.743 m (68.625 in.),
R_c = 1.765 m (69.5 in.),
H = 609.6 mm (24 in.),
H_c = 44.45 mm (1.75 in.)
R_f = 1.705 m (67.125 in.),
H_f = 165.1 mm (6.5 in.),
L = 304.8 mm (12 in.),
E = 172.37 x 10^3 MPa (25 x 10^6 psi),
E^* = 34.474 x 10^3 MPa (5.0 x 10^6 psi),
ν = 0.3,
ν^* = 0.76,
P = 289.58 KPa (42 psi),

It was found that

S_2 = 9.3956 KN/m (53.65 lb/in.),
M_1 = -16.0937 KN·m/m (-3618 lb·in./in.),
M_2 = 1.539 KN·m/m (346 lb·in./in.).

Note that the negative sign of the interactive moment (M_1) indicates that an additional rotation of the grid plate is caused by M_1 because of the larger rotation of the more flexible support cylinder. This result will be used to arrive at a satisfactory design configuration for the junction between the grid plate and the core support cylinder.

6. DISCUSSION AND CONCLUSIONS

A comprehensive study of the GCFR core support structure has been performed, including analysis of the grid plate, the grid support structure, and the structural interaction between the plate and the support structure. The effect of neutron irradiation on mechanical properties was not studied. Problems such as irradiation-induced swelling, creep, loss of ductility, thermal stress, and thermal fatigue will be studied during the next phase of this effort.

The stresses in the component of the core support structure subjected to pressure loading were found to be very low, as predicted. However, thermally induced stresses were not included in this analysis.

Three different theories were applied to the analysis of the grid plate: transversely isotropic elastic body theory, isotropic elastic body theory, and thin plate theory. The results show that the radial and tangential stresses for the three theories are almost identical. The axial stress and transverse shear distribution along the thickness of the grid plate for the transversely isotropic elastic body and isotropic elastic body analysis are also very close. The input for the isotropic elastic theory and thin plate theory solutions are identical. Therefore, the 32.6% difference in axial displacement at the center of the grid plate is considered to be due to the effect of transverse shear and normal stress.

There is a 21% difference in the displacement at the center of the grid plate for the transversely isotropic and isotropic solutions. Both theories consider transverse shear and normal stress, but the transversely isotropic elastic body solution considers the axial direction elastic modulus, which is much higher than the in-plane direction elastic modulus. This higher elastic constant plus the different Poisson's ratio contributes

the difference in the displacement. Indeed, thin plate theory is based on the assumption that E is infinite in the axial direction (rigid).

Prediction of displacements is much more sensitive to the method used than prediction of stress. The plot of radial displacement versus radial coordinate for the transversely isotropic solution is quite different from that for the isotropic case (Fig. 31). The maximum radial displacement for the transversely isotropic solution is -0.1196 mm (-4.71×10^{-3} in.) at r = 1.397 m (55 in.); for the isotropic case, it is -0.0813 mm (-3.2×10^{-3} in.) at r = 1.257 m (49.5 in.).

Comparison of axial displacement at the center of the grid plate for the three solutions gave the most significant results. The center axial displacement at the middle surface of the grid plate for the transversely isotropic solution (Fig. 32) is 0.5283 mm (0.0208 in.); the prediction made by the isotropic elastic body solution is 0.6401 mm (0.0252 in.), and thin plate theory gives the center displacement as 0.4826 mm (0.019 in.).

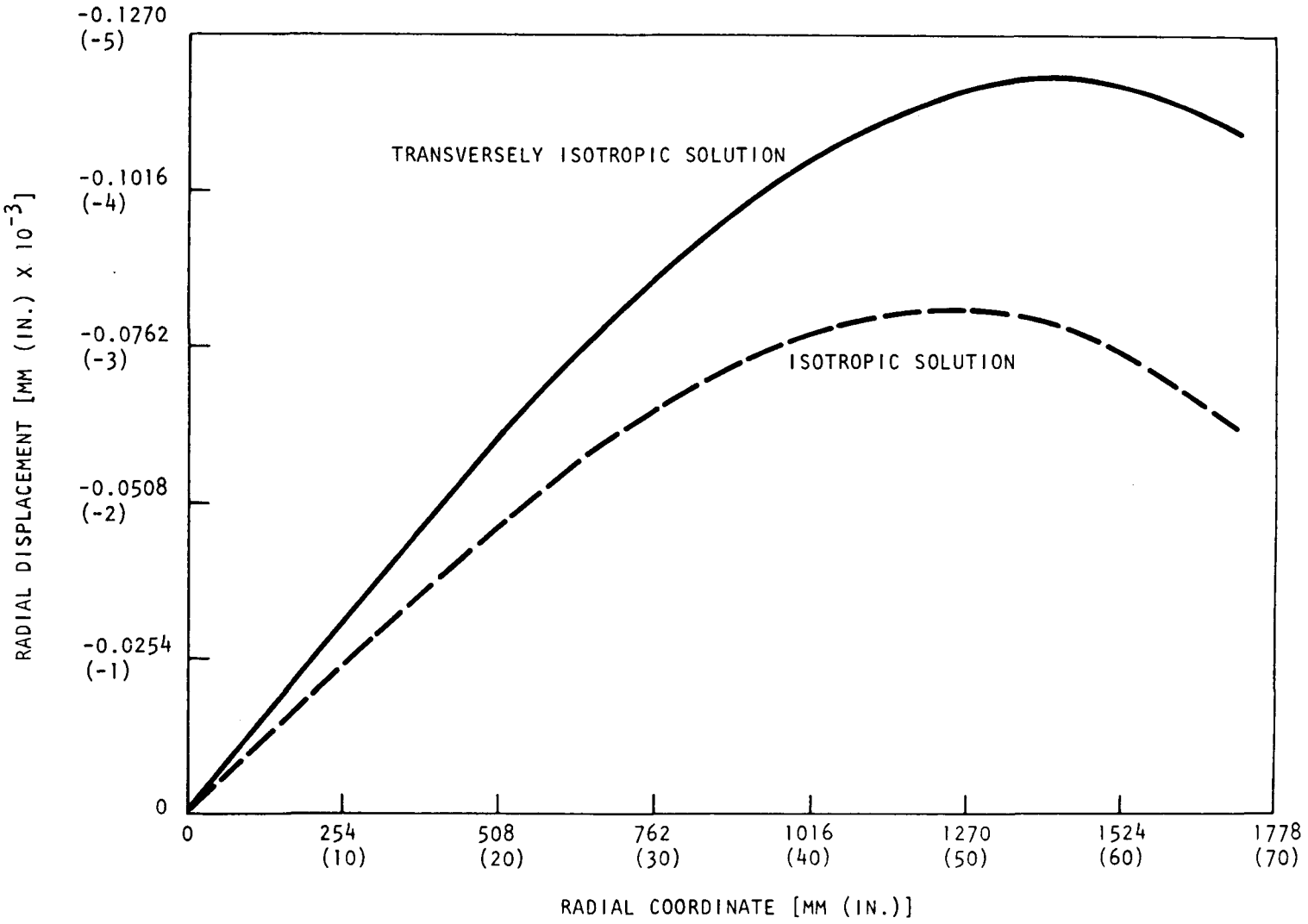

Fig. 31. Comparison of transversely isotropic and isotropic solutions, radial displacement vs radial coordinate at the top surface of the grid plate

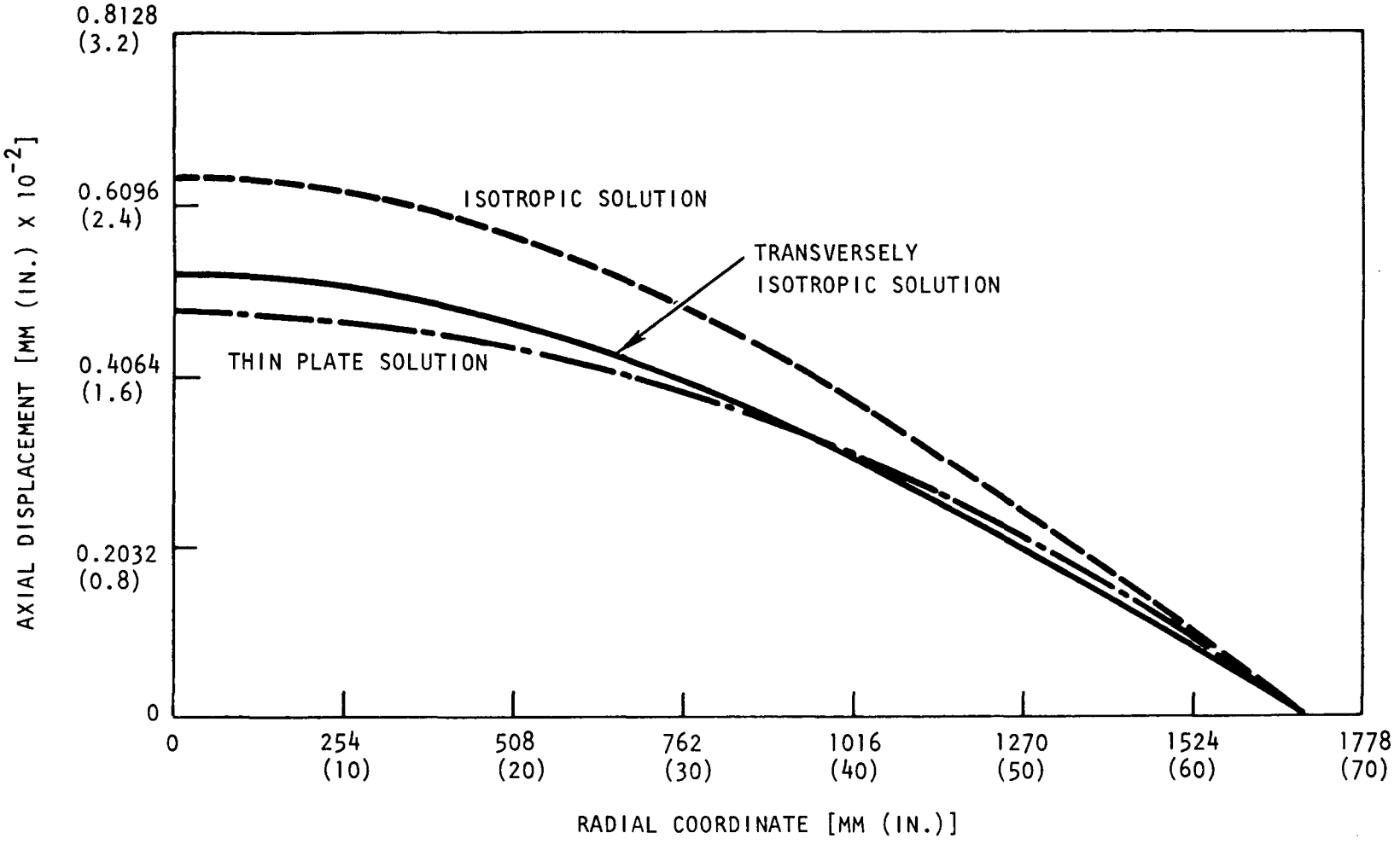

Fig. 32. Comparison of transversely isotropic, isotropic, and thin plate solutions, axial displacement vs radial coordinate at the middle surface of the grid plate

7. REFERENCES

1. Gardner, K. A., "Heat-Exchanger Tube-Sheet Design," J. Appl. Mech. 15, 377-385 (1948).
2. Gardner, K. A., "Heat-Exchanger Tube-Sheet Design - 2: Fixed Tube Sheets," J. Appl. Mech. 19, 159-166 (1952).
3. Gardner, K. A., "Heat-Exchanger Tube-Sheet Design - 3: U-Tube and Bayonet Tube Sheets," J. Appl. Mech. 27, 25-33 (1960).
4. Horvay, G., "Thermal Stresses in Perforated Plates," in Proceedings of the First U.S. National Congress of Applied Mechanics, Chicago, 1951, ASME, New York, pp. 247-257.
5. Horvay, G., "Bending of Honeycombs and of Perforated Plates," J. Appl. Mech. 19, 122-123 (1952).
6. Horvay, G., "The Plane-Stress Problem of Perforated Plates," J. Appl. Mech. 19, 355-360 (1952).
7. Malkin, I., "Notes on a Theoretical Basis for the Design of Tube Sheets of Triangular Layout," Trans. Am. Soc. Mech. Engrs. 74, 389-396 (1952).
8. Slot, T., "Orthotropic Analysis of a Thick Perforated Plate with Pressure on One Side," in Proceedings of the Second International Conference on Structural Mechanics in Reactor Technology, Berlin, Germany, September 10-14, 1973, v. 11.
9. Torri, A., and M. J. Driscoll, "Reactivity Insertion Mechanisms in the GCFR," General Atomic Report GA-A12934, April 10, 1974.
10. "ASME Boiler and Pressure Vessel Code," Section III (ASME 111/2).
11. O'Donnell, W. J., and B. F. Langer, "Design of Perforated Plates," J. Eng. Ind. 84, 307-320 (1962).
12. Roark, R. J., Formulas for Stress and Strain, 4th ed., McGraw-Hill, New York, 1965, p. 255.
13. Timoshenko, S., and S. Woinowsky-Krieger, Theory of Plates and Shells, 2nd ed., McGraw-Hill, New York, 1959.

14. Slot, T., "Stress Analysis of Thick Perforated Plates," Ph.D Dissertation, University of Technology Delft, September 1972.
15. Leknitskii, S. G., Theory of Elasticity of an Anisotropic Elastic Body, Holden-Day, San Francisco, 1963.
16. Timoshenko, S., and J. N. Goodier, Theory of Elasticity, 3rd ed., McGraw-Hill, New York, 1969, p. 386.
17. Love, A. E. H., A Treatise on the Mathematical Theory of Elasticity, 4th ed., Dover, New York, 1974, p. 481.

APPENDIX A

COMPUTER PROGRAM GRIPLAT

```
*FOR,IS   GRIPLAT,GRTPLAT
      REAL M,NU,NUP
      DIMENSION R(10),Z(10),STR(10,10),STT(10,10),STRZ(10,10),STZ(10),
     1          UR(10,10),W(10,10),WT(10)
      DIMENSION EXTRA(10),STRZ1(10),UR2(10),UR3(10),W4(10),W5(10),
     1          STR1(10,10),STT1(10,10),UR1(10,10),W1(10),W2(10),
     2          W3(10,10)
      READ(5,1)RO,H,Q,L,N
    1 FORMAT(3F10.3,2I3)
      READ(5,2)E,NU,EP,NUP,GP
    2 FORMAT(6E12.6)
      READ(5,2)(Z(I),I=1,L)
      READ(5,2)(R(I),I=1,N)
      WRITE(6,14)RO,H,Q,E,EP,GP,NU,NUP
   14 FORMAT(1H1,14X,'INPUT DATA'/
     1       15X,'OUTER RADIUS =',F7.3,1X,'IN.'/
     2       15X,'THICKNESS =',F7.3,1X,'IN.'/
     3       15X,'PRESSURE =',F7.3,1X,'PSI'/
     4       15X,'IN-PLANE YOUNG MODULUS =',E9.4,1X,'PSI'/
     5       15X,'AXIAL YOUNG MODULUS =',E9.4,1X,'PSI'/
     6       15X,'AXIAL SHEAR MODULUS =',E9.4,1X,'PSI'/
     7       15X,'IN-PLANE POISSON RATIO =',F5.3/
     8       15X,'AXIAL POISSON RATIO =',F5.3)
C     TRANSVERSELY ISOTROPIC CASE
      NN=1
      WRITE(6,3)
    3 FORMAT(///,10X,'TRANSVERSELY ISOTROPIC SOLUTION'//)
      M=E*(1./GP-NUP*(3.+NU)/EP)/(1.-NU)
      D=E*H**3/(12.*(1.-NU**2))
      DO 101 I=1,L
      EXTRA(I)=Q*M*((Z(I)/H)**3-0.15*(Z(I)/H))
      STZ(I)=0.5*Q*(-1.+3.*Z(I)/H-4.*(Z(I)/H)**3)
      STRZ1(I)=0.75*Q/H*(1.-4.*(Z(I)/H)**2)
      UR2(I)=0.3/H*(M*(1.-NU)+10.*E*NUP/EP)*Z(I)
      UR3(I)=(M*(1.-NU)-2.*E*NUP/EP)*(Z(I)/H)**3
      W4(I)=0.15*(M*NUP+5.)*Z(I)/H
      W5(I)=0.5*(M*NUP+1.)*(Z(I)/H)**3
      DO 101 J=1,N
      STR1(I,J)=0.75*Q*(3.+NU)*(RO**2-R(J)**2)*Z(I)/H**3
      STR(I,J)=STR1(I,J)+EXTRA(I)
      STT1(I,J)=0.75*Q*((3.+NU)*RO**2-(1.+3.*NU)*R(J)**2)*Z(I)/H**3
      STT(I,J)=STT1(I,J)+EXTRA(I)
      STRZ(I,J)=-STRZ1(I)*R(J)
      UR1(I,J)=0.75*(1.-NU)*((3.+NU)*RO**2-(1.+NU)*R(J)**2)*Z(I)/H**3
      UR(I,J)=Q*R(J)/E*(E*NUP/(2.*EP)+UR1(I,J)-UR2(I)+UR3(I))
      W1(J)=Q*(RO**2-R(J)**2)*((5.+NU)/(1.+NU)*RO**2-R(J)**2)/(64.*D)
      W2(J)=0.3*Q/H*(1./GP-NUP*(7.-NU)/(4.*EP))*(RO**2-R(J)**2)
      W3(I,J)=0.75*NUP*Z(I)*((3.+NU)*RO**2-2.*(1.+NU)*R(J)**2)/(EP*H**3)
      W(I,J)=W1(J)+W2(J)+Q*Z(I)/EP*(-0.5-W3(I,J)+W4(I)-W5(I))
  101 CONTINUE
 1001 WRITE(6,4)
    4 FORMAT(25X,'RADIAL STRESS,PSI'///,7X,'Z',61X,'R'//)
      WRITE(6,21)(R(I),I=1,N)
   21 FORMAT(15X,10E11.4)
      WRITE(6,5)(Z(I),(STR(I,J),J=1,N),I=1,L)
    5 FORMAT('0',E12.4,3X,5E11.4)
      WRITE(6,6)
```

```
    6 FORMAT(///25X,'TANGENTIAL STRESS,PSI'//7X,'Z',61X,'R'/)
      WRITE(6,21)(R(I),I=1,N)
      WRITE(6,5)(Z(I),(STT(I,J),J=1,N),I=1,L)
      WRITE(6,7)
    7 FORMAT(///25X,'AXIAL STRESS,PST'//69X,'Z'/)
      WRITE(6,21)(Z(I),I=1,L)
      WRITE(6,21)(STZ(I),I=1,L)
      WRITE(6,8)
    8 FORMAT(///25X,'TRANSVERSE SHEAR STRESS,PSI'//7X,'Z',61X,'R'/)
      WRITE(6,21)(R(I),I=1,N)
      WRITE(6,5)(Z(I),(STRZ(I,J),J=1,N),I=1,L)
      WRITE(6,9)
    9 FORMAT(///25X,'RADIAL DISPLACEMENT,IN.'//7X,'Z',61X,'R'/)
      WRITE(6,21)(R(I),I=1,N)
      WRITE(6,5)(Z(I),(UR(I,J),J=1,N),I=1,L)
      WRITE(6,10)
   10 FORMAT(///25X,'AXIAL DISPLACEMENT,IN.'//7X,'Z',61X,'R',/)
      WRITE(6,21)(R(I),I=1,N)
      WRITE(6,5)(Z(I),(W(I,J),J=1,N),I=1,L)
      IF(NN .EQ. 2) GO TO 1002
      NN=2
C     ISOTROPIC CASE
      WRITE(6,11)
   11 FORMAT(///,10X,'ISOTROPIC SOLUTION'//)
      DO 102 I=1,L
      EXTRA(I)=Q*(2.+NU)*((Z(I)/H)**3-0.15*(Z(I)/H))
      STZ(I)=0.5*Q*(-1.+3.*Z(I)/H-4.*(Z(I)/H)**3)
      STRZ1(I)=0.75*Q*(1.-4.*(Z(I)/H)**2)/H
      UR2(I)=0.15*Z(I)*(2.+9.*NU-NU**2)/H
      UR3(I)=(2.+NU-NU**2)*(Z(I)/H)**3
      W4(I)=0.15*(5.+2.*NU+NU**2)*Z(I)/H
      W5(I)=0.5*(1.+NU)**2*(Z(I)/H)**3
      DO 102 J=1,N
      STR1(I,J)=0.75*Q/H**3*(3.+NU)*(RO**2-R(J)**2)*Z(I)
      STR(I,J)=STR1(I,J)+EXTRA(I)
      STT1(I,J)=0.75*Q/H**3*((3.+NU)*RO**2-(1.+3.*NU)*R(J)**2)*Z(I)
      STT(I,J)=STT1(I,J)+EXTRA(I)
      STRZ(I,J)=-STRZ1(I)*R(J)
      UR1(I,J)=0.75*(1.-NU)/H**3.*((3.+NU)*RO**2-(1.+NU)*R(J)**2)*Z(I)
      UR(I,J)=Q*R(J)/E*(0.5*NU+UR1(I,J)-UR2(I)+UR3(I))
      W1(J)=Q*(RO**2-R(J)**2)*((5.+NU)/(1.+NU)*RO**2-R(J)**2)/(64.*D)
      W2(J)=0.075*Q*(8.+NU+NU**2)*(RO**2-R(J)**2)/(E*H)
      W3(I,J)=0.75*NU*Z(I)*((3.+NU)*RO**2-2.*(1.+NU)*R(J)**2)/(E*H**3)
      W(I,J)=W1(J)+W2(J)+Q*Z(I)/E*(-0.5-W3(I,J)+W4(I)-W5(I))
  102 CONTINUE
      GO TO 1001
C     THIN PLATE CASE
 1002 WRITE(6,12)
   12 FORMAT(///,10X,'THIN PLATE SOLUTION'//)
      DO 103 I=1,L
      DO 103 J=1,N
      STR(I,J)=0.75*Q*(3.+NU)*(RO**2-R(J)**2)*Z(I)/H**3
      STT(I,J)=0.75*Q*((3.+NU)*RO**2-(1.+3.*NU)*R(J)**2)*Z(I)/H**3
  103 CONTINUE
      DO 104 I=1,N
      WT(I)=Q*(RO**2-R(I)**2)*((5.+NU)/(1.+NU)*RO**2-R(J)**2)/(64.*D)
  104 CONTINUE
```

```
      WRITE(6,4)
      WRITE(6,21)(R(I),I=1,N)
      WRITE(6,5)(Z(I),(STR(I,J),J=1,N),I=1,L)
      WRITE(6,6)
      WRITE(6,21)(R(I),I=1,N)
      WRITE(6,5)(Z(I),(STT(I,J),J=1,N),I=1,L)
      WRITE(6,13)
   13 FORMAT(///25X,'AXIAL DISPLACEMENT,IN.'///,69X,'R'/)
      WRITE(6,21)(R(I),I=1,N)
      WRITE(6,21)(WT(I),I=1,N)
      STOP
      END
*XQT
10.        3.6          60.              5  5
0.2        E6 0.76        2.257        E6  0.3        0.4503     E6
0.           0.5            1.0            1.5          1.8
0.           2.             4.             6.           10.
```

APPENDIX B

COMPUTER PROGRAM INPUT

```
*FOR,SI      INPUT,INPUT
      DIMENSION R(3),R1(7),H(6),T1(8),T2(8),ETA(7)
      DATA (R(I),I=1,3)/77.5,79.5,81.5/
      DATA (H(I),I=1,6)/.5,.7,.9,1.1,1.3,1.5/
      DATA (T1(I),I=1,8)/16.,18.,20.,22.,24.,26.,28.,30./
      RO=70.6175
      P=8.767
      W=35.3
      DO 10 I=1,6
      ETA(I)=H(I)/P
      R1(I)=RO+(P-H(I))/4.
   10 CONTINUE
      DO 11 I=1,8
      T2(I)=T1(I)-1.5
   11 CONTINUE
      WRITE(6,100)
  100 FORMAT(1H1,6X,'R',9X,'R1',8X,'T1',8X,'T2',8X,'P',8X,'ETA',8X,'W',9
     1X,'E',9X,'E*',7X,'NU')
      DO 12 I=1,3
      DO 12 J=1,6
      DO 12 K=1,8
      WRITE(6,101) R(I),R1(J),T1(K),T2(K),P,ETA(J),W
      PUNCH 102, R(I),R1(J),T1(K),T2(K),W
   12 CONTINUE
  101 FORMAT(3X,7(E8.4,2X))
  102 FORMAT(5F12.4)
      STOP
      END
*XQT
```

APPENDIX C

COMPUTER PROGRAM GRID

```
*FOR,SI   GRID,GRID
      DIMENSION TITLE(18)
      REAL NU1,LIGEF,M
      READ(5,200)TITLE
200   FORMAT(18A4)
      WRITE(6,300) TITLE
300   FORMAT(6X,18A4)
      WRITE(6,100)
  100 FORMAT(1H1,5X,'GRID PLATE DEFLECTION DUE TO PRESSURE')
      WRITE(6,110)
110   FORMAT('0',5X,'R =RADIUS OF GRID PLATE,IN.'/
     16X,'R1=RADIUS OF PERFORATED PLATE,IN.'/
     26X,'T1=THICKNESS OF GRID PLATE,IN.'/
     36X,'T2=THICKNESS OF PLATE LESS BEVEL DEPTH,IN.'/
     46X,'W =LOAD,LBS/IN**2'/
     56X,'E =YOUNG MODULUS ,LBS/IN.**2'/
     66X,'E1=EFFECTIVE YOUNG MODULUS,LBS/IN.**2'/
     76X,'NU1=EFFECTIVE POISSON RATIO'/
     86X,'P =PITCH,IN.'/
     96X,'ETA=LIGAMENT EFFICIENY'/
     16X,'M =MOMENT AT JUNCTION OF PERFORATED PLATE AND SOLID RING,LB*IN
     2./IN.'/
     36X,'DELC=DEFLECTION AT PLATE CENTER,IN.'/
     46X,'RC=CORE RADIUS, IN.'/
     56X,'DYDRC=SLOPE AT CORE EDGE'/
     66X,'RHO=REACTIVITY, CENTS'//)
      BETA=0.0035
      EL=84.67
      RC=50.
      CN=0.512
      WRITE(6,111)
111   FORMAT(5X,'W=35.3 PSI  P=8.676 IN.  RC=50. IN.')
      WRITE(6,112)
112   FORMAT(//,8X,'R',9X,'R1',8X,'T1',8X,'T2',7X,'ETA',8X,'E',9X,
     1'E1',7X,'NU1',8X,'M',7X,'DELC',6X,'DYDRC',6X,'RHO')
      N=1
   10 READ(5,101) NEXT
  101 FORMAT(I3)
      READ(5,102) R,R1,T1,T2,W
      READ(5,102) E,E1,NU1, PITCH,LIGEF
102   FORMAT(5E12.6)
      B=(T2/T1)**3
      M1=(E1/E)*B*(R+R1)*(R**2+R1**2)/(R1*(1.-NU1))
      M2=4.*(E1/E)*B*(R+R1)/((1.-NU1)*(R-R1))
      M=(R1**2*W-M1*W)/(8.+M2)
      CM1=(6.*R1*(R+R1))/(E*T1**3)
      CM2=6.*(1.-NU1)*R1**2/(E1*T2**3)
      CW1=1.5*(R**4-R1**4)/(E*T1**3)
      CW2=3.*R1**4*(1.-NU1)*(5.+NU1)/(16.*E1*T2**3)
      DELC=(CM1-CM2)*M+(CW1+CW2)*W
      DYDRW=-3.*R1**2*W*(1.-NU1**2)*(2.*RC**3/R1**2-2.*(3.+NU1)*RC
     1       /(1.+NU1))/(8.*E1*T2**3)
      DYDRM=-12.*(1.-NU1)*RC*M/(E1*T2**3)
      DYDRC=DYDRW+DYDRM
      RHO=CN*DYDRC*EL*100./(RC*BETA)
      WRITE(6,113)R,R1,T1,T2,LIGEF,E,E1,NU1,M,DELC,DYDRC,RHO
113   FORMAT(4X,5F10.4,2E10.4,F10.4,4E10.4)
```

```
      N=N+1
      IF(NEXT.GT.0) GO TO 10
      STOP
      END
*XQT
```

APPENDIX D

COMPUTER PROGRAM GRISP

```
*FOR,SI    GRISP,GRISP
C     GRID PLATE SUPPORT STRUCTURAL ANALYSIS
C
      REAL NU
      DIMENSION TITLE(18),H1(10),T1(10),T(10),R(10),H2(10),T2(10)
      READ(5,10) TITLE
   10 FORMAT(18A4)
      WRITE(6,11)TITLE
   11 FORMAT(1H1,5X,18A4)
      READ(5,12) E,NU,W,PI,PO
12    FORMAT(5E12.6)
      READ(5,13) N1,N2,N3,N4,N5,N6
   13 FORMAT(6I6)
      READ(5,14) (H1(I),I=1,N1)
      READ(5,14) (T1(I),I=1,N2)
      READ(5,14) (T(I),I=1,N3)
      READ(5,14) (R(I),I=1,N4)
      READ(5,14) (H2(I),I=1,N5)
      READ(5,14) (T2(I),I=1,N6)
   14 FORMAT(6F12.4)
      WRITE(6,15)
   15 FORMAT('0',5X,'NOTATION EXPLANATION'/
     16X,'H1=UPPER FLANGE WIDTH, IN.'/
     26X,'T1=UPPER FLANGE THICKNESS, IN.'/
     36X,'T =CYLINDER WALL THICKNESS, IN.'/
     46X,'R =CYLINDER INNER RADIUS, IN.'/
     56X,'H2=LOWER FLANGE LENGTH, IN.'/
     66X,'T2=LOWER FLANGE THICKNESS, IN.'/
     76X,'E =ELASTIC MODULUS, LBS/IN**2'/
     86X,'NU=POISSON RATIO'/
     96X,'SZO=AXIAL STRESS AT OUTER SURFACE, PSI'/
     16X,'SZI=AXIAL STRESS AT INNER SURFACE, PSI'/
     26X,'STO=HOOP STRESS AT OUTER SURFACE, PSI'/
     36X,'STI=HOOP STRESS AT INNER SURFACE, PSI'/
     46X,'SR=MEAN RADIAL STRESS DUE TO INSIDE AND OUTSIDE PRESSURE,PSI'/
     56X,'SO=STRESS INTENSITY AT OUTER SURFACE, PSI'/
     66X,'SI=STRESS INTENSITY AT INNER SURFACE, PSI'/
     96X,'W=DEAD WEIGHT, LBS.'/
     76X,'PI=INSIDE PRESSURE, PSI'/
     86X,'PO=OUTSIDE PRESSURE, PSI')
      WRITE(6,16)E,NU,W,PI,PO
   16 FORMAT('0',5X,'E=',E12.4,3X,'NU=',F12.4,3X,'W=',F12.2,
     13X,'PI=',F12.2,3X,'PO=',F12.2)
C
C     STRESS ANALYSIS AT C/S A
C
      WRITE(6,17)
   17 FORMAT('0',5X,'STRESSES AT JOINT OF CYLINDER AND UPPER FLANGE'//
     16X,'R',6X,'T',5X,'H1',5X,'T1',6X,'V',8X,'SZO',6X,'SZI',
     26X,'STO',6X,'STI',6X,'SR',7X,'SO',7X,'SI')
      DO 100 I=1,N4
      V=W/(2.*3.14159*(R(I)+T(J)/2.))
      DO 100 J=1,N3
      D=E*T(J)**3/(12.*(1.-NU**2))
      BETA=(3.*(1.-NU**2)/((R(I)+T(J)/2.)**2*T(J)**2))**0.25
      DO 100 K=1,N1
      DO 100 L=1,N2
```

```
      R1=2.*R(I)+T(J)
      R2=2.*R(I)+H1(K)
      E1=E*T1(L)**2
      A11=1./(BETA*D)+3.*R1*R2/(E1*H1(K)*T1(L))
      A12=-1./(2.*BETA**2*D)+3.*R1*R2/(2.*E1*H1(K))
      A21=-1./(2.*BETA**2*D)+3.*R1*R2/(2.*E1*H1(K))
      A22=1./(2.*BETA**3*D)+R1*R2/(E*H1(K)*T1(L))
      B1=3.*R1*R2*V/(2.*E1*T1(L))
      B2=B1*T1(L)/2.-(PI-PO)*(R(I)+T(J)/2.)**2/(E*T(J))
      DELTA=A11*A22-A21*A12
      MA=(B1*A22-B2*A12)/DELTA
      SA=(A11*B2-A21*B1)/DELTA
      WC=SA/(2.*BETA**3*D)-MA/(2.*BETA**2*D) +
     1(PI-PO)*(R(I)+T(J)/2.)**2/(E*T(J))
      SZO=V/T(J)+MA/T(J)**2
      SZI=V/T(J)-MA/T(J)**2
      STO=E*WC/(R(I)+T(J)/2.)-NU*MA/T(J)**2
      STI=E*WC/(R(I)+T(J)/2.)+NU*MA/T(J)**2
      SR=(-PI-PO)/2.
      SO1=ABS(STO-SZO)
      SO2=ABS(SZO-SR)
      SO3=ABS(SR-STO)
      SO=AMAX1(SO1,SO2,SO3)
      SI1=ABS(STI-SZI)
      SI2=ABS(SZI-SR)
      SI3=ABS(SR-STI)
      SI=AMAX1(SI1,SI2,SI3)
      WRITE(6,19) R(I),T(J),H1(K),T1(L),V,SZO,SZI,STO,STI,SR,SO,SI
19    FORMAT(4X,F6.2,1X,F5.2,1X,F6.2,1X,F6.2,1X,8(F8.1,1X))
  100 CONTINUE
C
C     STRESS ANALYSIS AT C/S B
C
      WRITE(6,20)
   20 FORMAT(///,6X,'STRESSESS AT CYLINDER MID-SECTION'//
     18X,'R',9X,'T',9X,'V',8X,'SZ',8X,'ST',8X,'SR',8X,'S')
      DO 101 I=1,N4
      V=W/(2.*3.14159*R(I))
      DO 101 J=1,N3
      SZ=V*R(I)/((R(I)+T(J)/2.)*T(J))
      ST=(PI-PO)*(R(I)+T(J)/2.)/T(J)
      SR=(-PI-PO)/2.
      S1=ABS(ST-SZ)
      S2=ABS(SZ-SR)
      S3=ABS(SR-ST)
      S=AMAX1(S1,S2,S3)
      WRITE(6,22)R(I),T(J),V,SZ,ST,SR,S
   22 FORMAT(4X,7(F8.2,2X))
  101 CONTINUE
C
C     STRESS ANALYSIS AT C/S C
C
      WRITE(6,23)
   23 FORMAT(///,6X,'STRESSES AT JOINT OF CYLINDER AND LOWER FLANGE'//
     16X,'R',6X,'T',5X,'H2',5X,'T2',6X,'V',8X,'SZO',6X,'SZI',
     26X,'STO',6X,'STI',6X,'SR',7X,'SO',7X,'SI')
      DO 102 I=1,N4
```

```
      V=W/(2.*3.14159*R(I))
      DO 102 J=1,N3
      D=E*T(J)**3/(12.*(1.-NU**2))
      BETA=(3.*(1.-NU**2)/((R(I)+T(J)/2.)**2*T(J)**2))**0.25
      DO 102 K=1,N5
      DO 102 L=1,N6
      DF=E*T2(L)**3/(12.*(1.-NU**2))
      BETAF=(3.*(1-NU**2)/((R(I)+T(J)-T2(L)/2.)**2*T2(L)**2))**0.25
      DIVD=2.*((SINH(BETAF*H2(K)))**2-(SIN(BETAF*H2(K)))**2)
      B11F=(SINH(2.*BETAF*H2(K))-SIN(2.*BETAF*H2(K)))/DIVD
      B12F=(COSH(2.*BETAF*H2(K))-COS(2.*BETAF*H2(K)))/DIVD
      B22F=(SINH(2.*BETAF*H2(K))+SIN(2.*BETAF*H2(K)))*2./DIVD
      C11=1./(BETA*D)+B22F/(BETAF*DF)
      C12=-1./(2.*BETA**2*D)+B12F/(2.*BETAF**2*DF)
      C21=C12
      C22=1./(2.*BETA**3*D)+B11F/(2.*BETAF**3*DF)
      D1=B22F*T2(L)*V/(4.*BETAF*DF)
      D2=B12F*T2(L)*V/(4.*BETAF**2*DF)+
     1(PI-PO)*(R(I)+T(J)/2.)**2/(E*T(J))
     2-(PI-PO)*(R(I)+T(J)-T2(L)/2.)**2/(E*T2(L))
      DELTA=C11*C22-C12*C21
      MC=(D1*C22-D2*C12)/DELTA
      SC=(C11*D2-C21*D1)/DELTA
      WC=MC/(2.*BETA**2*D)-SC/(2.*BETA**3*D)+
     1(PI-PO)*(R(I)+T(J)/2.)**2/(E*T(J))
      SZO=V/T(J)-MC/T(J)**2
      SZI=V/T(J)+MC/T(J)**2
      STO=E*WC/(R(I)+T(J)/2.)+NU*MC/T(J)**2
      STI=E*WC/(R(I)+T(J)/2.)-NU*MC/T(J)**2
      SR=(-PI-PO)/2.
      SO1=ABS(STO-SZO)
      SO2=ABS(SZO-SR)
      SO3=ABS(SR-STO)
      SO=AMAX1(SO1,SO2,SO3)
      SI1=ABS(STI-SZI)
      SI2=ABS(SZI-SR)
      SI3=ABS(SR-STI)
      SI=AMAX1(SI1,SI2,SI3)
      WRITE(6,24) R(I),T(J),H2(K),T2(L),V,SZO,SZI,STO,STI,SR,SO,SI
24    FORMAT(4X,F6.2,1X,F5.2,1X,F6.2,1X,F6.2,1X,8(F8.1,1X))
  102 CONTINUE
      STOP
      END
@XQT
   300MW DEMO PLANT GRID SUPPORT STRUCTURAL ANALYSIS
25.       E06  0.3        1174000.       1305.         1263.
     6      6      6      1      6      6
3.5            4.5            5.5            6.5            7.5            8.5
1.5            2.0            2.5            3.0            3.5            4.0
1.0            1.25           1.5            1.75           2.0            2.25
68.625
8.             10.            12.            14.            16.            18.
3.5            4.5            5.5            6.5            7.5            8.5
@PMD,8RDL
```